การจัดเรียงตัวของท่อคาร์บอนขนาดนาโนเมตรในพอลิอิไมด์ภายใต้สนามไฟฟ้าและสนามแม่เหล็ก

นายณัฐกานต์ ร่มเย็น

วิทยานิพนธ์นี้เป็นส่วนหนึ่งของการศึกษาตามหลักสูตรปริญญาวิศวกรรมศาสตรมหาบัณฑิต
สาขาวิชาวิศวกรรมเคมี ภาควิชาวิศวกรรมเคมี
คณะวิศวกรรมศาสตร์ จุฬาลงกรณ์มหาวิทยาลัย
ปีการศึกษา 2551

ALIGNMENT OF CARBON NANOTUBES IN POLYIMIDE UNDER
ELECTRIC AND MAGNETIC FIELD

Mr. Natthakarn Romyen

A Thesis Submitted in Partial Fulfillment of the Requirements
for the Degree of Master of Engineering Program in Chemical Engineering
Department of Chemical Engineering
Faculty of Engineering
Chulalongkorn University
Academic Year 2008

Thesis Title   ALIGNMENT OF CARBON NANOTUBES IN
POLYIMIDE UNDER ELECTRIC AND MAGNETIC FIELD

By   Mr. Natthakarn Romyen

Field of study   Chemical Engineering

Advisor   Associate Professor ML. Supakanok Thongyai, Ph.D.

Accepted by the Faculty of Engineering, Chulalongkorn University in Partial Fulfillment of the Requirements for the Master's Degree

…………………………...… Dean of the Faculty of Engineering
(Associate Professor Boonsom Lerdhirunwong, Dr.Ing.)

THESIS COMMITTEE

……………………………………Chairman
(Professor Suttichai Assabumrungrat; Ph.D.)

……………………………….…...Advisor
(Associate Professor ML. Supakanok Thongyai, Ph.D.)

……………………………………Examiner
(Assistant Professor Bunjerd Jongsomjit, Ph.D.)

…………………………………... Examiner
(Assistant Professor Anongnat Somwangthanaroj, Ph.D.)

…………………………………….External Examiner
(Assistant Professor Sirirat Wacharawichanant, D.Eng.)

ณัฐกานต์ ร่มเย็น: การจัดเรียงตัวของท่อคาร์บอนขนาดนาโนเมตรในพอลิอิไมด์ภายใต้สนามไฟฟ้าและสนามแม่เหล็ก. (ALIGNMENT OF CARBON NANOTUBES IN POLYIMIDE UNDER ELECTRIC AND MAGNERTIC FIELD) อ.ที่ปรึกษาวิทยานิพนธ์หลัก: รศ. ดร. มล. ศุกกนก ทองใหญ่, 127 หน้า.

การศึกษาคอมโพสิตระหว่างคาร์บอนแบล็กกับพอลิอิไมด์ทำขึ้นเพื่อใช้เป็นข้อมูลพื้นฐานสำหรับการศึกษาการจัดเรียงตัวของท่อนาโนคาร์บอนในพอลิอิไมด์ การกระจายตัวที่ดีของคาร์บอนแบล็กในพอลิอิไมด์โดยใช้สารลดแรงตึงผิวร่วมกับการสั่นเหนือคลื่นเสียง ถูกเตรียมขึ้นด้วยวิธีการเกิดพอลิเมอร์แบบสองขั้นตอน ซึ่งมี 4,4' ODA และ PMDA เป็นสารตั้งต้น การวิเคราะห์ด้วยกล้องจุลทรรศน์แบบส่องกราด ร่วมกับ ยูวี-วิสิเบิลสเปกโตมิเตอร์ เผยให้เห็นถึงอัตราส่วนโดยน้ำหนักระหว่างคาร์บอนแบล็กต่อสารลดแรงตึงผิวที่เหมาะสมที่สุดสำหรับการเกิดคุณสมบัติความโปร่งใสมากที่สุดในแผ่นคอมพอสิต เท่ากับ 1:2 ค่าคงที่ไดอิเล็กทริกของคอมพอสิตเพิ่มสูงขึ้นตามปริมาณของคาร์บอนแบล็กที่เพิ่มขึ้น และลดลงเมื่อเติมสารลดแรงตึงผิวลงไปในคอมพอสิต ผลการทดสอบเชิงกลของคอมพอสิตพบว่า ที่ปริมาณคาร์บอนแบล็ก 5 เปอร์เซ็นต์โดยน้ำหนักและมีอัตราส่วนระหว่างคาร์บอนแบล็กต่อสารลดแรงตึงผิวเท่ากับ 1:2 ให้คุณสมบัติการทนต่อแรงดึงยืดสูงที่สุดและคุณสมบัตินี้จะลดลงเมื่อสัดส่วนระหว่างคาร์บอนแบล็กต่อสารลดแรงตึงผิวในคอมพอสิตเพิ่มขึ้น

การเรียงตัวของท่อนาโนคาร์บอนในพอลิอิไมด์ทำขึ้นภายใต้สภาวะที่ดีสุดของระบบคาร์บอนแบล็ก/พอลิอิไมด์ นาโนคอมพอสิต สนามแม่เหล็กปริมาณคงที่ 2 เทสลา และสนามไฟฟ้าที่ความเข้มแตกต่างกันคือ 150 300 450 และ 600 โวลต์ต่อเซนติเมตร ถูกใช้เพื่อเหนี่ยวนำท่อนาโนคาร์บอนให้จัดเรียงตัวในพอลิอิไมด์ การสังเกตด้วยกล้องกำลังขยายสูงพบว่า ที่ความเข้มของสนามสูงสุด (2 เทสลาและ600โวลต์ต่อเซนติเมตร) จะเห็นการเรียงตัวของท่อนาโนคาร์บอนชัดเจนที่สุดและจะลดลงเมื่อความเข้มของสนามไฟฟ้าลดลง การประเมินระดับการจัดเรียงของท่อนาโนคาร์บอนในพอลิอิไมด์ด้วยโพลาไรเซอร์รามานเผยให้เห็นว่า ที่ปริมาณความเข้มของสนามไฟฟ้าเท่ากันระบบที่มีสนามแม่เหล็กร่วมด้วยในทิศทางที่เสริมกันได้ให้ระดับการจัดเรียงของท่อนาโนคาร์บอนสูงที่สุดเนื่องจากเสริมกันของแรงที่เหนี่ยวนำท่อนาโนคาร์บอนให้มีการเรียงตัวจากสนามไฟฟ้าและสนามแม่เหล็ก

ภาควิชา	วิศวกรรมเคมี	ลายมือชื่อนิสิต	
สาขาวิชา	วิศวกรรมเคมี	ลายมือชื่ออ.ที่ปรึกษาวิทยานิพนธ์หลัก	
ปีการศึกษา	2551		

##5070271621: MAJOR CHEMICAL ENGINEERING

KEYWORDS: ALIGNMENT/CARBON NANOTUBES/POLYIMIDE/ELECTRIC FIELD/ MAGNETIC FIELD

NATTHAKARN ROMYEN: ALIGNMENT OF CARBON NANOTUBES IN POLYIMIDE UNDER ELECTRIC AND MAGNETIC FIELD. ADVISOR: ASSOC.PROF.ML.SUPAKANOK THONGYAI, Ph.D., 127 pp.

The carbon black (CB)/polyimide nanocomposite films were investigated as basic information for studying the alignment of carbon nanotubes in polyimide. The efficiently disperse carbon black in polyimide using both of surfactant and ultrasonication was prepared by two step polymerization method, with 4'4-ODA and PMDA is a starting materials. TEM images and UV-vis spectra were evidenced that the appropriate CB to surfactant ratio, which achieve to improve the transparent properties, was 1:2. Dielectric properties of the CB/polyimide nanocomposite films without surfactant increase with increasing the CB loading and decreased as the addition of surfactant. The tensile properties of the CB/polyimide nanocomposite films were improved by surfactant amount up to 1:2 of CB to surfactant ratio and were optimized at 0.5 wt% of CB in composites.

Alignment of carbon natubes in polyimide was performed under the optimize condition of the CB/polyimide nanocomposites. 2 Tesla of magnetic field and various electric field, included 150, 300, 450 and 600 V/cm, were employed to induce the alignment of nanotubes in matrix. Optical microscopy observation indicated that an alignment could clearly be found when field strength is highest and would be decreased when field strength was decreased. Polarizer Raman spectroscopy was used to assess the degree of alignment of nanotubes in polyimide. At the same electric field strength, incorporation of magnetic field will be enhance the level of alignment to be better than only using electric or magnetic field alone. The three forces from electric and magnetic field were displayed important role for improving the degree of alignment in composites.

Department :   Chemical Engineering   Student's Signature : ....

Field of Study : Chemical Engineering   Advisor's Signature : ....

Academic Year : ....2008............

ACKNOWLEDGEMENTS

I would like to express my deeply gratitude to my advisor, Associate Professor Dr. ML. Supakanok Thongyai, Ph.D. to his continuous guidance, enormous number of invaluable discussions, helpful suggestions, warm encouragement and patience to correct my writing. I am grateful to Professor Suttichai Assabumrungrat, Ph.D., Assistant Professor Anongnat Somwangthanaroj, Ph.D., Assistant Professor Bunjerd Jongsomjit Ph.D. and Assistant professor Sirirat Wacharawichanant, D.Eng. for serving as chairman and thesis committees, respectively, whose comments were constructively and especially helpful.

Sincere thanks are made to Mektec Manufacturing Corporation (Thailand) Ltd. for supporting the materials for synthesis polyimide and the characterize equipments, the financial support from the graduate school at Chulalongkorn University, and Department of Chemical Engineering ,Faculty of Engineering Chulalongkorn University.

Sincere thanks to all my friends and all members of the Center of Excellent on Catalysis & Catalytic Reaction Engineering (Petrochemical Engineering Research Laboratory), Department of Chemical Engineering, Chulalongkorn University for their assistance and friendly encouragement.

Finally, I would like to dedicate this thesis to my parents and my families, who generous supported and encouraged me through the year spent on this study.

CONTENTS

LIST OF TABLES

LIST OF FIGURES

CHAPTER I

INTRODUCTION

Nowadays polymers play a very important role in numerous fields of everyday life due to their advantages over conventional materials (e.g. wood, clay, metals) such as lightness, resistance to corrosion, ease of processing, and low cost production. Besides, polymers are easy to handle and have many degrees of freedom for controlling their properties. Further improvement of their performance, including composite fabrication, still remains under intensive investigation. The altering and enhancement of the polymer's properties can occur through doping with various nano-fillers such as metals, semiconductors, organic and inorganic particles and fibers, as well as carbon structures and ceramics [1-4]. Such additives are used in polymers for a variety of reasons, for example: improved processing, density control, optical effects, thermal conductivity, control of the thermal expansion, electrical properties that enable charge dissipation or electromagnetic interference shielding, magnetic properties, flame resistance, and improved mechanical properties, such as hardness, elasticity, and tear resistance [5-7].

The discovery of carbon nanotubes (CNT) opens the door to enhance the properties of polymer composites by adding them to the matrix materials for structural and multifunctional applications. Unique properties of carbon nanotubes (CNT) such as extremely high strength, lightweight, high elasticity, high thermal and air stability, high electric and thermal conductivity, and high aspect ratio offer crucial advantages over other nano-fillers. Therefore, CNT-based composites have attracted great interest due to an increasing technological demand for multifunctional materials with improved mechanical, electrical, and optical performance, complex shapes, and patterns manufactured in an easy way at low costs. However, several fundamental processing challenges as follows must be overcome to enable applicable composites with carbon nanotubes :

- Proper selection of the polymer matrix
- High purity of carbon nanotubes used in the composites
- Uniform dispersion of carbon nanotubes within the polymer matrix during

and after manufacturing process

- Controllable alignment of carbon nanotubes in the composites
- Good interfacial bonding between the nanotubes and polymer matrix in the composites.

First of all, the polymer matrix should be properly chosen before processing of carbon nanotube/polymer composites. Both thermosetting and thermoplastic polymers have been used as matrix materials in carbon nanotube/polymer composites. Polyimides (PI) are a class of polymers that are known for their stability at high temperature, high glass transition temperature, flexibility, excellent thermal stability, favorable dielectric properties, chemical resistance and easy processability, which have widely been found applications in the composite and microelectronics industries [8]. Therefore, CNT/polyimide nanocomposite is of particular interest [9–15]. Regarding the issues of interfacial strength, purity, dispersion and alignment of carbon nanotube, these could be achieved by precisely controlling the manufacturing processes of carbon nanotubes and nanotube/polymer composites.

CNT are highly anisotropic in nature because of their high aspect ratio. It is important to have aligned CNT in the polymer matrix to take advantage of their anisotropic structure and to have improved properties in the direction of the alignment. By aligning the CNT in the polymer matrix, the strength, stiffness, electrical and thermal properties of the composite can be controlled than the randomly CNT in polymer matrix. Numerous alignment techniques have been employed to produce this effect, including fiber spinning with drawing and/or with a rotating collector, shearing, plasma enhanced deposition, electric-induced alignment, and magnetic alignment. However, the studies on the combination effects of electric and magnetic field induced the alignment of CNT in polymer matrix have not been conducted yet.

In this research, the aligned SWNT/PI nanocomposites were performed by simultaneously applied of DC electric and magnetic fields to induce the formation of an aligned structure. Sodium dodecyl sulfate (SDS) as ionic surfactant in presence of ultrasonication was also used to assist homogeneous dispersion of SWNT in polyimide matrix. Different type of filler, the CB/PI nanocomposites were also established in order to compare with the aligned SWNT/PI nanocomposites.

1.1 The Objectives of This Thesis

1.1.1. To efficiently disperse carbon black and carbon nanotubes to in the polyimide matrix by using combination of surfactant and ultrasonication.

1.1.2 To characterize of the carbon black/polyimide nanocomposite films

1.1.3 To effectively align carbon nanotubes in the polyimide using both of electric and magnetic field.

1.1.4 To investigate the degree of alignment of the carbon nanotube/polyimide nanocomposite films.

1.2 The Scope of This Thesis

1.2.1 To synthesize the carbon nanotubes and carbon black/polyimide from 4,4'-oxydianiline(ODA), pyromellitic dianhydride (PMDA) and 4,4′-(Hexafluoro-isopropylidene) diphthalic anhydride (6 FDA).

1.2.2 Synthesize polyimide film by using two-step polymerization method.

1.2.3 Synthesize aligned carbon nanotube/polyimide nanocomposites from SWNT and SWNT-COOH by using a DC electric field and 2 Tesla magnetic fields.

1.2.4 To Characterize carbon nanotubes and carbon black/polyimide nano-composites by using Fourier Transform Infrared Spectroscopy (FT-IR), Fourier Transform Raman Spectroscopy (FT-Raman), Transmission Electron Microscope (TEM), dielectric, conductivity and mechanical properties.

CHAPTER II

THEORY

2.1 Polyimide

Polyimide (sometimes abbreviated PI) is a polymer of imide monomers. Polyimides are step or condensation polymers derived from both aliphatic or aromatic dianhydrides and diamines, or their derivatives, and contain a heterocyclic imide linkage in the repeat unit, as shown in Figure 2.1.
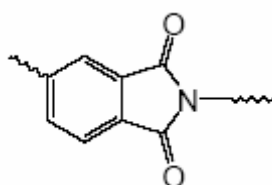
Figure 2.1 A heterocyclic Imide Linkage.

The comparatively rigid structure of polyimides provides high glass transition temperatures (Tg > 300°C) and imparts good mechanical strength and high modulus. The linearity and stiffness of the cyclic backbone allow molecular ordering. This phenomenon results in lower coefficients of thermal expansion (CTE) than those found for thermoplastic polymers having coiled, flexible chains. Additionally, the morphology of long, linear ordered chains provides solvent resistance to the aromatic polyimides.

2.2 Synthesis of Polyimides

2.2.1 One-Step Method Polymerization

2.2.1.1 High-Temperature Solution Polymerization

A single-stage homogeneous solution polymerization technique can be employed for polyimides which are soluble in organic solvents at polymerization temperatures. In this process, a stoichiomeiric mixture of monomers is heated in a high boiling solvent or a mixture of solvents in a temperature range of 140-250°C, where the imidization reaction proceeds rapidly. Commonly used solvents are nitrobenzene, benzonitrile, α-chloronaphthalene, o-dichlorobenzene, trichloro-benzenes and phenolic solvents such as m-cresol and chlorophenols in addition to

dipolar aprotic amide solvents. Toluene is often used as a cosolvent to facilitate the removal of the water of condensation. During polymerization, water is distilled off continually as an azeotrope along with the solvent. Preparation of high-molecular-weight poly(amic acid) is not necessary in this procedure. Imidization still proceeds via amic acid intermediate. However, the concentration of amic acid group is very small at any time during the polymerization because it is unstable at high temperature and rapidly imidizes, or reverts to amine and anhydride. Because water is formed as the result of the imide formation, some of the anhydride groups are rapidly hydrolyzed to o-dicarboxylic acid. When a mixture composed of diamine, dianhydride, and a solvent is heated, a viscous solution is formed at intermediate temperature of 30-100°C. The composition of the product is mainly poly(amic acid). At this stage, phase separation is usually observed in nonpolar solvents such as chlorinated aromatic hydrocarbons. However, on raising the temperature to 120-160°C, a vigorous evolution of water occurs and the reaction mixture suddenly becomes homogeneous. At this stage the product is essentially a low molecular-weight polyimide having o-dicarboxy and amino end groups.

2.2.1.2 Low-Temperature Solution Polymerization

Kim and Moore [16] synthesized a dicyanomethylidene derivative of phthalic anhydride, as shown in Figure 2.2. The compound reacted with aniline in NMP to produce an intermediate of amic acid analog that gradually transformed during 24 h at room temperature to N-phenylphthalimide, co producing malonitrile as condensation byproduct. Subsequently, bis(dicyanomethylidene) derivative of PMDA and ODA were reacted in NMP to afford poly(amic acid) analog intermediate, which underwent partial imidization at room temperature in the homogeneous solution, as illustrated in Figure 2.3.

The extent of imidization reached approximately 75% over 24 h, after which time the polymer began to precipitate. The solid-state imidization of films prepared from the poly(amic acid) analog intermediate behaved similarly to that of poly(amic acid). However, the imidization could be achieved at lower temperature; it was nearly complete at 120°C in 20 h.
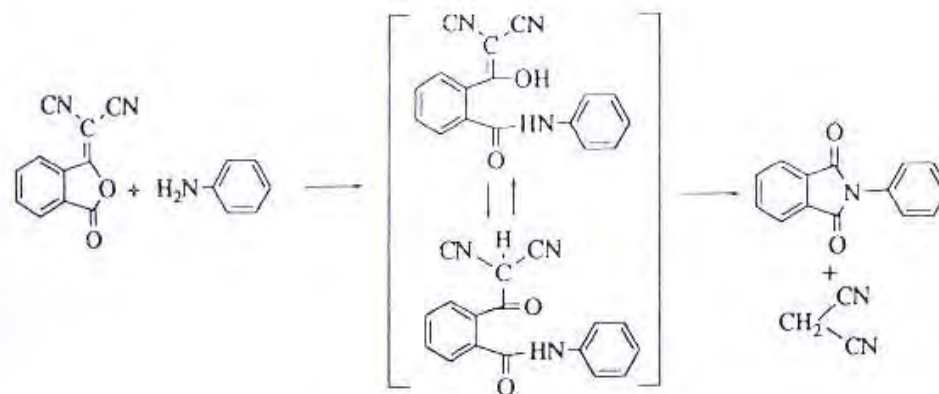
Figure 2.2 Reaction of dicyanomethylidenephthalide with aniline.
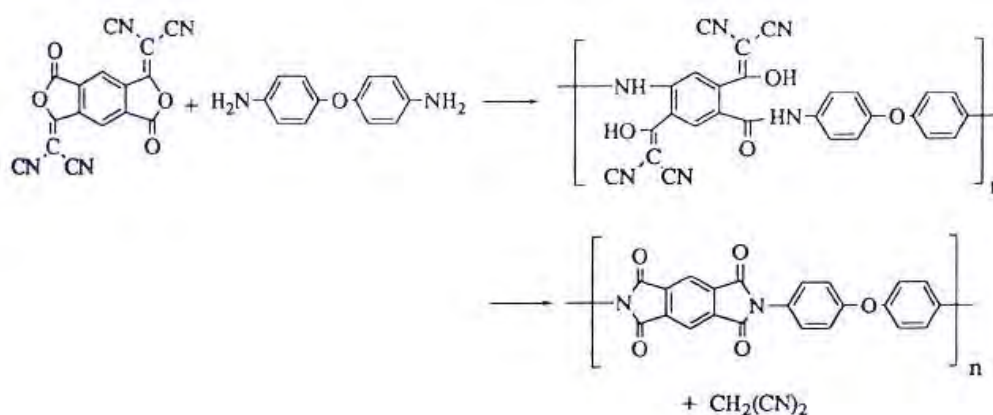
Figure 2.3 Polymerization of bisdicyanomethylidene derivative of PMDA with ODA.

2.2.2 Two-Step Method Polymerization

The majorities of polyimides possess extended rigid planar aromatic and hetero aromatic structures and are infusible and insoluble. The earlier pioneers at Dupont Co. coped with this common problem of intractability generally associated with high-temperature polymers by synthesizing the soluble polymer precursor, namely "poly(amic acid)" and converting it to the final polyimide. Figure 2.4 presents an example of the synthesis of Kapton polyimide. This highly elegant process made it possible to bring the first significant commercial polyimide products into the market namely Du Pont's Kapton[TM] and it is still the method of choice in majority of applications. However, the seemingly simple process involves several elementary reactions interrelated in a complex scheme. In the following sections important parameters that govern these complex interrelations will be discussed in terms of

reaction mechanisms in relation to the chemical and physical natures of monomers and intermediates as well as solvents involved.
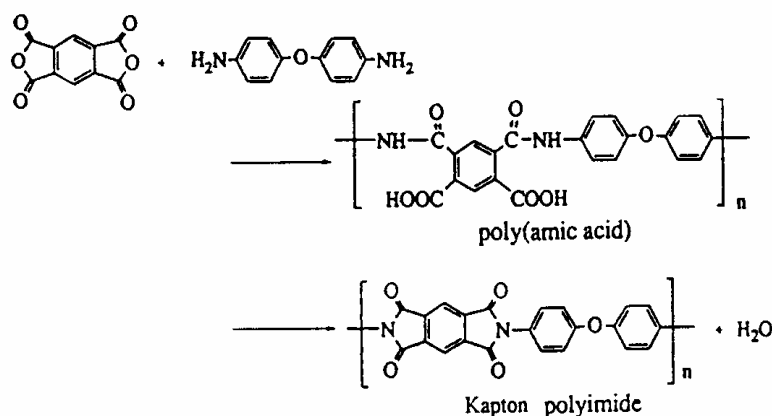
Figure 2.4 Preparation of Kapton polyimide.

2.2.2.1 Formation of Poly(amic acid)s

When a diamine and a dianhydride are added into a dipolar aprotic solvent such as N,N-dimethylacetamide (DMAc), poly(amic acid) is rapidly formed at ambient temperatures. The reaction mechanism involves the nucleophilic attack of the amino group on the carbonyl carbon of the anhydride group, followed by the opening of the anhydride ring to form amic acid group as illustrated in Figure 2.5.

The most important aspect of this process is that it is an equilibrium reaction. Often it appears to be an irreversible reaction because a high-molecular-weight poly (amic acid) is readily formed in most cases as long as pure reagents are used. This is because the forward reaction is much faster than the reverse reaction, often by several orders of magnitude. If the large reaction rate difference is not met, the high-molecular-weight poly(amic acid) can not be formed. Therefore, it is important to examine the driving forces that favor the forward reaction over the reverse reaction. It should also be noted that the acylation reaction of amines is an exothermic reaction and that the equilibrium is favored at lower temperatures. The forward reaction in dipolar solvents is a second-order-reaction and the reverse reaction is a first-order reaction. Therefore, the equilibrium is favored at high monomer concentrations to form higher molecular-weight poly (amic acid).
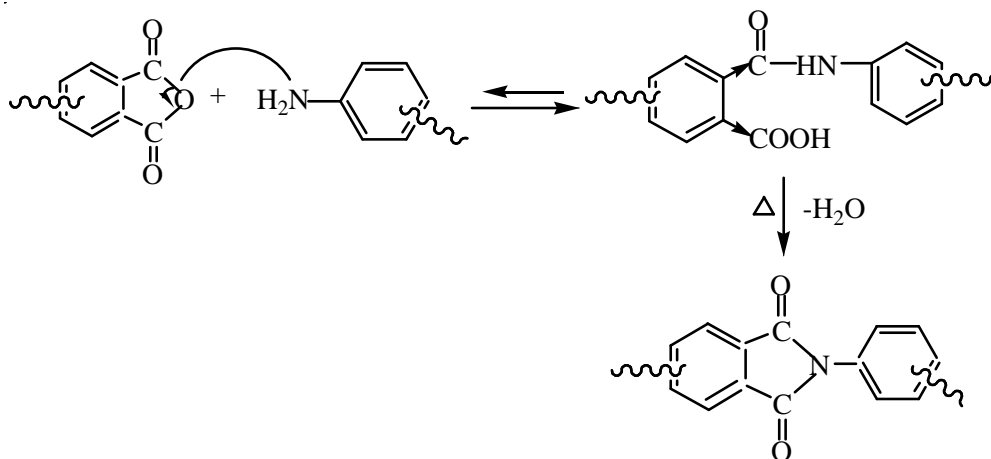
Figure 2.5 Reaction mechanism of imide formation.

2.2.2.2 Effect of Solvents

Solvents used in the formation of poly(amic acid)s play an important role. Most commonly used solvents are dipolar aprotic amide solvents such as N,N-dimethylformamide (DMF), *N,N*-dimethylacetamide (DMAc), N-methylpyrrolidinone (NMP), and tetramethylurea (TMU). Sulfoxides such as dimethylsulfoxide (DMSO) can also be used. However, lesser thermal stability and difficulty in removing it in the following imidization process argue against its use. One of the important properties of these solvents is the basicity (Lewis' base). It is interesting and worthy to note that the starting reagents are weakly basic aromatic amine and nonprotic anhydride, and yet the product is a strong protic acid. In other words, the starting mixture is basic and the product is an acid. The orthoamic acid is a relatively strong carboxylic acid because of the electron-withdrawing effect of the orthoamide group and the stabilization by internal hydrogen bonding of dissociated carboxylate with amide hydrogen. The strong acid-base interaction between the amic acid and the amide solvent is a major source of exothermicity of the reaction and one of the most important driving forces. Therefore, it is expected that the rate of poly(amic acid) formation is generally faster in more basic and more polar solvents. The rate of reaction measured for phthalic anhydride and 4-phenoxyaniline increased with solvent in the order of tetrahydrofuran (THF) < acetonitrile < DMAc (Table 2.1) [17].

Table 2.1 Rates of amic acid formation at 30°C and effects of solvents.

Anhydrides	Solvents	k_1 (1/mol·s)	k_2 (1/mol·s^2)
Phthalic anhydride	DMAc	0.0850	–
	Acetonitrile	0.00102	33.63
	THF	0.000387	7.17
	m-Cresol	0.685	7.34
Tetrahydrophthalic anhydride	DMAc	0.000583	0.0378
	Acetonitrile	0.00750	0.116
	THF	0.158	2.16
	m-Cresol	0.0412	7.92

k_1, rate constant of second-order reaction; k_{-1}, rate constant of reverse reaction;

k_2, rate constant of autocatalytic reaction.

2.2.2.3 Thermal Imidization of Poly(amic acid)s

The intermediate poly(amic acid) is usually converted to the final polyimide by the thermal imidization route. This process is especially useful when the final product is desired as a film or a coating form. Films are firstly cast on a substrate and then undertaken through a thermal cycle with temperatures ranging from 100°C to 350°C. There has been considerable debate in the literature regarding the exact thermal cycle to be utilized for achieving close to 100% imidization of the poly(amic acid). While the types of thermal cycles utilized are many, they can essentially be divided into two different types

1) Heating gradually to 250°C-350°C, depending on the stability and Tg of the polyimide.

2) Heating the poly(amic acid) mixture to 100°C and holding for one hour, heating from 100°C to 200°C and holding for one hour, heating from 200°C to 300°C and holding for one hour and slow cooling to room temperature from 300°C.
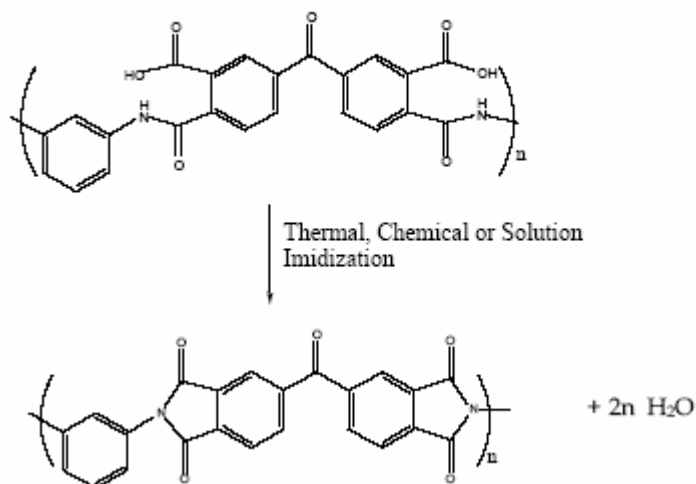
Figure 2.6 Three common routes to facilitate the conversion of Polyamide acid to Polyimides.
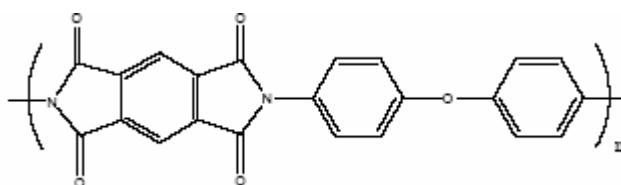
Figure 2.7 The repeat unit of Kapton-H formed from PMDA and ODA.

However, irrespective of the type of thermal cycle utilized, it is important to recognize that there are several complicating factors involved in these seemingly simple thermal imidization processes, which finally determine the degree of imidization of the polyimide product. It needs to be emphasized that the imidization reactions take place in a very concentrated viscous solution (during initial and intermediate stages) and the presence of residual solvent plays a very important role during imidization at the later stages of the reaction. In this regard, the imidization proceeds faster in the presence of dipolar amide solvents due to several reasons, some of which are;

1) Specific solvation allows the favorable conformation of the amic acid groups to cyclize.
2) Plasticizing effect of the solvent to increase the mobility of the reacting functional groups.

3) The basicity of the amide solvent allows it to accept protons and may be responsible for the specific effect.

A simple kinetic expression for the imidization reaction is often not possible as the overall process involves several interrelated elementary reactions which dynamically changed physical properties such as diffusion rate, chain mobility, solvation and acidity. The rate of imidization is usually faster during the initial stages due to the presence of solvent and shorter chain sizes resulting in increased chain mobility. However, during the later stages of the reaction the rate tapers off due to primarily the reasons listed below:

1) Loss of residual solvent which occurs due to the extended heating.
2) The Tg of the polymer increases as the degree of imidization reaction proceeds and as the Tg approaches the reaction temperature, the imidization rate slows down markedly due to the decreased chain mobility.

Lastly, the rate of imidization may be dependent upon the availability of suitable conformations for the amic acid group to decyclohydrate in to an imide. The slower rate of imidization during the later stages of imidization is attributed to unfavorable conformations, which have to rearrange to favorable conformations before imidization can take place. Such a conformational rearrangement is only possible if the rotation of the adjoining polymer chain and strongly bound solvent molecules takes place.

2.2.2.4 Mechanism of Chemical Imidization

The kinetic study of model compounds revealed that isoimides and imides are formed via a mixed-anhydride intermediate (7), which is formed by acylation of the carboxylic group of amic acid (6), as illustrated in Figure 2.8. The presence of the intermediate mixed-anhydride was detected by IR as well as proton nuclear magnetic resonance (NMR). Convincing evidence was also presented when di- functional acid chloride such as sebacoyl chloride was used instead of acetyl chloride for cyclization of poly(amic acid). The solution viscosity temporarily increased during the reaction because of the interchain mixed-anhydnide formation. The viscosity gradually

decreased back to the normal level as the cyclization proceeded. Imides are formed by intramolecular nucleophilic substitution at the anhydride carbonyl by the amide nitrogen atom *(8a-9a)*, while isoimides are formed as a result of substitution by the amide oxygen *(8b-9b)*. The cyclization of N-phenylphthalamic acids with acetic anhydride proceeds smoothly at room temperature in DMAc in the presence of a tertiary amine. The amine acts as a catalyst as well as an acid acceptor. Use of a less than stoichiometric amount of amine still leads to completion of the reaction, only at a slower rate. Use of triethylamine (pk_a 10.6) as a catalyst produced exclusively normal imides. However, a mixture of imide and isoimide was formed when less basic pyridine (pk_a 5.2) was used as a catalyst.
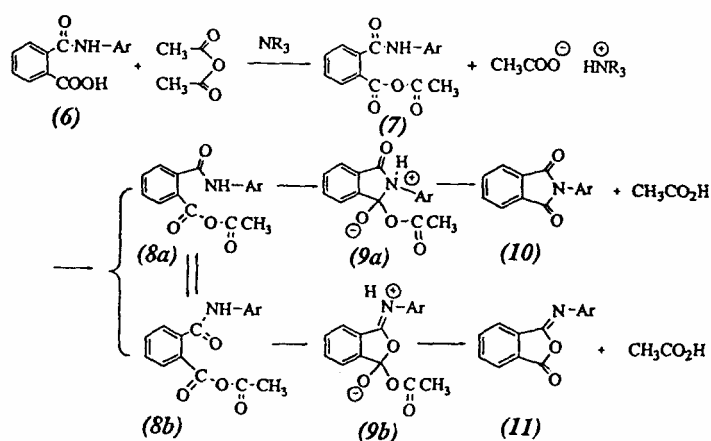
Figure 2.8 Mechanism involved in chemical dehydration of amic acid. R, ethyl; Ar, phenyl.

2.3 Carbon nanotube

2.3.1 Carbon Nanotube Fundamentals

Iijima. S first observed carbon nanotubes while studying another class of macromolecules called fullerenes in 1991. Carbon Nanotubes are made up of graphene molecules. They are composed only of four carbon atoms arranged in a three- dimensional cage like structure. Carbon nanotubes are fullerenes, which are extended in one dimension with a high aspect ratio, acquiring a cylindrical structure. Although graphite and diamond are also composed of only carbon atoms, the properties of carbon nanotubes vary due to their unique atomic arrangement. The geometry of a single walled nanotube structure can be best described as one layer of
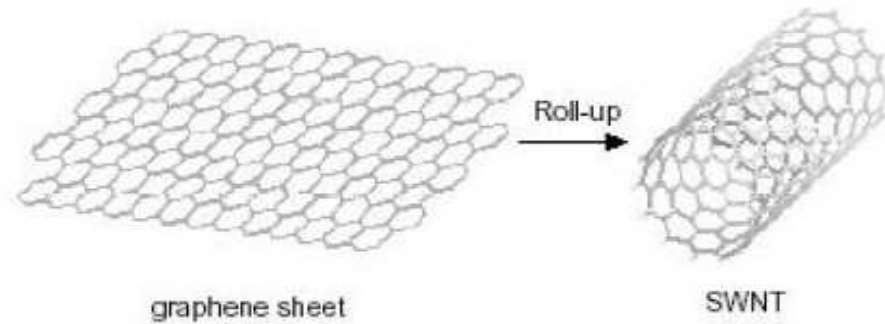
Figure 2.9 Structure of a Carbon Nanotube.

grapheme rolled in a seamless cylinder with an average diameter of 1-2 nm as illustrated in Figure 2.9. There are two main types of carbon nanotubes that can have high structural perfection, as single-walled carbon nanotubes and multiwalled carbon nanotubes.

- Singlewall carbon nanotubes (SWNT) are hollow single cylinders of a graphene sheet, which are defined by their diameter and their chirality. The diameter of SWNT varies from 0.5 to 5 nm. Depending on the chirality, SWNT may either be metallic or semiconducting.

- Multiwall carbon nanotubes (MWNT) are a group of concentric SWNT often capped at both ends, with diameters in the range from several nanometers up to 200 nm. These concentric nanotubes are held together by van der Waals bonding. MWNT form complex systems with different wall numbers, structures, and properties, a photo of MWNT underneath a microscope shown in Figure 2.11.

Figures of SWNT and MWNT are shown in Figure 2.10(a) and Figure 2.10(b). Single-walled carbon nanotubes tend to be stronger and more flexible than their multi-walled counterparts. One reason multiwalled carbon nanotubes are weaker, is because the individual cylinders slide inside one another. Single-walled carbon nanotubes are also better electrical conductors and are more transparent. However, their production is difficult and they are challenging to purify. Single-walled carbon nanotubes are also more expensive to make and this may not change until there is a large-scale market for Single-walled carbon nanotubes. Currently, multiwalled carbon nanotubes are

more widely used in composite materials than Single-walled carbon nanotubes for these reasons.

(a)   (b)
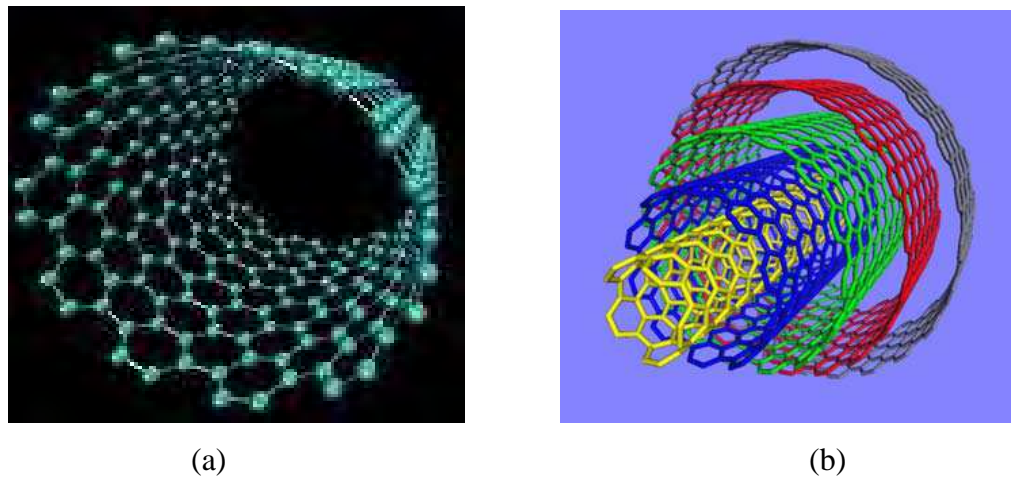
Figure 2.10 (a) Image of SWNT with one tube, (b) image of MWNT with concentric tubes.
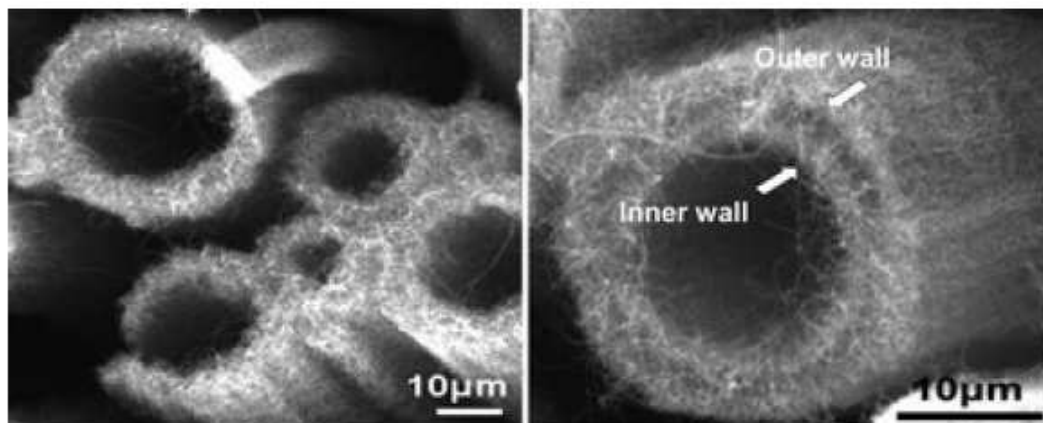
Figure 2.11 Multi-walled carbon nanotubes underneath a microscope.

The properties of CNT depend on chirality, diameter and length of the tubes. Chirality is defined by the symmetry and the chiral angle formed between the carbon bonds. The graphene sheet can be rolled up with varying degrees of twist along its length resulting in CNT having a variety of chiral structures. The atomic structure of CNT is described in terms of the tube chirality, or helicity, which is defined by the chiral vector Ch and the chiral angle θ which is shown in Figure 2.12. The chiral vector is Ch= na1 + ma2, where the integers (n,m) are the number of steps along the

zig-zag carbon bonds of the hexagonal lattice and a1 and a2 are unit vectors whose lengths are equal to √3 dc-c with dc-c indicating the C-C bond length.
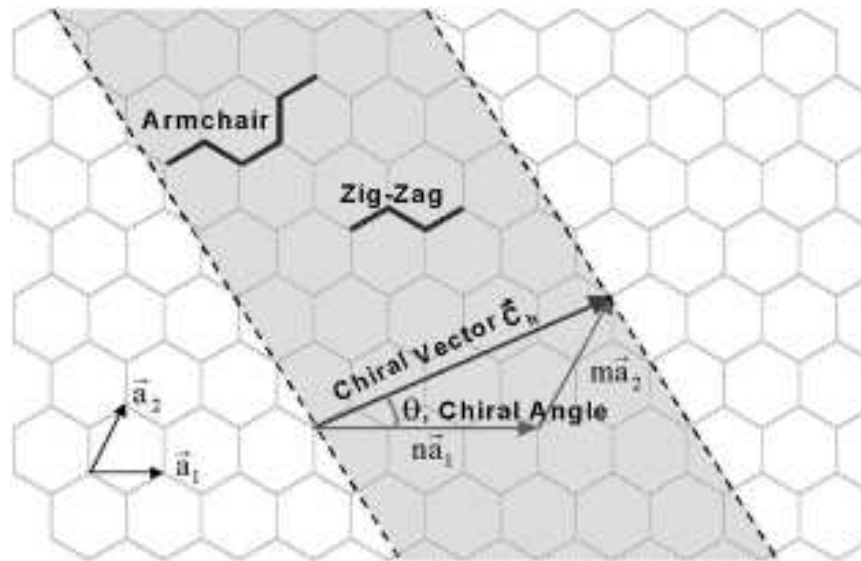
Figure 2.12 Chiral vector and chiral angle explained on a graphene sheet [18].

The different pairs of integers (n,m) define a different way of rolling the graphene sheet to form a CNT. The diameter D of tube (n,m) and the chiral angle θ with equal dc-c are given by

$$D = \frac{\sqrt{3d_{c-c}}}{\Pi} \cdot \sqrt{n^2 + nm + m^2} \quad \text{and} \quad \theta = arccos \ \frac{2n + m}{2\sqrt{n^2 + nm + m^2}}.$$

Armchair CNT are formed when n=m and the chiral angle is 30°. In zig-zag CNT, n or m = 0 and θ = 0°. All other chiral CNTs have chiral angles between 0° and 30° (as shown in Figure 2.13). Depending on the tube chirality the electrical properties of the CNT differ; they can be metallic or semiconducting. When n-m=3p, where p is an integer, the CNT are metallic and when n-m≠3p, the CNT are semiconducting.

2.3.2 Carbon nanotube properties

Carbon nanotubes have properties unlike any other substance on earth of which we currently know. Even though carbon nanotubes are made out of graphite carbon, they have different properties than bulk graphite because of their size, shape, and crystallography. While carbon nanotubes may have the potential for being the

next supermaterial for our society, actually utilizing all of their mechanical, thermal, and electrical properties is still an unsolved challenge.
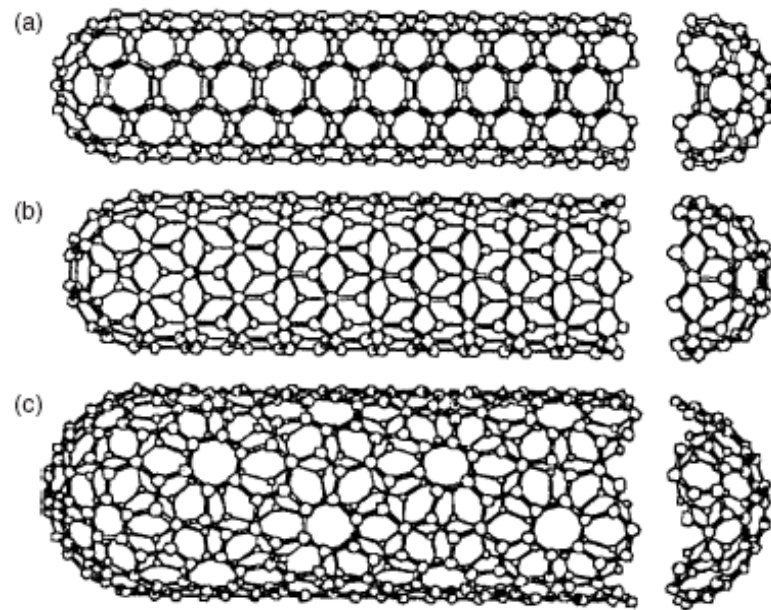
Figure 2.13 Classification of carbon nanotubes: (a) armchair, (b) zigzag, and (c) chiral nanotubes [19].

2.3.2.1 Mechanical properties

The structural properties of CNT with strong σ bonds between the carbon atoms give nanotubes a very high Young's modulus and tensile strength. The strength of the carbon carbon bonds in-plane, along the cylinder axis, retains the structure exceptionally strong resistance to any failure. CNT also have very good elasto-mechanical properties. The two dimensional (2D) arrangement of the carbon atoms in a graphene sheet permits a large out-of-plane distortion. Both experimental and theoretical investigations show extraordinary mechanical properties of individual MWNT with Young's modulus being over 1 TPa and a tensile strength of 10 - 200 GPa [20-22], which is several hundred times more than that of steel, while they are only one-sixth as heavy. The elastic response of a nanotube to deformation is also remarkable: CNT can sustain up to 15 % tensile strain before fracture. Nanotubes are shown to be very flexible, with the reversible bending up to angles of 110º for both SWNT and MWNT [23]. Due to the extremely high strength of CNT, they can bend

without breaking. All of these properties open up broad possibilities for the use of CNT as lightweight, highly elastic, and very strong composite fillers.

2.3.2.2 Electrical properties

Carbon nanotubes have the unique ability to be insulators, semiconductors, or conductors, depending on the way the carbon atoms are arranged. Carbon nanotubes can have an electrical conductivity up to 1000 times that of copper. If the carbon atoms in the carbon nanotubes are arranged a certain way, they can be almost perfect conductors along their axial direction (almost no electrical resistance) at temperatures close to absolute freezing (-273 °C), which is very rare. Given their high thermal conductivity, tolerance for high current density, and sharp tips, carbon nanotubes are the best field emitters of any material, meaning they are ideal for flat panel displays, such as the ones on tvs, phones, or computers. Single-walled carbon nanotubes can also carry the highest current density of any known material, measured as high as 109 amps/cm^2.

2.3.2.3 Chemical properties

Functionalization of the carbon nanotubes (chemical or physical modification of the surface of CNT, e.g. by the attachment of certain molecules or functional groups) is a very important issue in order to overcome their poor solubility in solvents. Functionalized CNT are very attractive for chemical and biological applications because of their strong sensitivity to chemical or environmental interactions. This leads to a broad range of applications, e.g. as sensors. Covalent and non-covalent functionalization, doping, decoration with organic as well as inorganic species of the surface of CNT lead to direct changes of the properties of carbon nanotubes (optical, electrical, and mechanical).

2.3.2.4 Themal properties

The thermal conductivity of carbon nanotubes is very high in the axial direction and very low in the lateral direction, which makes them a subject of great interest. Thermal conductivity, along the axial direction, has been found to be at least double that of diamond (1000: 3000 W/m·K) and diamond has the highest thermal conductivity of any substance we know of today.

Table 2.2 shows theoretical and experimental properties of carbon nanotubes. From Table 2.2, it is clear that CNT have unique mechanical, electrical, magnetic, optical and thermal properties. In some special applications, such as space explorations, high-performance lightweight structural materials are required, and they can be developed by adding CNT to polymers or other matrix materials.

Table 2.2 Theoretical and experimental properties of carbon nanotubes [24-25].

Property	CNTs	Graphite
Specific gravity	0.8 g/cm^3 for SWCNT; 1.8 g/cm^3 for MWCNT (theoretical)	2.26 g/cm^3
Elastic modulus	$\sim$1 TPa for SWCNT; $\sim$0.3–1 TPa for MWCNT	1 TPa (in-plane)
Strength	50–500 GPa for SWCNT; 10–60 GPa for MWCNT	
Resistivity	5–50 $\mu\Omega$ cm	50 $\mu\Omega$ cm (in-plane)
Thermal conductivity	3000 W m^{-1} K^{-1} (theoretical)	3000 W m^{-1} K^{-1} (in-plane), 6 W m^{-1} K^{-1} (c-axis)
Magnetic susceptibility	22 $\times$ 10^6 EMU/g (perpendicular with plane), 0.5 $\times$ 10^6 EMU/g (parallel with plane)	
Thermal expansion	Negligible (theoretical)	-1×10^{-6} K^{-1} (in-plane), 29 $\times$ 10^{-6} K^{-1} (c-axis)
Thermal stability	>700 °C (in air); 2800 °C (in vacuum)	450–650 °C (in air)
Specific surface area	10–20 m^2/g	

Moreover, although graphite is a semi-metal, CNT can be either metallic or semi-conducting due to the topological defects from the fullerene-like end caps in CNT (pentagons in a hexagonal lattice). Thus, the physico-mechanical properties of CNT are dependent upon their dimensions, helicity or chirality.

2.3.3 Carbon nanotube synthesis

There are many different methods and variations for producing carbon nanotubes, but this section will only cover the three principal methods for carbon nanotube synthesis: chemical vapor deposition (CVD), arc discharge, laser ablation, and High pressure conversion of carbon monoxide (HiPCO). There are continual improvements in each of the methods in an effort to produce more nanotubes quicker, and for a lower cost.

- Chemical vapor deposition (CVD): This technique involves the decomposition of hydrocarbon gases on the substrate in the presence of metal catalyst particles (Fe, Ni, Co). The synthesis of CNT is often thermally or plasma-enhanced. MWNT are mainly obtained by this method, with high purity but

with limited control of the structure and diameter. Long nanotubes with diameters ranging from 0.6 - 4 nm (SWNT) and 10 - 200 nm (MWNT) can be produced. The CVD technique is suitable for a large-scale industrial production of nanotubes. If plasma is generated by the application of a strong electric field during the growth process (plasma enhanced CVD), then the nanotube growth will follow the direction of the electric field forming vertically aligned carbon nanotubes (e.g. perpendicular to the substrate).

- Arc discharge method: This base on an electric arc discharge generated between two graphite electrodes under an inert gas atmosphere (argon, helium). This method requires very high temperatures (>5000 ^{o}C) and produces a mixture of different components (including fullerenes, amorphous carbon, and some graphite sheets). The carbon nanotubes need to be separated from the soot and the catalytic metals present in the crude product. Depending on the variation of the parameters (e.g. temperature, pressure, different gases and catalytic metals) employed in this technique, it is possible to selectively grow SWNT or MWNT. CNT produced this way are normally tangled with poor control over the length and diameter. CNT are short with diameters ranging from 1.2 - 1.4 nm (SWNT) and 1 - 3 nm (MWNT).

- Laser ablation: A graphite target is vaporized by laser irradiation under flowing inert gas atmosphere at high temperature. Nanotubes produced in this way are very pure but the process is not effective for a large scale synthesis. Only bundles of individual SWNT of 5 - 10 μm in length and 1 - 2 nm in diameter are being fabricated in this way.

- High pressure conversion of carbon monoxide (HiPCO): This method is considered as an improved CVD process which bases on the gas-phase growth of single wall carbon nanotubes with carbon monoxide as a carbon source at high temperature and pressure. This technique is suitable for the production of large quantities of SWNT with high purity.

All of these methods are still under development; there are numerous variations of these techniques operating under different conditions, with different set-ups, and process parameters. Every technique provides diverse advantages and disadvantages over the quality and kinds of synthesized CNT. An overview of these techniques is given in Table 2.3. Nowadays, the main issue concerns the large-scale and low-cost production of nanotubes for industrial applications.

Table 2.3 An overview on the most common CNTs synthesis techniques and their advantages and disadvantages.

Method	CVD	Arc Discharge	Laser Ablation	HiPCO
Basics	Decomposition of hydrocarbon gases in the presence of metal catalyst particles	Electric arc discharge generated between two graphite electrodes under an innert atmosphere (argon, helium)	Graphite target is vaporized by laser irradiation under flowing innert atmosphere and high temperature	Gas-phase growth of singlewall carbon nanotubes with carbon monoxide as a carbon source at high temperature and pressure
SWNT	long, 0.6 - 4 nm diameter	short, 1.2 - 1.4 nm diameter	long, 1-2 nm diameter	~0.7 nm diameter, various lengths
MWNT	long, 10-200 nm diameter	short, 1-3 nm diameter	not applicable but possible	not applicable
Yield	up to 100 %	up to 90%	up to 65 %	up to 70 %
Advantages	high purity, large scale production, simple	easy, defect-free nanotubes, no catalyst	high purity, defect free SWNTs	large scale, high purity
Disadvantages	limited control over the structures, defects	short, tangled nanotubes, random structures	expensive, low scale production	defects

2.3.4 Dispersion Techniques

The practical applications of CNT composites have so far been largely limited by their poor processibility. The intrinsic van der Walls attraction among the tubes in combination with their high surface area and high aspect ratio often leads to significant agglomeration of CNT. The surface of CNT is also non reactive which makes it difficult in achieving efficient dispersion, as they mix and blend with the host matrix. To effectively use CNT as intrinsic reinforcements in composite structures and ensure a good stress transfer between CNT and the polymer matrix, uniform dispersion within the polymer matrix and improved nanotube/matrix wetting and adhesion are critical. Different methods have been used to efficiently disperse the CNT in polymer matrices.

Dispersion broadly falls into two main categories; mechanical/physical methods and chemical methods. The mechanical techniques involve physically separating out the tubes from each other, but can also fragment the tubes and decrease their aspect ratio. Chemical methods often use surfactant or chemical functionalization of the tube surface, which in turn can affect surface energies as well as wetting and/or adhesion characteristics, leading to prevention of aggregation and/or re-aggregation. However, certain types of aggressive chemical treatment can lead to the key nanotube properties being compromised.

2.3.4.1 Physical Methods of Dispersion

To physically separate tubes that are bundled together, and tightly held by van der Waals forces, requires a mechanical force as opposed to a force arising from chemical potentials between different species. To this end, three main mechanical processes have been partially successful in dispersing tubes in various media: ultrasonication, milling, and shear mixing.

(a) Ultrasonication

This is a rather ubiquitous technique. However, overexposure to ultra-sonication is known to lead to tube rupture, which may have negative consequences for the polymer–nanotube composite properties. Clearly, due care is required with all mechanical processes. For ultrasonication, the nanotube specimens are first mixed with a solvent and then placed into an ultrasonic regime. Two main instruments are used:
- Ultrasonic bath
- Ultrasonic horn/tip

The ultrasonic process delivers high levels of vibrational energy to the system and is thought to create expansion and peeling/fractionation of the graphene layers making up the multi walled tube. The process starts from the outside and works its way in, with each layer fractionating independently from preceding and subsequent layers. So the process has the potential to make the tube thinner as well as shorter.

The ultrasonic process has three particular mechanisms: bubble nucleation and subsequent implosion (cavitation), localized heating, and the formation of free radicals. It is the cavitation mechanism that causes much of the dispersion but also

much of the tube damage. Low frequencies (20 kHz) produce larger bubbles, which lead to a larger energy distribution as they collapse. Increasing the frequency leads to lower energy dissipation as the bubble radius is smaller and cavitation is thus reduced. When an ultrasonic horn is used, the mechanical tip oscillates, normally at lower frequencies than for a bath, leading to high-energy cavity formation (which can result in rapid sample heating if due care is not taken). In this case the dispersive energy is very high and localized around the oscillating tip. Prolonged exposure to such techniques is not recommended. An ultrasonic bath works in much the same way except that the cavitation zone is not well-defined and the frequencies of oscillation are normally higher (~40–50 kHz). The dispersive energy is lower than that for an ultrasonic horn.

The use of an ultrasonic horn leads to the formation of a conical field of high energy around the oscillating tip. Solvent within this "dispersion zone" experiences fierce cavitation (mentioned above) which in turn induces a flow that moves material away from the tip which then recirculates inside the conical field again. The size of the dispersion zone depends on a number of factors, including solvent properties, mixture phase viscosity, and the geometry of the system. However, it is *wrong* to think that by increasing the viscosity of the solvent, overall dispersion would be linearly improved due to higher stress transmission. It is an attractive idea, since many monomer solvents could then have purified nanotubes directly added to them so that the ultrasonic regime would disperse them directly in the monomer before the final polymerized matrix is formed. A higher viscosity solvent, in addition to the beneficial higher levels of shear energy in the matrix, also may result in poor recirculation of the material only a local region within the mixture will be well dispersed. Overall, beyond a certain optimum viscosity, the dispersion quality is reduced as solvent viscosity is increased. The optimum viscosity at which to operate the ultrasonic tip is (at this time) a matter of experimentation. The exact value will vary for different systems and will be a function of container and tip geometry as well as the operating frequency applied.

(b) Milling and Grinding

This method uses a rotating cylinder (or several, such as in the 4-mill mixer) filled with grinding media such as iron balls to wear down the aggregated tubes. Ball-

milling can be used to break up multi-walled nanotube aggregates and reduce nanotube length and diameter distributions. There is also good evidence in the literature that the ball-milling technique is among the most destructive toward nanotubes and produces a large amount of amorphous carbon. At a laboratory scale it is not a favored route toward dispersion because of the difficulty in controlling amorphous particle build-up. However, industrial scale dispersion techniques might employ ball milling of a polymer–nanotube viscous fluid as a "cheap-and-fast" physical dispersion alternative, given the right criteria. On a laboratory scale, a gentler route to break up large nanotube aggregates is to use the traditional mortar and pestle before more aggressive physical or chemical treatments are employed.

(c) Shear Mixing

High-shear mixing is another dispersive option with which nanotube aggregates can be mechanically forced apart in a viscous monomer or polymer solvent. A relatively high-shear regime needs to be applied. The benefits of this technique are clear:

- Direct dispersion into the host matrix
- No chemical modification is required
- Nanotubes are prevented from re-aggregation by viscous forces

However, this technique is only applicable to MWNT as the physics behind SWNT entwined aggregates is different and requires more careful treatment. Additionally, shear flow dispersion is limited to viscous fluids within a finite range of viscosities between, say, $\eta \sim 10^{-3}$ and 20 Pa. If the viscosity is too low, separated aggregates are able to overcome viscous forces and re-aggregate, driven by their attractive van der Waals potentials. If the viscosity is too high, dispersive mixing is not efficient and greatly impeded. There are indications of successful application of melt-mixing for SWNT, but this will inevitably only disperse large aggregates and not solve the inter-tube tapestry formed between single tubes.

2.3.4.2 Chemical Methods of Dispersion

There has thus been much interest in mastering chemical functionalization of the nanotube surface to make the tubes more soluble and/or separable in a given

solvent. A chemical route toward dispersion would be scalable by default. It would also ensure homogeneous dispersion throughout the solvent and thus a host matrix, giving much technical flexibility to polymer-nanotube composite manufacture. Two general classes of chemical dispersion methods are considered covalent and non-covalent.

(a) Covalent Methods

Covalent methods refer to functionalization treatments involving covalent bond breakage across the nanotube surface, which disrupts the delocalized π-electrons and σ-bonds, and hence incorporate other species across the exterior of the shell. The mechanisms may preferentially occur at defect sites (Figure 2.14), or where tube curvature is highest, i.e., tube-ends. A functionalized tube is more soluble in organic solvents, hence spectroscopic characterization in the liquid phase is much more amenable. It is the sidewalls of a nanotube that tend to experience chemical attack during oxidative work-up (Figure 2.14(a)).
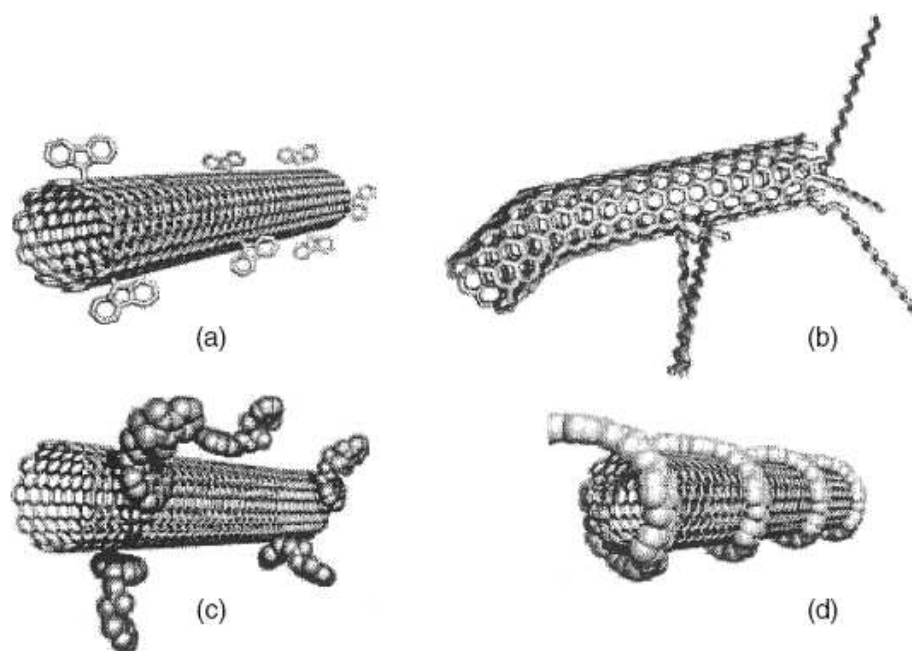
Figure 2.14 Chemical methods for dispersing nanotubes: (a) Covalent sidewall functionalization, (b) defect group functionalization, (c) noncovalent exohedral functionalization with surfactants, (d) noncovalent exohedral functionalization with polymers [26].

A classical example of nanotube treatment is by refluxing in 2.6-M nitric acid. The acidic attack forms defect sites which are in turn saturated with –COOH groups. These side groups are what functionalizes the tube and makes it more receptive to further treatments, such as attachment of long alkyl chains via amide formation. Covalently attaching alkene groups to nanotubes has been shown to increase solubility in organic solvents such as tetrahydrofuran (THF), chloroform, methylene chloride and dimethylformamide (DMF).

(b) Non-Covalent Methods

Non-covalent functionalization generally involves the use of surfactant to bind ionically to the nanotube surface and prevent the tubes aggregating (Figure 2.14(c)). This can be a much less destructive route toward dispersion than covalent bonding/acidic boiling. Surface active molecules such as sodium dodecylsulfate (SDS) or benzylalkonium chloride have proven successful in dispersing nanotubes into an aqueous phase. The mechanism is thought to involve the nanotubes residing in the hydrophobic interiors of the micelles. If the hydrophobic region of the amphiphile contains an aromatic group, π-π stacking interactions occur with the nanotube sidewalls. Interestingly, they went on to show that parts of the amphiphile can be substituted with amino groups from proteins causing immobilization of the biopolymers a useful development in biosensor research.

Non-surfactant-mediated dispersion has been carried out using anilines, amines, and, more recently, DNA, to name just a few. For anilines and amines interacting with nanotubes, it is thought that donor-acceptor complexes are formed. Strong curvature of the tubes imparts acceptor character to the corresponding macromolecular carbon networks.

Supramolecular complexes can also be formed between SWNT and certain polymers. The polymer wraps around the tube when in solvent, leading to a stable dispersion of the polymer–nanotube complex (Figure 2.14(d)). A number of polymers can be used so long as they have a suitably polar side-chain. Some of these nanotube–polymer complexes have shown liquid crystalline behavior. However, a word of caution is warranted here. Using surfactant-and/or non-surfactant mediated techniques alone is not always a successful affair, because coating of individual tubes is much

harder than it seems. Many groups reported successes in dispersing SWNT but in truth only managed to separate out the bundles and not the individual tubes themselves, resulting only in partial exfoliation. This remark applies to both the covalent and non-covalent methods. The techniques are more successfully applied to MWNT, but, even then, attempts at coating the tubes can sometimes backfire, with aggregates being coated instead, and making it even more difficult to disperse the tubes. Indeed, there appears to be a limit to the percentage of tubes, at around 1%, that are possible to be dispersed in solvent using surfactants. Consideration must also be given to the polymers and surfactant adsorbed onto the nanotube surface and their possibly reduced compatibility with the host matrix in a composite.

2.3.5 Nanotube Alignment

CNT are highly anisotropic in nature because of their high aspect ratio. It is important to have aligned CNT in the polymer matrix to take advantage of their anisotropic structure and to have improved properties in the direction of the alignment. By aligning the CNT in the polymer matrix, the strength, stiffness, electrical and thermal properties of the composite can be controlled. The requirement for anisotropic properties at the nanometer-level highlights the driving motivation and significant contribution made by the polymer–nanotube composite field to the wider nanoscience community. Control and manipulation of nanometer-sized objects to affect macroscopic properties is at the very heart of modern nanotechnology. With this in mind, control over orientation of nanotubes in a matrix is of significant importance in tailoring the composite's performance. The specific examples of the critical role, that the orientation order of nanotubes plays in the macroscopic properties of nanocomposites, for instance leading to a complete reversal in the material behavior.

Electric and magnetic fields can be used to induce tube alignment, due to the very high anisotropy of their polarizability. This anisotropy originates from the delocalized π-electrons along the nanotube axis, thus producing a substantial dielectric torque when they are exposed to an external field. In the presence of an electric field $\bar{E}$, each conductive nanotube experiences a polarisation P. This polarisation can be divided into two contributing components, i.e. one parallel to the tube axis $P_{//}$ and one in the radial direction $P_{\perp}$. The magnitude of both components

depends on the polarisability tensor of the nanotube. For single-wall carbon nanotubes, it has already been suggested that the static polarisability in the direction of the tube axis is much larger than across the diameter. To a first approximation a similar behaviour might be expected for multi-wall carbon nanotubes exposed to low-frequency electric fields. This polarisation leads to a torque N_E acting on the nanotube. Under the given conditions, this torque aligns the nanotube against the viscous drag of the surrounding medium in the direction of the electric field. A comparable behaviour has already been observed for multi-wall carbon nanotubes in different solvents [27, 28]. An illustration of the behaviour of a cylindrical particle exposed to a homogeneous electric field is given in Figure 2.15. Apart from this rotation and alignment, the behaviour of a carbon nanotube depends on the type of the applied electric field and its surface charge. In case of a DC field, charged carbon nanotubes move according to their electrophoretic mobility μ [29], where

$$\mu = \frac{v}{E} = \frac{\varepsilon \zeta}{\eta},$$

towards the electrode with the opposite sign, where they discharge. Here, ε is the dielectric constant and η the viscosity of the epoxy resin, respectively, and ζ is the zeta potential of the carbon nanotube, which is a measure of the surface charge [29]. In case of an AC field, the net electrophoretic mobility due to the zeta potential equals zero. However, aligned metallic carbon nanotubes cause inhomogeneities in the electric field, as shown schematically in Figure 2.16.
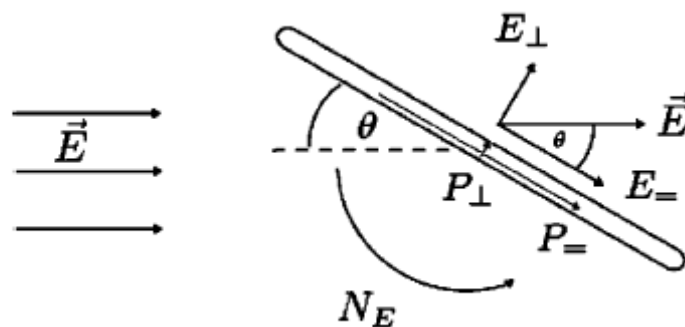
Figure 2.15 Schematic illustration of a polarised cylindrical particle in an electric field.

One effect is a Coulombic attraction between oppositely charged ends of the nanotubes. In addition, the non-uniform electric field in the vicinity of the nanotube tips results in the movement of induced dipoles towards the area with the highest field strength, a behaviour which is called dielectrophoresis. This effect can also induce nanotube movement towards the electrode for those nanotubes in close proximity to the electrodes.

Magnetic fields have recently shown promise in encouraging nanotube alignment along specific directions. Theory suggests that carbon nanotubes should have anisotropic magnetic susceptibility. Metallic tubes are calculated to be paramagnetic in the direction of their long axis. Paramagnetic character causes such tubes to align parallelly to the applied field. All other nanotube variations are thought to be diamagnetic. The diamagnetic susceptibility is most negative in the direction perpendicular to the tube axis, causing tubes with these chiralities to also align parallelly to the magnetic field. Interestingly, the alignment energy is proportional to the overall amount of carbon. Hence, a rope of SWNT or a multi-walled carbon nanotube requires less magnetic field for alignment than an individual single-walled carbon nanotube of the same length.
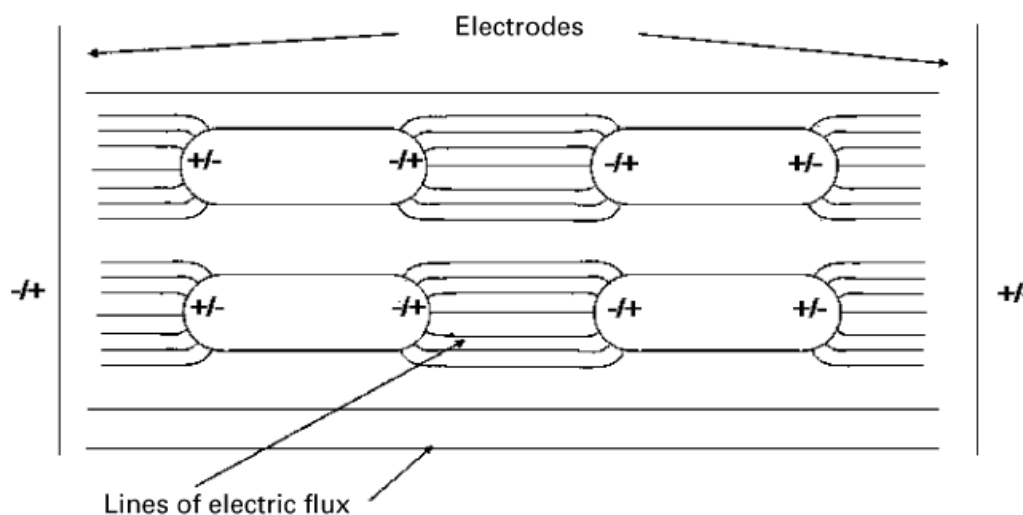
Figure 2.16 Schematic illustration of the interaction between aligned and polarised metallic cylindrical particles in an electric field.

CHAPTER III

LITERATURE REVIEWS

3.1 The CNT/Polyimide nanocomposite films

Cheol park *et al*. [30] used in situ polymerization and sonication to develop a efficient method to disperse single-walled (SWNT) bundle into polyimide matrix in order to produce an electrically conductive (antistatic) and optically transparent nanocomposite films. Single-walled carbon nanotube reinforced polyimide nanocomposites were fabricated by in situ polymerization using 1,3-bis (3-aminophenoxy) benzene (APB) and 2,2-bis(3,4-anhydrodicarboxyphenyl) hexafluoropropane (6FDA) in the presence of sonication with SWNT concentration ranging from 0.01 to 1.0 vol%. Opical microscopy and TEM of the composites show the uniform dispersion of SWNT bundles in the polymer matrix which imply the success of the process. The developed SWNT-polyimide nanocomposite films exhibited significant conductivity enhancement (10 order of magnitude) at a very low loading (0.1 vol%). The incorporation of the SWNT improved the mechanical properties as well as thermal stability of polyimide.

Hyang Hwa So *et al.* [31] synthesized Polyimide(PI)-carbon nanotubes nanocomposites by in situ polymerization using Multi-walled carbon nanotubes (MWNT), with 4,4'-oxydianilline and pyromellitic dianhydride, followed by casting, evaporation and thermal imidization. The incorporation of MWNT and MWNT-COOH in polymer matrix enhanced the mechanical properties of the polyimide. The presence of hydrogen bonds between the MWNT-COOH and PI chain exhibited strong interfacial interaction and a homogeneously dispersion. Thus, the overall mechanical performances of PI/MWNT-COOH nanocomposites were higher than pure PI and PI/raw MWNT composites. The PI film with 0.1 wt% MWNT-COOH content was transparent. The electrical conductivity of the PI/MWNT nano-composites were increased with increasing MWNT content and the percolation threshold for the electric conductivity of the resultant PI/MWNT nanocomposites was at 3wt%.

Siu-Ming *et al*. [32] used 4,4'-oxydianiline (ODA) with 3,3',4,4'-benzophenone tetracarboxylic dianhydride (BTDA) to produce polyimide (PI) and polyamic acid (PAA) precursor solution, that prepared from the reaction between ODA and BTDA. This solution was separately mixed by unmodified, acid-modified and amide-modified MWNT, followed by casting, evaporation and thermal imidization at 300 ^{0}C to produce polyimide/carbon nanotube nanocomposites. The scanning electron microscopy (SEM) and atomic force microscopy (AFM) show the uniformly dispersed acid and amine-modified MWNT in the polymer matrix, while unmodified MWNT became aggregated. Comparing the electrical properties between unmodified MWNT and modified MWNT at a high MWNT content (6.98 wt%), the surface electrical resistivity of the unmodified MWNT was decreased lower than modified MWNT, from $1.28*10^{-15}$ Ω/cm^2 (neat PI) to $7.59*10^6$ Ω/cm^2, as same as the volume electrical resistivity. The incorporation of the MWNT significance enhanced the mechanical properties of polyimide. The tensile properties of MWNT/PI nanocomposites could be improved by mixing with modified MWNT. Moreover, the tensile strength of the amino-MWNT/PI nanocomposites was higher than acid-MWNT/PI nanocomposites. However, the opposite trend was found when MWNT content was over 2.44 wt%.

Aiping Yu *et al*. [33] have developed a novel in situ polymerization to disperse single-walled carbon nanotube (SWNT) in the form of individual nanotube and small bundles in a polyimide matrix. Due to the higher aspect ratio of individual SWNT than a bundle of SWNT of the same length, the individual SWNT composites have lower percolation threshold and a better transfer of properties. In this study, SWNT/polyimide composite film with SWNT concentration ranging form 0.02-1 wt% was synthesized by the in situ polymerization reaction of 1,3-bis(3-amino phenoxy) benzene (APB) and 4,4'-hexafluoroisopropylidiene diphthalic anhydride (6-FDA), followed by spin coating on a glass substrate. Optical microscopy, SEM and TEM showed the homogenously distributed of SWNT in the polymer matrix, and AFM observations indicated that more than 80% of the dispersed SWNT are stabilized as individual nanotubes. Thus, individual SWNT distribution led to efficient network formation because of the much higher aspect ratio than the bundled SWNT. Furthermore, the carboxylic acid groups contributed to crosslink of the SWNT within the polymer matrix. The freestanding SWNT composite films have very good optical,

thermal and mechanical properties as well as the better electrostatic charge dissipation properties.

3.2 Alignment of CNT in polymer matrix

Martin C.A. *et al*. [34] synthesized MWNT-epoxy composites, with MWNT loading fraction containing from 0.005 to 0.02 wt%, as an electrically conductive filler. An epoxy system composed of a bisphenal-A resin and an amine hardener. The present work, investigated the influence of both AC and DC electric field on dispersion of MWNT in an epoxy matrix during cure. The formations of aligned conductive nanotube network between the electrodes were observed. The network formation process and resulting network structure depended on the field strength, the nanotube weight fraction and the curing time. In situ optical microscopy revealed that both AC and DC electric field can induce the formation of aligned carbon nanotube network across the electrodes. However, the network structure formed in AC field was more uniform and more aligned compare to the rather inhomogeneous and branches structure obtained in the case of DC field. The bulk conductive nanotube-polymer nanocomposites showed promising anisotropic electrical properties and degrees of optical transparency.

Cheol park *et al*. [35] utilized AC field to control over the electrical and dielectric properties of a SWNT/UH nanocomposites, with SWNT concentration 0.03 wt%, compared with shear alignment method. In this process, SWNT were aligned via an AC field in liquid matrix, followed by matrix immobilized by photopolymerization under continuous application of the electric field. The degree of SWNT alignment was achieved by adjusting the applied field strength, the frequency and the application time. High-resolution scanning electron microscopy (HRSEM) showed the aligned SWNT along the field and also the laterally migrated thick SWNT near the electrodes, which was not observed in shear aligned SWNT. The aligned SWNT polymer composites exhibited anisotropic characteristics and the alignment can be controlled by tuning the applied field parameters.

Donglu Shi *et al*. [36] present the solution-coating method of NiO and CoO onto the surface of the carbon nanofibers (CNF) by magnetically aligned the carbon nanofibers in polymer composites under moderate magnetic field (3T). Due to the extremely low magnetic susceptibility carbon nanofibers, the magnetically induced alignment cannot be made. Because of NiO/CoO coating, coated carbon nanofibers can be magnetically induced to rotate in viscous polymer liquid. Both transmission electron microscopy (TEM) and scanning electron microscopy (SEM) showed the well-aligned nanofibers in a polymer matrix. The pronounced anisotropy in tensile strength in directions normal (12.1 MPa) and parallel (22 MPa) to the applied field were observed. Such a method can be applied to other nano- and micro-species for various composite materials in any general alignment of nonmagnetic substances.

Torsten Prasse *et al*. [37] report the application of AC and DC electric field for the alignment and the formation of network of carbon nanofiber (CNF) dispersion during epoxy resin curing. The network formations of CNF in the amine curing agent between silver strip electrodes with an electrode spacing of 500 µm, on DC or an AC electric filed in the range of 400 to 800 V/cm, were investigated. In situ optical microscopy reveal that the fiber deposition onto the anode after 17 min of DC electric filed of 800V/cm gave a direct evidence for negative excess charge on the particle surface, but the web-like structure dispersion fiber with the electrostatic stabilization by AC electric field with an amplitude of 400 V/cm and a frequency of 1 KHz was observed. For the cured composites, the structural anisotropy of the fiber network with a fiber loading ≥ 1wt% showed the maximal anisotropy for the DC resistivity of about 10 and for the dielectric constant of about 20 at 1 kHz.

Torsten Prasse *et al*. [38] used the DC electric or magnetic filed at two direction, parallel and perpendicular, to induce the alignment of vapor-grown carbon fibers (VGCFs) in polydimethylsiloxane at room temperature. In this study, the fixed magnetic of 0.23 T or the fixed DC electric filed of 18V was applied. The gap between the indium-tin-oxide (ITO) electrodes was 125 µm. In situ transmission optical microscopy demonstrated that the application of a DC electric field originated an aligned ramified network structure of VGCFs between the electrodes. In the formation of the network structure, end of VGCFs become connected to end of other VGCFs, followed by rotation and orientation of the VGCFs along the direction of

electrode flux. The resulting network had a reduced percolation threshold of below 1 wt%. In contrast, when applied a magnetic field, the VGCFs were only rotated without the formation of a network, resulting in no reduction in volume resistivity up to 1wt%. The network formation speed was almost proportional to the matrix viscosity.

Bangwen Zhang *et al*. [39] used the hybrid electric and magnetic fields to prepare a novel 1–3 nanocomposites consisting of one-dimensional-aligned carbon-coated nickel (Ni@C) nanoparticles in epoxy resin matrix. The experimental equipments for the curing of composites consist of a permanent magnet, an electrostatic generator and a mold, as illustrated in Figure 3.1. The magnet, with pole section area of 5 * 5 cm^2 and pole-to-pole gap of 2 cm, can produce a magnetic field of 0.8 T. The electric field is supplied by the electrostatic generator with a voltage output range of 0–8 kV. The mold includes a small container and two brass sheets closed at sides. The container, cut from a polytetrafluoroethylene (PTFE) plate, is 25 mm in diameter and 2 mm in thickness, with an entry in the top for resin injection. The brass sheets service as electrodes, connecting with the electrostatic generator. A PTFE adhesive tape of 0.1 mm thickness is stuck inside the brass sheets for electrical insulation and demoulding.
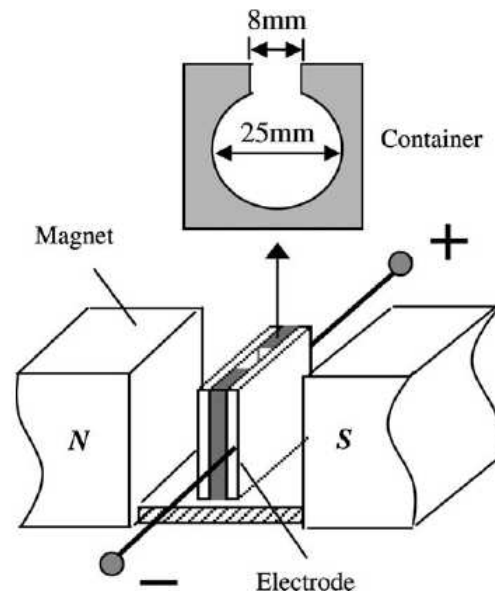
Figure 3.1 Schematic of experimental equipment for the curing of composite samples under external fields.

The results showed the alignment attributed to the dipolar interaction between Ni@C nanoparticles in the liquid-state resin under external fields, among which firstly, hybrid electric and magnetic fields play the important role on the alignment of nanoparticles, secondly is magnetic field, and lastly is electric field. The resistivity of aligned composites decreases by 3–4 orders of magnitude than that of random composites in the loading content range of 3-10 wt%, accompanied with an increase in dielectric constant and dielectric loss.

Erin Camponeschi *et al*. [40] utilized both SWCNT and MWCNT to embed in two different epoxy matrices, Aeropoxy (AP) and Coldfix (CF), in order to determine the effect of alignment on the mechanical properties of the resulting composites. The samples varied by epoxy type, carbon nanotube type, and magnetic field strength. A detailed summary of the sample experimental and calculated data is shown in Table 3.1. The changes in polymer chain conformation induced by an external magnetic field as illustrated in Figure 3.2.

Table 3.1 Summary of the measured and calculated mechanical properties for the various samples characterized in this work

Epoxy	CNT type	Magnetic field (T)	Tan δ	Modulus		T_g (°C)		Young's modulus (MPa)
				Loss (MPa)	Storage (MPa)	DSC	DMA	
AP	None	15	0.817	3070	2508	58.8	75.6	3964
AP	SWNT	0	0.752	248	1330	55.1	80.6	1353
AP	SWNT	15	0.649	224	2277	70.9	77.2	2288
AP	SWNT	25	0.726	219	2002	55.6	83.8	2014
AP	SWNT	25	0.634	270	2760	62.5	72.4	2773
AP	MWNT	0	1.120	22	1099	54.2	70.8	1099
AP	MWNT	15	0.825	86	1295	64.6	65.6	1298
AP	MWNT	25	0.565	117	3377	64.3	86.5	3379
AP	MWNT	25	0.530	150	2492	48.1	63.7	2497
CF	None	15	1.139	205	1914	60.2	79.1	1925
CF	None	25	1.260	285	2900	45.5	64.3	2914
CF	SWNT	0	0.764	249	1330	54.9	80.6	1353
CF	SWNT	15	1.127	117	1099	51.1	77.1	1105
CF	SWNT	25	1.093	244	982	68.3	73.5	1012
CF	SW/MW	0	1.102	274	2051	52.4	85.2	2069
CF	MWNT	15	0.916	201	1952	79.1	97.9	1963
CF	MWNT	25	1.174	113	1192	54.8	64.6	1197
CF	MWNT	25	1.197	244	1430	52.0	65.8	1450

The results showed the changes in the thermo-mechanical properties of the nanocomposites, i.e. the glass transition temperature, Young's modulus and elastic and viscous moduli, as a function of the magnetic field strengths used for the alignment of the carbon nanotubes, and the epoxy system used. Moreover, CNT alignment, actually occurs at high magnetic fields, caused the properties of the composites to be superior than the unexposed to a magnetic field composites.
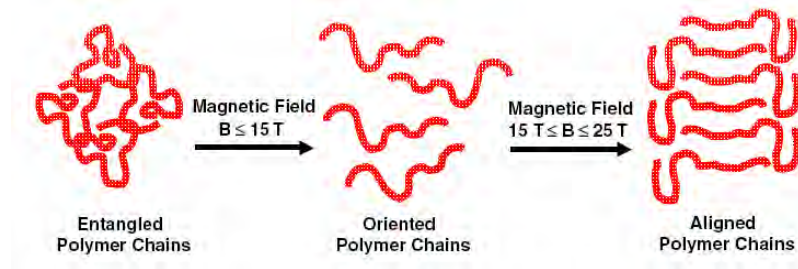
Figure 3.2 The predicted effect of the application of an external magnetic field on the orientation and alignment of polymer chains.

Haiquan Wang *et al*. [41] described the method to orient the graphite nanosheet (GNs) in one direction in the unsaturated polyester resin by the electrical field. The electric field is applied by two parallel electrodes and the electric field-induced torque is the driving force for the orientation of the GNs. Figure 3.3 illustrates the experimental setups used to apply a DC field. The electric field of 18 Volts DC was applied using parallel electrodes which were fabricated by etching indium-tinoxide (ITO) onto a glass substrate. The gap between the electrodes was 0.20 mm, so 90 V/mm was applied to the dispersion. Under this condition, the matrix will cure in a few minutes.
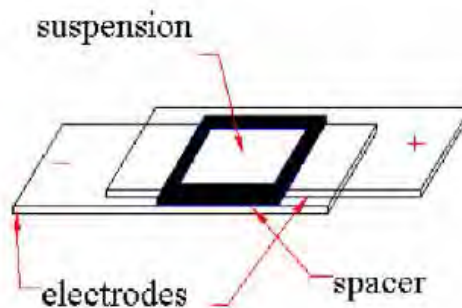
Figure 3.3 Schematic illustration of experimental setup for preparation of oriented specimens.
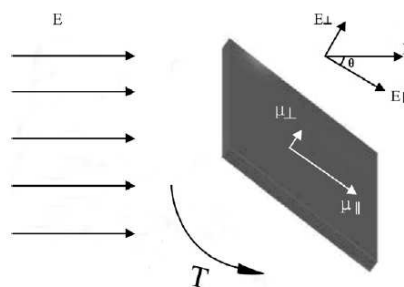
Figure 3.4 Schematic illustration of a polarized flake in an electric field.

The results demonstrated that the GNs were oriented with their flakes along the   electric flux under the influence of a DC electric field. The optical properties of the field-induced composite films showed significant improvement in visible light transmittance compared with those prepared without the electric field within the visible wavelength range. The oriented composite film tended to absorb and scatter less light than the random one.

Brian W. Steinert *et al.* [42] dispersed Single-wall carbon nanotubes (SWNT) in a polyethylene terephthalate (PET) matrix by solution blending and casting onto a glass substrate to create flexible films. Various SWNT loading concentrations were implemented (0.5, 1.0, and 3.0 wt%), and the processing method was repeated to produce films in the presence of magnetic fields (3 and 9.4 Tesla). Raman spectroscopy and TEM determined that the field strength and filler concentration play the most important roles in determining the degree of alignment. Low concentration and high magnetic field strength produced the most highly aligned samples. The electrical properties showed the sufficient conductivity for antistatic and electrostatic dissipation purposes at concentrations as low as 0.5 wt% SWNT. It was also concluded that dispersion and filler concentration have the greatest effect upon electrical conductivity, while alignment plays a secondary role.
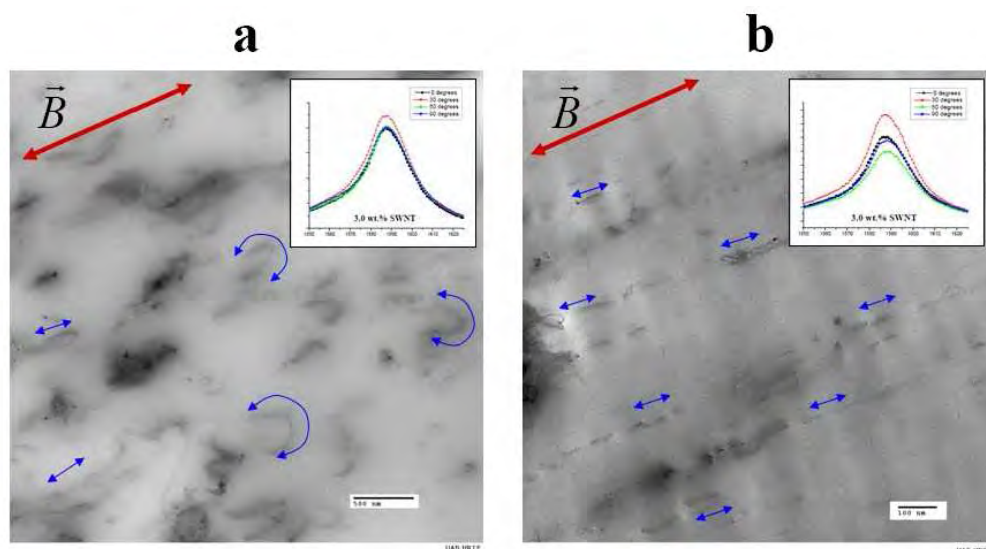
Figure 3.5 TEM micrographs showing the effect of magnetic field strength at a constant SWNT loading (3.0 wt%), but with varying magnetic field strengths of (a) 3.0 Tesla and (b) 9.4 Tesla.

CHAPTER IV

EXPERIMENT

The experimental procedures of polymer nanocomposites in this section were classified into two main part: CB/PI nanocomposite and aligned SWNT/PI nanocomposites. Carbon Black was used for comparison with SWNT material in the same matrix, and for determination of the fine conditions of SWNT in matrix from limitation of the CB/PI nanocomposites conditions. The entire experiments can be divided into five parts which can be explained as follows,

(i) Materials and chemicals

(ii) Equipments

(iii) The CB/PI nanocomposite films

(iv) The aligned SWNT/PI nanocomposite films

(v) Characterization of all polyimide films

The details of each part can be explained as followed.

4.1 Materials and Chemicals

1. 4,4′-(Hexafluoroisopropylidene) diphthalic anhydride (6 FDA) purchased from Aldrich chemical Company, Inc .

2. Pyromellitic dianhydride (PMDA) purchased from Aldrich chemical Company, Inc.

3. 4,4′-Oxydianiline (ODA) purchased from Aldrich chemical Company, Inc.

4. N-Methyl-2-pyrrolidinone (NMP) purchased from Merck KGaA Germany.

5. Sodium dodecyl sulfate purchased from Aldrich chemical Company, Inc.

6. Carbon black (N347 grade) was kindly provided by Thai Carbon Black public Co.,Ltd.

7. Single-walled carbon nanotube (SWNT) and acid modified Single-walled carbon nanotube (SWNT-COOH) purchased from Nanostructured & Amorphous Materials Inc.

4.2 Equipments

4.2.1 Polyimide synthesis part

Since most of the reagents were very sensitive to the oxygen and moisture therefore the special techniques were undertaken during the handling of reagents and the loading of ingredient into the reactor. Such equipments utilized for this purpose are listed as follows:

(a) Glove box (Vacuum Atmospheres) with oxygen and moisture analyzer for handling solid reagents under inert atmosphere and for storing air-sensitive reagents. Inside the glove box, oxygen and moisture levels are normally controlled to below 0.1 ppm. The glove box is shown in Figure 4.1.
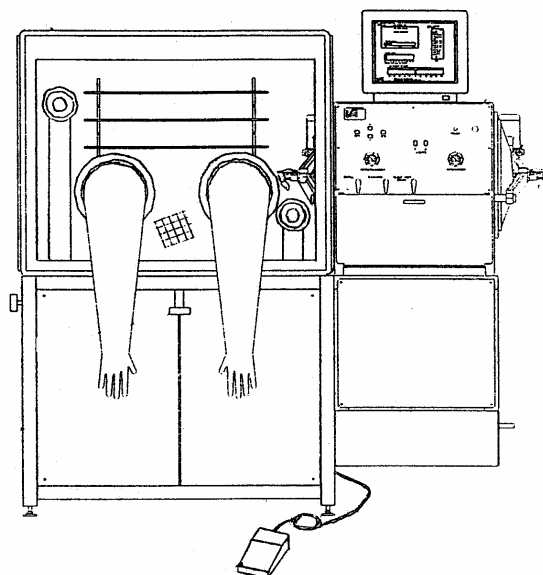
Figure 4.1 Glove box.

(b) Schlenk line consisted of vacuum line connected to vacuum pump and argon line for purging when reagents are transferred. The schlenk line was shown in Figure 4.2
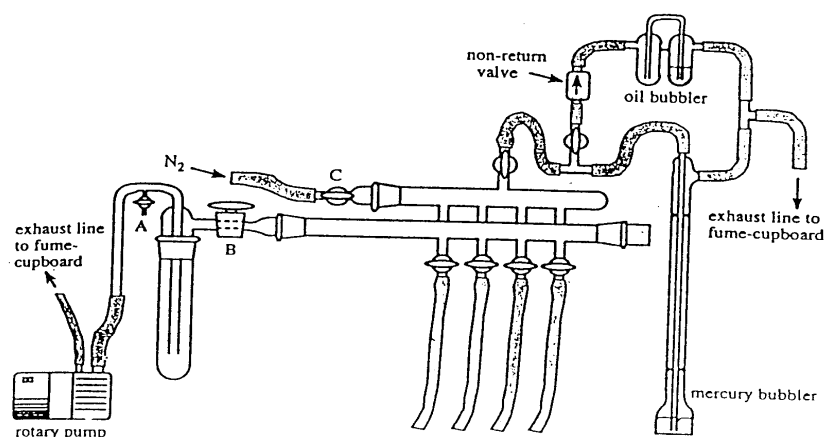
Figure 4.2 Schlenk line.

(c) Schlenk tube for keeping reagents under argon atmosphere outside the glove box. It was used accompanied with the Schlenk line. Schlenk tube is the tube with a ground joint and a side arm which connected with three ways glass valve. The Schlenk tube picture is shown in Figure 4.3.
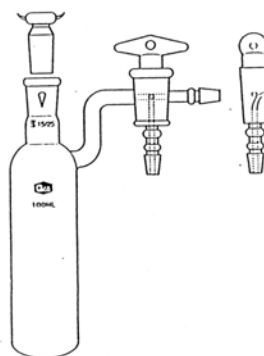
Figure 4.3 Schlenk tube.

(d) The inert gas (argon) from the cylinders was passed through columns of oxygen trap (BASF catalyst, R3-11G), moisture trap (molecular sieve), sodium hydroxide (NaOH) and phosphorus pentaoxide (P_2O_5) in order to purifying the argon gas to obtain ultra high purity argon which was used in Schlenk line and solvent distillation column. The inert gas supply system can be shown in Figure 4.4.
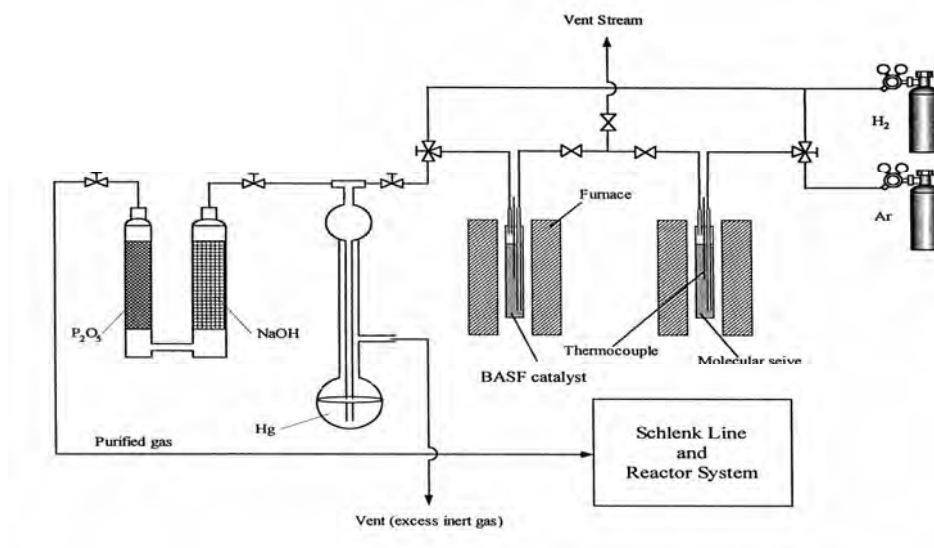
Figure 4.4 Inert gas supply system.

(e) **The vacuum pump** model 195 from Labconco Coporation was used. The produced low pressure of 10^{-1} to 10^{-3} mmHg was adequate for utilizing as the vacuum supply to the vacuum line of the Schlenk line. The vacuum pump is shown in Figure 4.5.
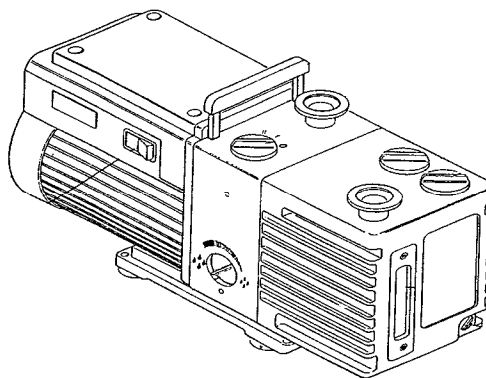
Figure 4.5 Vacuum pump.

(f) Magnetic Stirrer and Hot Plate

The magnetic stirrer and hot plate model RCT basic from IKA Labortechnik were used.

(g) Syringe, Needle

The syringe used in these experiments had a volume of of 50 and 10 ml and the cooperated needles were of No. 17 and 20, respectively.

4.2.2 Film preparation part

(a) Vacuum oven

A Cole-Parmer vacuum oven model 282A was used for removing solvent from freshly cast films and used for thermal treated the film polyimide. This vacuum oven can be programmed. All functions can be set from digital panel and display their status on LCD. The temperature, pressure and time are controllable variables. The maximum working temperature of this machine is 500°C.

4.2.3 Gold electrodes preparation part

(a) Metal evaporator

Metal evaporator model univex 300 was used for evaporating the gold metal under the plasma state to cover glass substrates and make the gold electrodes. It is universally usable for almost all vacuum coating processes. The high-vacuum pump system has been intergrated in the cabinet section and consists as standard of turbolecular pump and backing pump. Film thickness measuring instruments is added as auxiliary components. It is a kind of physical vapor deposition (PVD).

Figure 4.6 Metal evaporator Equipment.

4.3 Preparation of the CB/PI nanocomposite films

The CB/polyimide nanocomposites were synthesized by in-situ polymeri-zation base on PMDA, ODA and CB as starting materials. SDS was employed as surfactant to reduce the agglomeration of CB. First, CB (0.15 g) was added to NMP (100 ml) with vigorous stirring at ambient temperature. Then, the appropriate amount of surfactant (SDS) was combined with the homogeneous CB suspension of 0.15 wt/v% by ultrasonication (40 kHz) for 1-2 hours to obtain the homogeneous individual CB suspension. A set of concentration with ratio of CB to SDS varied from 1:0.4 to 1:100 by weight was performed.

The diamide (ODA) was completely dissolved in NMP with stirring to obtain the ODA solution. After stirring, the homogeneous individual CB suspension was added into ODA solution, it was continuously mixed by stirred for 10 min before adding the dianhydride (PMDA). The reaction was carried out under ultrasonic bath (40 kHz) while the solution viscosity gradually increased and stabilized. The mixture was stirred continuously overnight to form the CB/poly(amic acid) (PAA) solution. The PAA solution with CB was then cast onto clean, dry plate glass and subjected to thermal imidization for 1 hr each at $100\,^{\circ}$C, $150\,^{\circ}$C and $300\,^{\circ}$C to produce the CB/PI nanocomposite films with CB concentration ranging from 0.025-0.5 wt%.
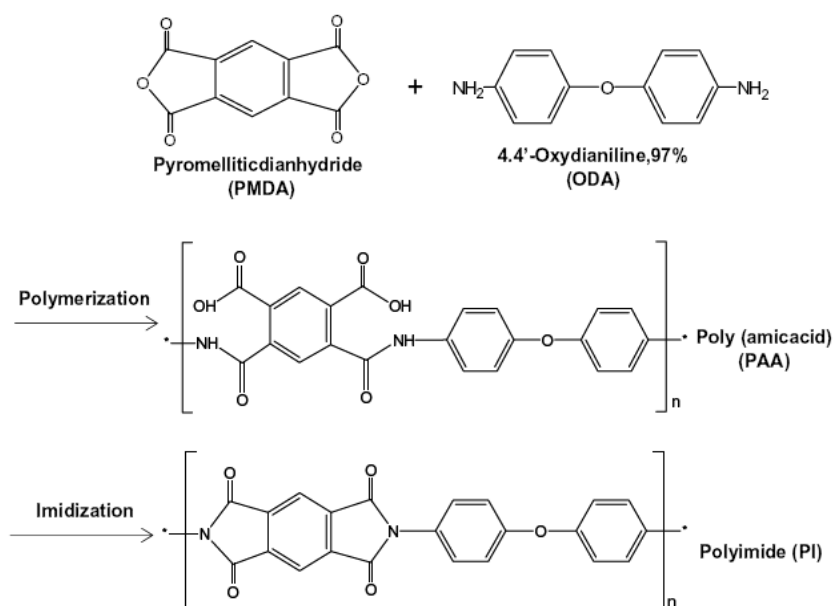
Figure 4.7 The synthesis procedure of polyimide.

4.4 Preparation of the aligned SWNT/PI nanocomposite films

In this process, 0.0203g of unmodified SWNT and acid-modified SWNT were first dispersed in Non-aqueous solution (0.03045 and 0.3g of sodium dodecyl sulfate and 100 ml of NMP solvent) containing SDS as ionic surfactant in presence of ultrasonication (40 kHz) for 1 hr in order to exfoliate the SWNT bundle into individual tubes. The individual SWNTs suspension was introduced as an electrical conductive filler in polyimide matrix based on 4,4'-oxdianilline (ODA) and 4,4′-(Hexafluoroiso-propylidene) diphthalic anhydride (6FDA) precursor. The homo geneous SWNT/PI solution were cast onto a dried glass plate, a DC electric and magnetic field were separately and simultaneously applied to induce the formation of an aligned structure, followed by evaporation and thermal imidization to produce the aligned SWNT/PI nanocomposite films. The summery of entire samples are shown in table 4.1.

Table 4.1 Summery of composites sample for experiment

Sample	CNT content (wt %)	Electric field (Volt)	Magnetic field (Tesla)	Electrode spacing (cm)	Thickness of electrode (kA°)	External field applied time (min)
Random	0.5	-	-	-	-	-
2T	0.5	-	2	-	-	7
150 V	0.5	150	-	1	300	7
300 V	0.5	300	-	1	300	7
450 V	0.5	450	-	1	300	7
600 V	0.5	600	-	1	300	7
[n]150 V+2T	0.5	150	2	1	300	7
[n]300 V+2T	0.5	300	2	1	300	7
[n]450 V+2T	0.5	450	2	1	300	7
[n]600 V+2T	0.5	600	2	1	300	7
*600 V+2T	0.5	600	2	1	300	7

[n] Two alignment system (A and B)

* Condition of SWNT-COOH/PI nanocomposites
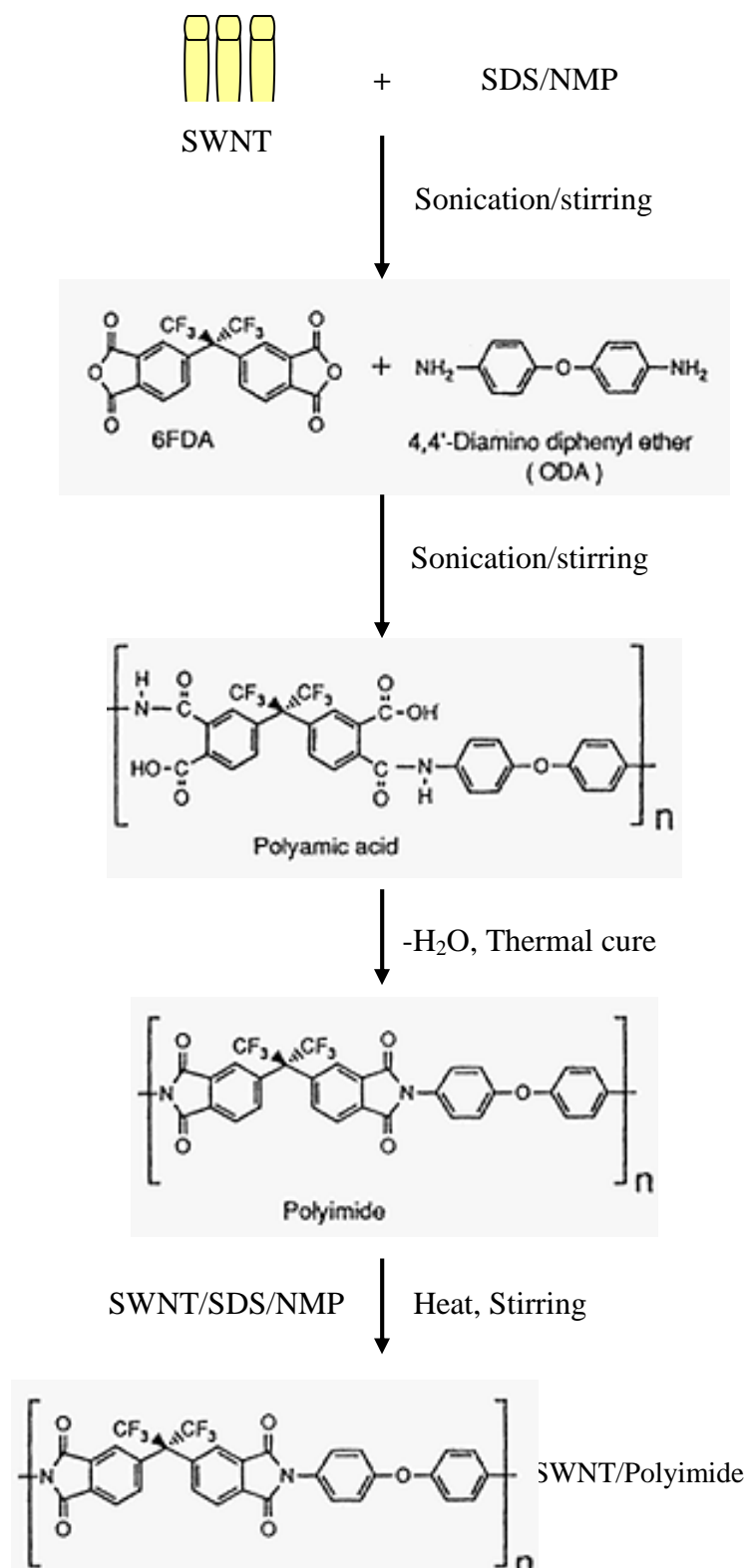
Figure 4.8 The synthesis procedure of SWNT/polyimide.

Power supply

+   -

EF →

Au electrode

SWNT/Polymer solution
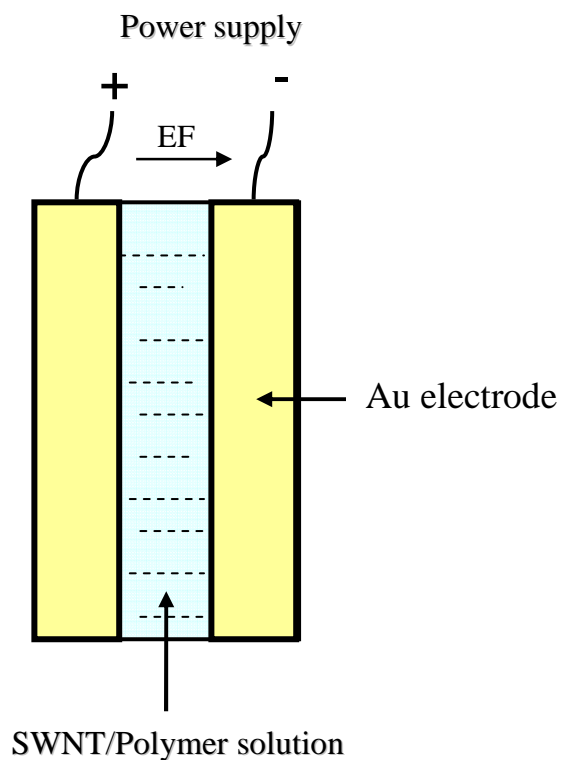
Figure 4.9 Schematic of the DC electric field alignment set up of SWNT in polyimide (Top view).

+   -

Power supply

EF →

MF →

N

S

Au

SWNT/Polymer solution
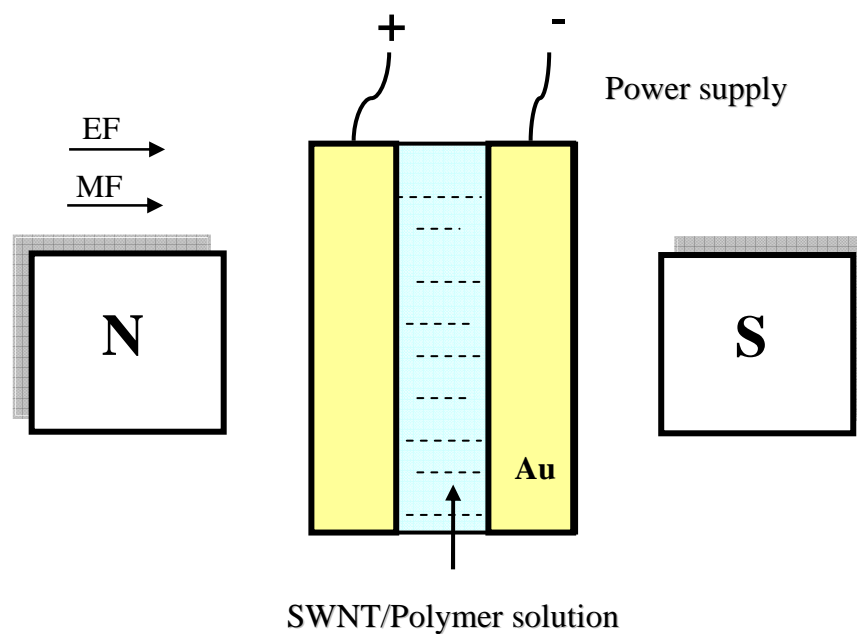
Figure 4.10 Schematic of the DC electric and magnetic field alignment set up of SWNT in polyimide (Top view). It was defined as A system.
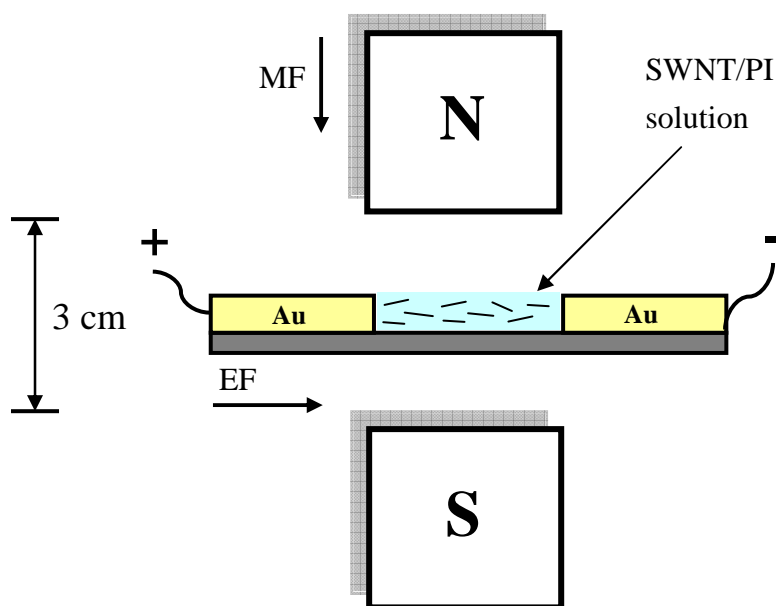
Figure 4.11 Schematic of the DC electric and magnetic field alignment set up of SWNT in polyimide (Side view). It was defined as B system.

4.5 Characterization Instruments

4.5.1 Infrared Spectroscopy (FTIR)

Infrared survey spectra were recorded with Nicolet 6700 FTIR spectrometer. The scanning ranged from 400 to 4000 cm^{-1} with scanning 64 times. The functional group of the composite films (1.5*1.5 cm^2) was identified.

Figure 4.12 Fourier transform infrared spectroscopy (FTIR) Equipment.

4.5.2 UV-VIS spectrometer (UV/VIS)

Transparent properties of the CB/PI nanocomposite films were characterized using Lambda 650 UV-VIS spectrometer. The sample films (1.5*1.5 cm^2) were investigated at 500 nm wavelength of absorbance mode.
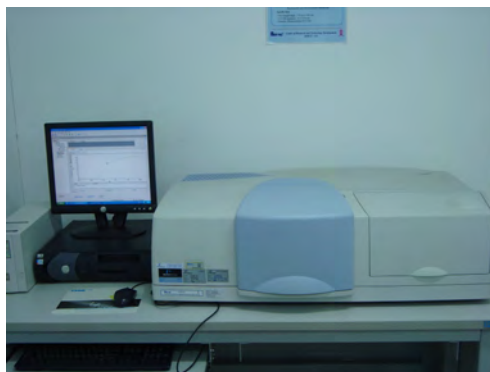
Figure 4.13 UV-VIS spectrometer (UV/VIS) Equipment.

4.5.3 Dielectric properties

The dielectric properties of the polyimide films were obtained via the capacitance method and were measured at room temperature and 1V with Agilent E 4980A Precision LCR Meter. The films for dielectric properties analysis were coated with gold layer by JEOL JFC-1100E ion sputtering device on both sides to provide electrical contact to the specimens. The specimens size were 1.5 x1.5 (cm).

Figure 4.14 LCR Meter Equipment.

4.5.4 Tensile testing machine

Tensile properties were characterized using an Instron universal testing machine with a test speed of 5 mm/min. Sample size 2 x 10 cm^2. The tests were conducted according to ASTM D 882-02. The tensile testing machine of a constant-rate-of-crosshead movement is used. It has a fixed or essentially stationary member carrying one grip, and a moveable member carrying a second grip. Self-aligning grips employed for holding the test specimen between the fixed member and movable member to prevent the alignment problem. An extension indicator is used for determination of the distance between two designated points located within the length of the test specimen as the specimen is stretched.

Figure 4.15 Tensile testing machines Equipment

4.5.5 Fourier Transform Infrared Spectometer and Raman Microscope (FT-IR/Raman)

Carbon nanotubes identification and degree of alignment of the CNT/PI nanocomposite films were assessed using FT-Raman spectroscopy with a laser in the near infrared-usually at 1064 nm. The spectral range form stokes 3500-100 cm^{-1} and sampling 180° reflective was also performed.
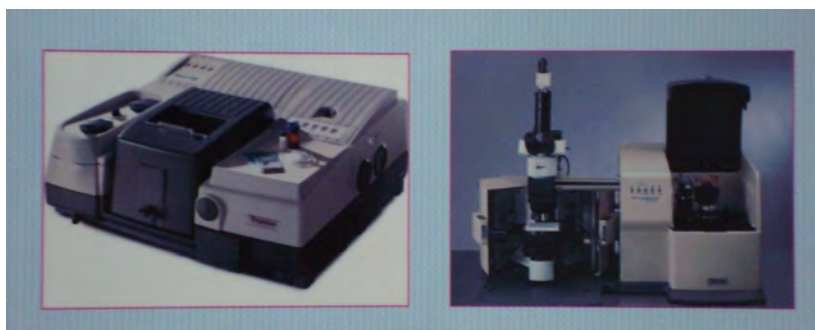
Figure 4.16 FT-Raman spectroscopy Equipment.

4.5.6 Transmission electron microscopy (TEM)

The morphology and dispersion state of CB within matrix polymer of nanocomposite films was observed using Transmission electron microscopy (TEM, JEOL JEM-2010). The specimens (~0.1*1 cm^2) were coated by epoxy resin to be cylindrical shape and cross-section by microtome.

4.5.7 Optical microscopy

The development of alignment structure of the CNT in composites was investigated by optical microscopy. The aligned films were observed under the magnification rang 0.67x-4.5x, and a commonly camera was also used to take a photo.

RESEARCH METHODOLOGY
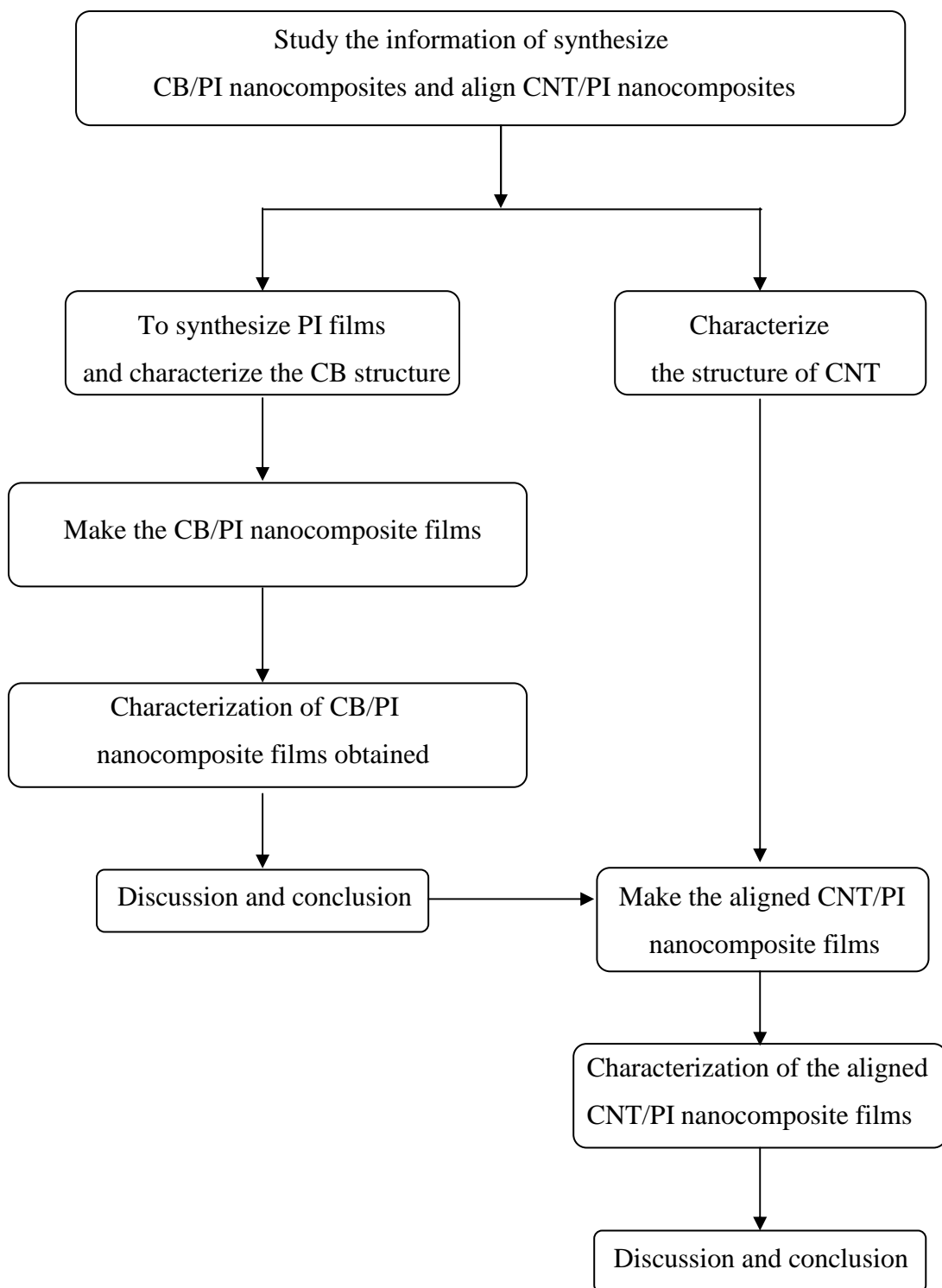
Figure 4.17 Flow diagram of research methodology.

CHAPTER V

RESULTS AND DISCUSSION

This chapter provides the information of the CB/PI nanocomposite films and the aligned SWNT/PI nanocomposite films such as thermal properties, electrical properties, mechanical properties and morphologies. The special characteristics method, UV-vis absorption spectroscopy observed the dispersion state of the CB/PI nanocomposite films, while Raman spectroscopy was also used for assessing the degree of alignment of the aligned SWNT/PI nanocomposite films.

5.1 The CB/polyimide nanocomposite films

5.1.1 Preparation of polyimide films

In this research, the polyimide films were synthesized by a two-step method. The polymerization was done by reaction between Pyromellitic dianhydride (PMDA) and 4,4´-oxydianiline (ODA) in N-methyl pyrrolidinone (NMP) solvents to form poly(amic acid) (PAA). The PAA solution was then cast onto clean, dry plate glass, and subjected to thermal imidization to produce the PI films. The structure of PI films was investigated by FT-IR, as shown in Figure 5.1.
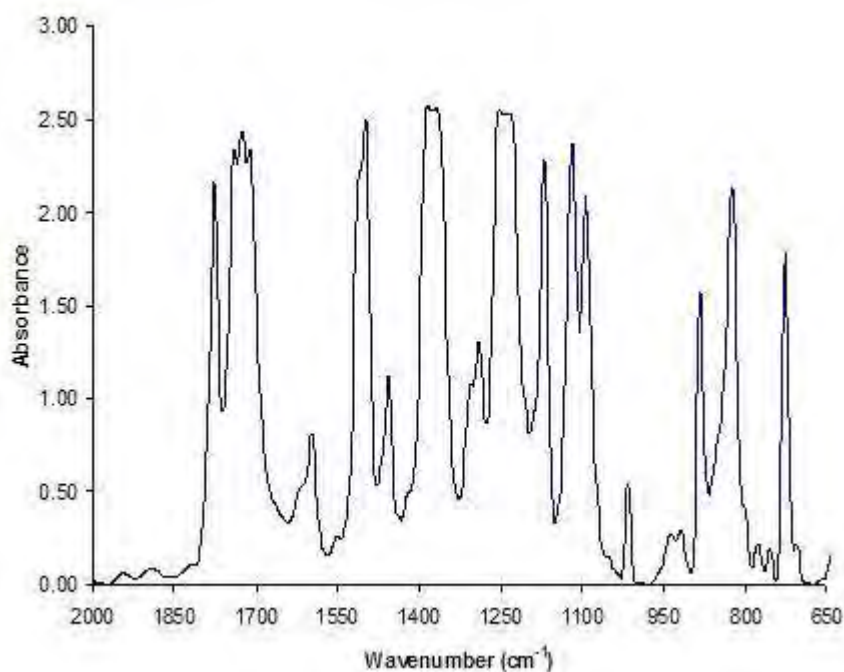
Figure 5.1 FT-IR spectra of pure polyimide films.

The features at wavenumber near 1780, 1730 and 1370 cm^{-1} were observed in the FT-IR spectra correspond with C=O (sym. str.), C=O (asym. str.) and C-N (str.) respectively, which as commonly the characteristic absorption peaks of the imide group as displays in table 5.1. The FT-IR spectra of the absoption peaks of PAA were not appeared, indicated that the imidization reaction was completed. Moreover, these results confirmed that polyimide films were successfully developed.

Table 5.1 Characteristic IR absorptions of poly(amic acid) and polyimide [43].

Wave number (cm^{-1})	Polyamic acid	Polyimide
3501 (imide ring)	No	Strong
3400–3200 (secondary amide)	Strong	No
3200–2800 (carboxylic acid)	Strong	Weak
1780 (C=O imide)	No	Weak
1720 (C=O stretching vibration)	Strong	Very strong
1640 triplet (secondary amide)	Strong	Very weak
1515 (aromatic C=C stretching)	Strong	Strong
1395 (imide stretching)	No	Strong
830 (trisubstituted C-H vibration)	Strong	Strong
690 (C=O imide)	Very weak	Strong

5.1.2 Surfactant assisted CB dispersion

In this section, the dispersion assisted by surfactant in the polymer will be studied. In order to achieve the well dispersion state of CB suspension and to understand the dispersion mechanism, the morphology and size of CB should be examined. Figure 5.2 shows TEM microphotographs of CB particles. It was clearly seen that the majority of CB particles formed self-aggregation, which has particle size larger than 200 nm, because of the strong van der Waal interaction force between carbon-carbon. The magnification image indicated that a diameter of individual CB was approximately 28 nm which corresponded to the supplier specification.

In this studied, CB were dispersed in NMP as organic solvent (0.15wt/v%) with various SDS amount, in which ratio of CB to SDS were 1:0.4, 1:0.8, 1:2, 1:5, 1:10 and 1:100. All of these suspensions were sonicated for 1 hour before using as filler into matrix medium, as show in Figure 5.2.
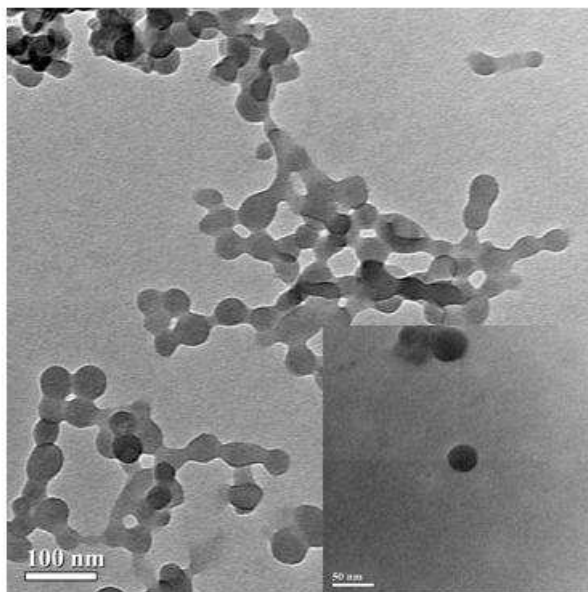
Figure 5.2 TEM images of CB particle.

After the sonication, the CB suspensions stabilized with SDS were kept for several months (Figure 5.3(1-3)) while the absorption of SDS on CB surface resulted in electrostatic repulsion force. However, a few carbon aggregated can be observed in Figure 5.3(1, 2) because of insufficient of surfactant, but the most of suspension were still homogeneous. Figure 5.3(3), the homogeneous and single-phase suspension was obtained. The appropriated SDS concentration, slightly below the CMC, can prevent carbon-carbon attraction and limit the aggregate size resulted in the stability of CB dispersion. Whereas CB suspension showed in Figure 5.3(4-6) contained aggregation of CB at the bottom of their respective vials after 36-48 hours due to the reduction of electrostatic repulsion force between CB. The similar result can be also found by [44, 45], in the dispersion of CNT in aqueous solution with SDS as dispersing agent. Comparable to the stability of all these suspensions, it can be conclude that the stability tends follows: (3) > (2) > (1) > (4, 5 and 6).

Figure 5.3 Vials (6mL) containing the CB suspension (0.15 wt/v%), in which the CB to SDS ratio were 1:0.4 (1), 1:0.8 (2) and 1:2 (3) sample were imaged after sonication 3 months whereas 1:5 (4), 1:10 (5) and 1:100 (6) sample were imaged after sonication 36-48 hours.

5.1.3 The optical images of the CB/PI nanocomposite films

In order to observe the effects of anionic surfactant on optical properties of the CB/PI nanocomposite films, a series of the CB/PI nanocomposite films with various SDS content were performed. The suitable suspension amount with ratio of CB to SDS varies from 1:0.4 to 1:100 by weight in presence of ultrasonication for 1 hour was added into PAA monomer to make the CB/PAA mixture. The mixture of 4 ml were cast onto $10*10 \ cm^2$ clean, dry plate glass and subject to thermal imidization to produce the CB/PI nanocomposite films with CB concentration followed : 0.025, 0.05, 0.1, 0.2, 0.3 and 0.5 wt% and have thickness of 30-40 µm. The partial nanocomposite films obtained as show in Figure 5.4.

After imidization, the synthesized pure polyimide film was yellow which correspond to PI commercial. It is well known that the optical properties of nanocomposite films were damaged when increased the CB loading in nanocomposite films, due to the agglomeration of CB in continuous phase impeded a light transmission. Therefore, the optical properties of nanocomposite films without surfactant-assisted dispersion depended strongly on amount of CB loading in nanocomposite films.
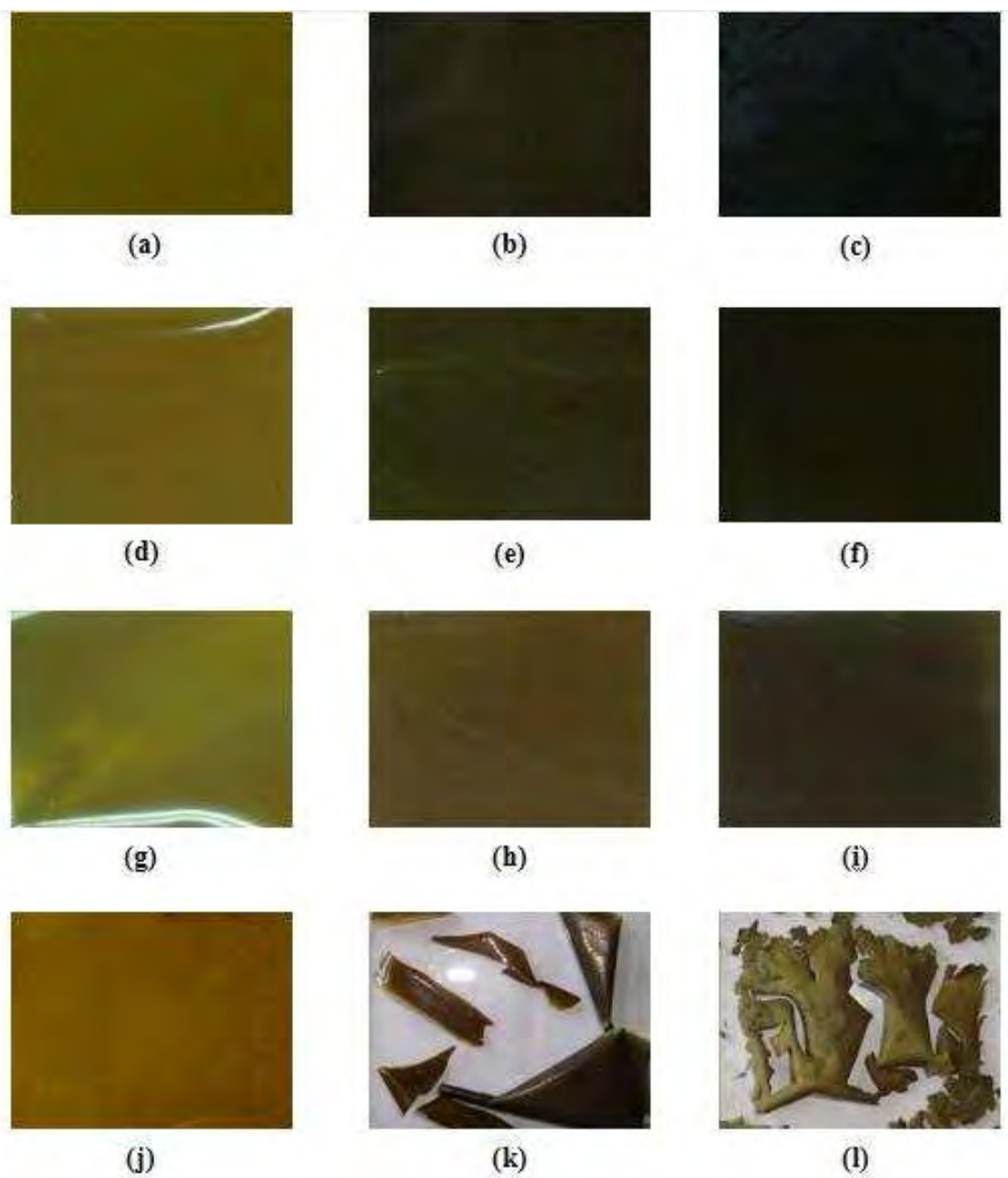
Figure 5.4 Photo images of 0.025wt% CB/PI nanocomposite films with CB/SDS ratio were 1:0 (a), 1:0.4 (d), 1:2 (g) and 1:100 (j). The 0.2wt% CB/PI nanocomposite films with CB/SDS ratio were 1:0 (b), 1:0.4 (e), 1:2 (h) and 1:100 (k). The 0.5wt% CB/PI nanocomposite films with CB/SDS ratio were 1:0 (c), 1:0.4 (f), 1:2 (i) and 1:100 (l).

From Figure 5.4, it was clearly seen that the addition of dispersing agent (SDS) into the CB/PI nanocomposite films improved the optical properties of these films, when compared to nanocomposite films without surfactant-assisted CB dispersion at the same weight fraction of CB. It is due to the rule of SDS in matrix medium was displayed as compatibilizer, in which aid a filler homogenous in matrix medium, and can also transferred the properties of filler to polymer matrix. However, the key factors of formation of translucent films depended on filler, dispersing agent, solvent and polymer matrix. In the case of 1:0.4 CB/SDS ratio in nanocomposite films, the all prepared films were more dark and opaque than the CB/SDS ratio of 1:2, but slightly transparent than the nanocomposite without surfactant at the same CB loading. These results demonstrated that the translucent films were achieved when the appropriated CB/SDS ratio was introduced into matrix media. At the 1:100 CB/SDS ratio, nanocomposite films with the CB fraction loading more than 2 wt% were broke, as show in Figure 5.4(k and l). It is due to a variation of SDS amount in nano-composite films, which dominated bulk properties of those films, meaning the fragile films were occurred from intrinsic properties of anionic surfactant. Nevertheless, the optical properties of nanocomposite films were also verified by absorption technique.

5.1.4 UV-vis spectra of the CB/PI nanocomposite films

In order to investigate the effects of surfactant on the CB dispersion in composite films, UV-vis absorption spectroscopy and TEM were utilized. After thermal imidization, the synthesized films with various SDS amount were investigated by scanning mode of UV-vis spectroscopic to search for the suitable wavelength applicable to films analysis. It was found that the wavelength at 500 nm was appropriate as showed in Figure 5.5. However, the synthesized films have thickness ranging from 30-40 μm. Therefore, to eliminate the effect of PI film thickness on absorbance, a linear calibration curve of pure PI were also established at 500 nm as a reference, showed in Figure 5.6. The absorbance value of pure PI (calibration curve) and nanocomposite films were denote Ao and A respectively. Figure 5.7 displays the absorbance value ratio at 500 nm of the CB/PI nanocomposite films of CB concentration as 0.5 wt% versus various SDS concentrations after subtraction of film thickness.
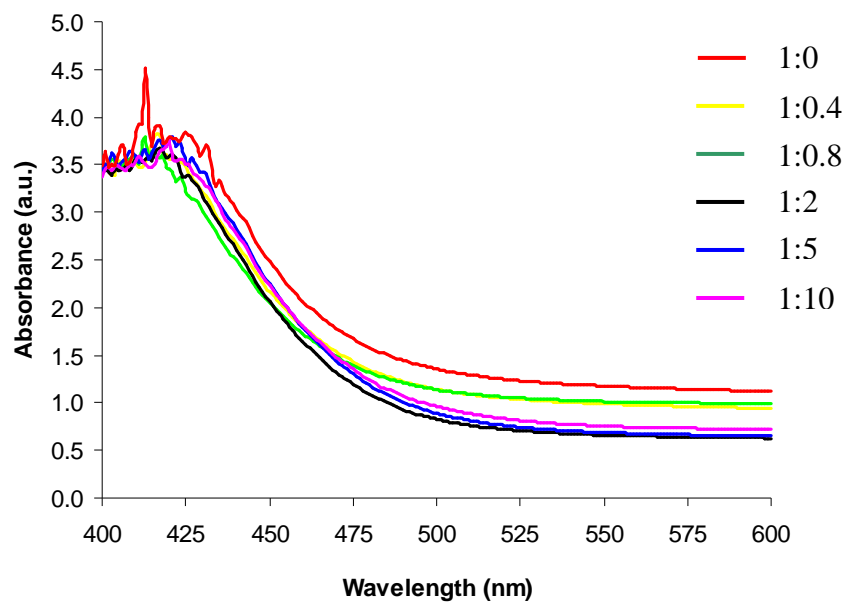
Figure 5.5 UV-vis spectra of the 0.5wt% CB/PI nanocomposite films as function of CB/SDS ratio.
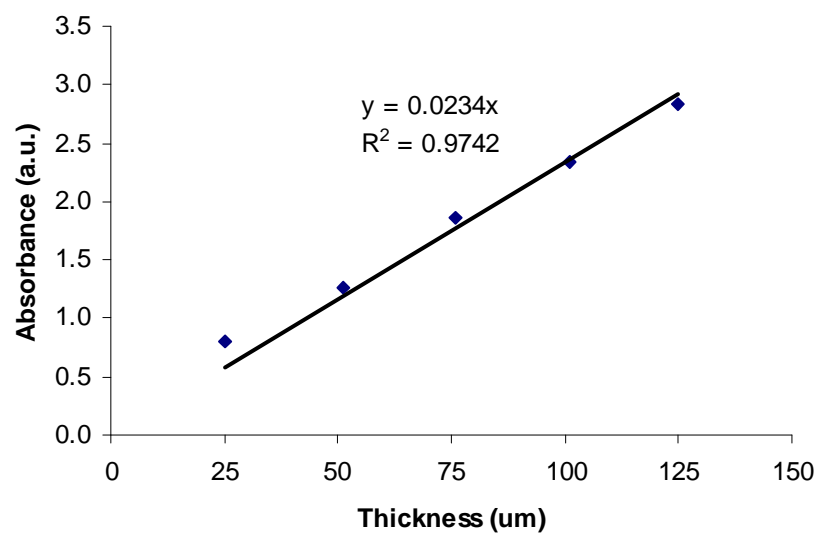
Figure 5.6 The calibration curves of pure PI at 500 nm, this absorbance value were denote Ao.
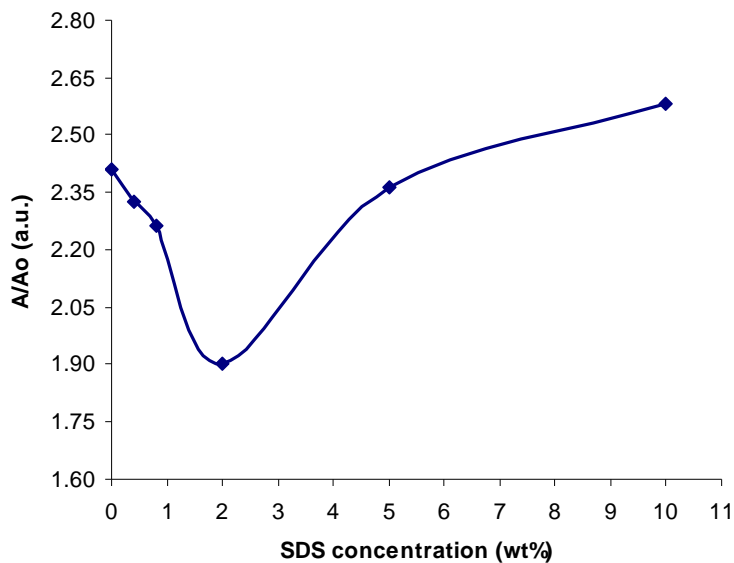
Figure 5.7 UV-vis spectra of 0.5wt% of CB in polyimide as a function of SDS concentration (wt%) at 500 nm.

The absorbance of nanocomposite films was sharply dimished when SDS concentration reached to 2wt% (CB/SDS = 1:2). At this point, the curve exhibited the optimum ratio of CB to SDS on the well dispersed, aggregated size reduction and interaction with matrix medium of CB in nanocomposites that affect the transparent properties. In contrast, when SDS concentration grew greater than optimum point, the absorbances of nanocomposite films were increased. This phenomenon demonstrated that at higher SDS concentration, CB particulates were clusters and became larger and denser. Such behaviors can considerably be adsorbing the spectra which result in losing transparent properties. This is also verified in the TEM image of polyimide nanocomposite films.

5.1.5 The effect of SDS on morphology of nanocomposite films

The effects of SDS concentration on the dispersion state and agglomeration behavior of CB in polymer matrix were studied using TEM, because it is a key factor that influences the composite properties. Figure 5.8 show TEM micrographs of 0.5 wt% CB in polyimide matrix contained various ratio of CB to SDS. The entire specimens were prepared by surface cross-section before analysis. Fig. 5a exhibit nanocomposite films without surfactant, the cross-section fracture surface is rather rough because of the presence of large CB particles in the form of agglomerates that separated from the matrix. The similar result was also observed in nanocomposite

films contain 1:0.4 and 1:0.8 CB/SDS ratio, in Figure 5.8(b) and (c) respectively. At this SDS amount, the addition of SDS was not concentrated enough to isolate CB aggregates to form small particles. The result demonstrated that the dispersion of CB in PI matrix was poor and inhomogeneous due to the weak interfacial interaction between CB and polymer matrix. Therefore, the fracture surface of the CB/PI nanocomposites with a tiny SDS amount tend to maintain their original shape (Composites without SDS) result in slightly decrease of absorbance value of UV-vis spectra (Figure 5.7). The TEM image of nanocomposite films with 1:2 CB/SDS ratio more clearly highlight the difference between these nanocomposites, show in Figure 5.8(d). It was found that the obtained nanocomposite films have smallest partly of CB aggregates in homogeneous PI matrix, that mean the preparation of nanocomposite films with 1:2 CB/SDS ratio in presence of ultrasonication can be overcome interparticular force of CB.

The SDS could dramatically decrease size of CB agglomerates while increase the dispersion between CB and matrix due to the complete coverage of CB surface by a thin surfactant layer cause electrostatic or steric repulsion reversed to carbon-carbon attraction. This clearly demonstrated that CB and polymer were compatible with each other, resulted in the significant decreasing of the absorbance value (Figure 5.7, 1:2 CB/SDS ratio) and the improved transparent properties of films. For the greater amount of SDS (more than 1:2 CB/SDS ratio), CB was re-agglomerated and randomly distributed. When the concentration of SDS was far over CMC point, CB tended to clusters and became the aggregates in the suspension that probability prone to incorporate into polymer matrix. Figure 5.8(e) show the inhomogeneous CB in polyimide matrix and the micro-agglomerated CB size was achieved when ratio of CB/SDS was over 1:10 (Figure 5.8(f)). Thus, the absorbances of UV-vis spectra in nanocomposite films were increased in both concentrations. The agglomerated sizes were larger in lower viscosity polymer matrix due to the dispersion in the low viscosity are easier to agglomerate together by Brownian movement. The differences in distributed state, particles size and compatibility with polymer matrix come from the appropriated ratio of CB to SDS in media.

(a)

(b)

(c)

(d)

(e)

(f)
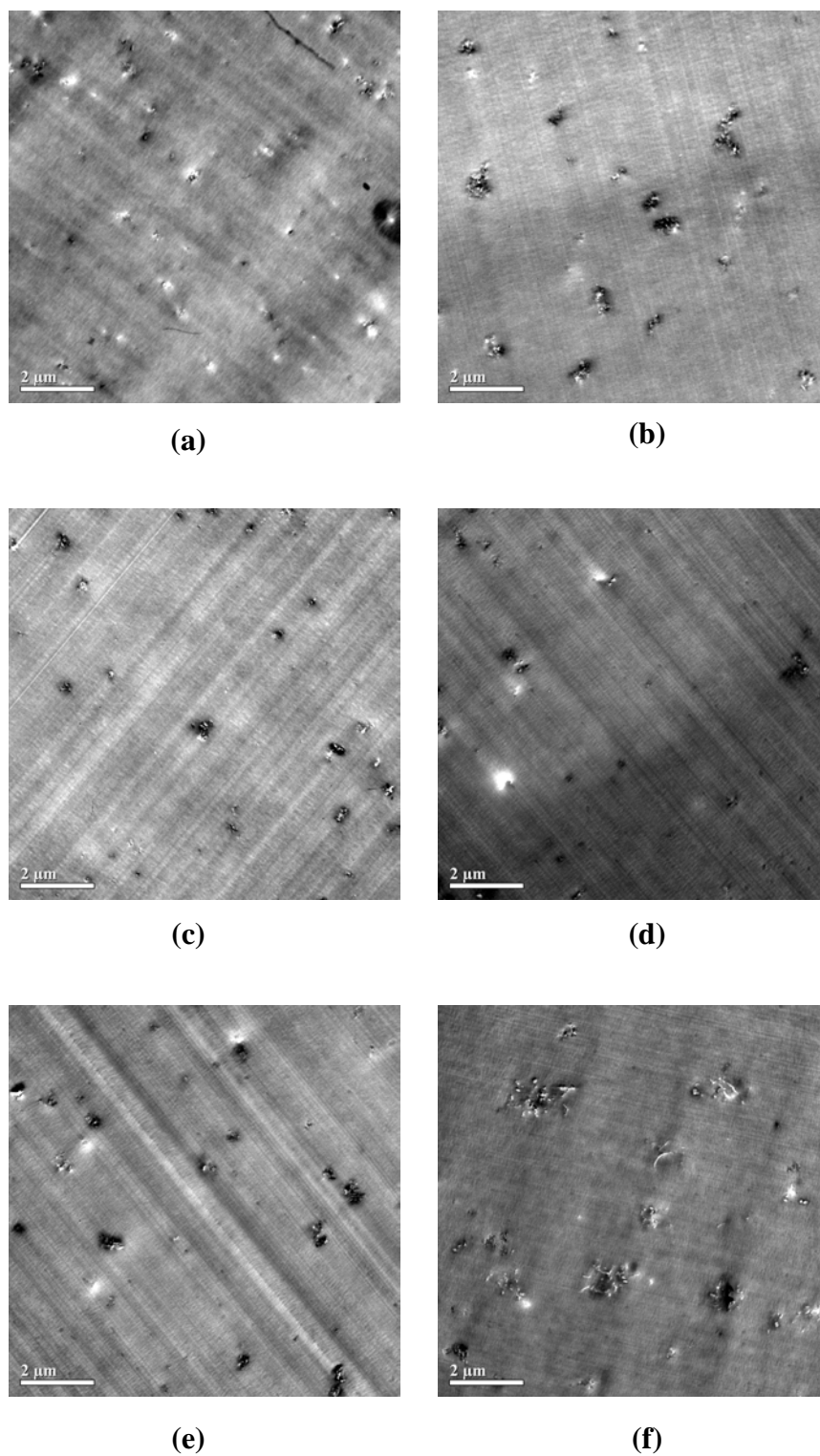
Figure 5.8 TEM images of 0.5wt%CB/PI nanocomposite films (a) contain various CB/SDS ratio 1:0.4 (b), 1:0.8 (c), 1:2 (d), 1:5 (e) and 1:10 (f). The entire specimens were prepared by surface cross-section.

5.1.6 The electrical properties of the nanocomposite films

It is well known that the incorporation of conductive filler can greatly alter the electrical properties of the polymer medium. The conducting behavior of carbon black filled polymer matrix depends strongly on the gaps between aggregate structures. When the aggregates are closely packed, the conductive networks are well established throughout the matrix which allowed electrons to pass the particles and the tunnel between the gaps resulted in the insulating properties of the PI matrix. Figure 5.9 shows the dielectric constant of the CB/PI nanocomposite films without the surfactant as a function of CB content. The addition of CB will directly influence the dielectric properties of CB containing nanocomposites. The dielectric constant of the nanocomposites increased with an increase in the CB content. The sharp increase when the mass loading of CB up to 0.1 wt% suggested the critical value of the aggregates that touched each other to form a conducting network as known as percolated structure. When the carbon black concentration was increased further, the dielectric constant increased slowly due to the electrons tunnel becomes saturated.
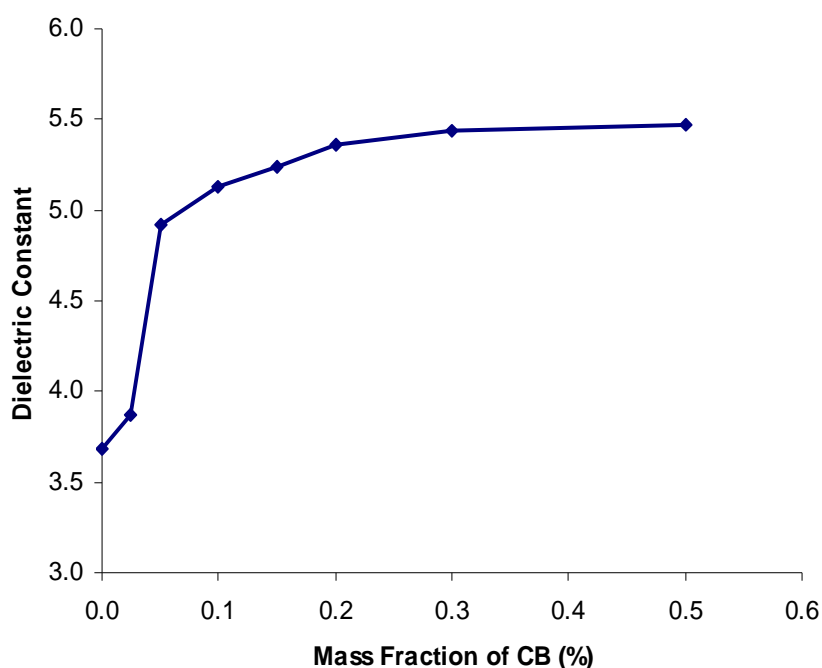
Figure 5.9 Dielectric constant of the CB/PI nanocomposites with the content of CB (1 kHz).
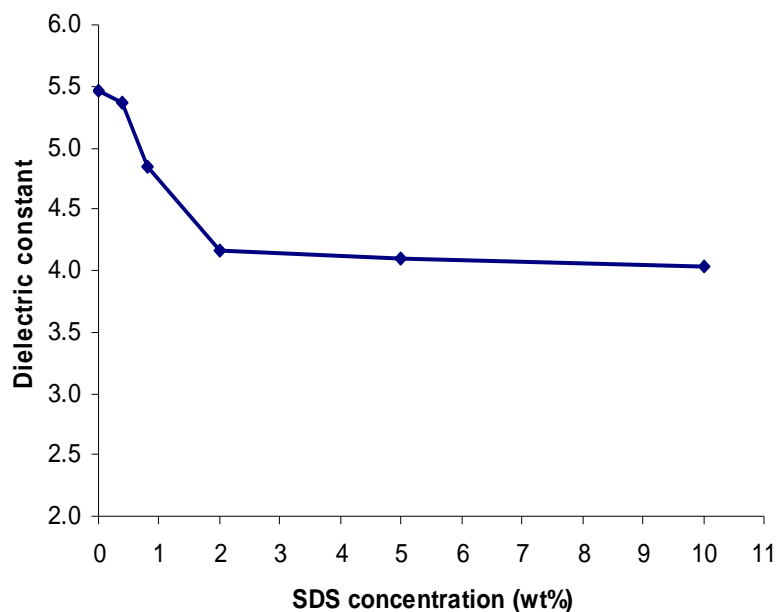
Figure 5.10 Dielectric constant of the CB/PI nanocomposites contain 0.5wt%CB as function with SDS concentration (1 kHz).

Figure 5.10 shows the effect of surfactant on the dielectric constant of nanocomposites containing 0.5wt% of CB. The dielectric constant of the nanocomposites decreases with increasing the content of SDS, which significant declined from 5.46 to 4.16 when SDS concentration up to 2wt%. This result is due to the reduction in the agglomerated size and the remains well dispersed of CB in polymer matrices result in the electrical short the network of conducting pathways, which make it difficult for the charge carriers to pass through the material. At the higher SDS concentration, TEM images of nanocomposites containing 5 and 10 wt% of SDS loading (Figure 5.8(e) and (f)) show the large aggregates of CB in polymer matrix, however, the dielectric constant of these composites were gradually decreased. This phenomenon related to the specific properties of SDS which caused the dielectric constant of pure PI films to decline from 3.50 to 3.09 when adding 0.5wt% SDS into PI matrix. Thus, we are suggested that at the higher SDS concentration in the CB/PI nanocomposite films (CB/SDS ratio more than 1:5), the dielectric constant were dominated by the influence of surfactant.

5.1.7 The mechanical properties of nanocomposite films

The influences of filler and surfactant content on the mechanical properties of the reinforced-polymer were investigated as in Table 5.2. At least five specimens were tested for each loading fraction. It was clear that incorporation of CB in the polyimide bulk have better tensile strength and Young's modulus than the pure polyimide. As the CB in the polymer increases, the tensile strength gradually improves from 84.60 MPa for pure PI to 90.11 MPa for the 0.5wt% CB/PI nano-composites (CP2). At the same weight CB loading in the polyimide, 0.5wt%CB/PI nanocomposites, the tensile strength of the nanocomposites increased at lower CB/SDS ratio but decreased at higher content. The maximum value of 107.60 MPa for 1:2 CB/SDS ratio nanocomposite films was reached. In order to explain these results, it should be mentioned that, in relation to what observed on Figure 5.8, it has been widely accepted that interfacial interaction between the filler and matrix was an important factor affecting the mechanical properties of the nanocomposites. Thus, by increasing the CB/SDS ratio in the nanocomposite films, the well dispersion states of CB were improved and optimum at CB/SDS ratio up to 1:2.0 as showed in Figure 5.8(a-d).

Table 5.2 Mechanical properties of the CB/PI nanocomposite films.

Composites	CB loading (wt%)	CB/SDS ratio (wt%)	Tensile strength (MPa)	Young's Modulus (MPa)
pure PI	0	0	84.60	2418.47
CP1	0.2	0	88.01	2463.05
CP2	0.5	0	90.11	2482.92
CP3	0.5	1:0.4	93.14	2578.41
CP4	0.5	1:0.8	101.76	2620.03
CP5	0.5	1:2.0	107.60	2628.23
CP6	0.5	1:5.0	92.52	2655.39
CP7	0.5	1:10.0	87.57	2662.72

The improvement in these dispersion states may be caused by the strong interaction between CB and polyimide chain, which leaded to increasing the tensile strength performance of the composites. On the other hand, at the higher CB/SDS ratio in the composites the formation of aggregate is higher (Figure 5.8(e) and (f)), which diminished the interfacial filler-polymer adhesion resulted in the decrease of the tensile strength. The Young's modulus of the nanocomposites increased with increasing CB/SDS ratio indicating that the incorporation of SDS surfactant in the nanocomposites makes them more brittle. The relation curves between absorbance (A/Ao) and mechanical and electrical properties of the CB/PI nanocomposite films were displayed in figure 5.11.
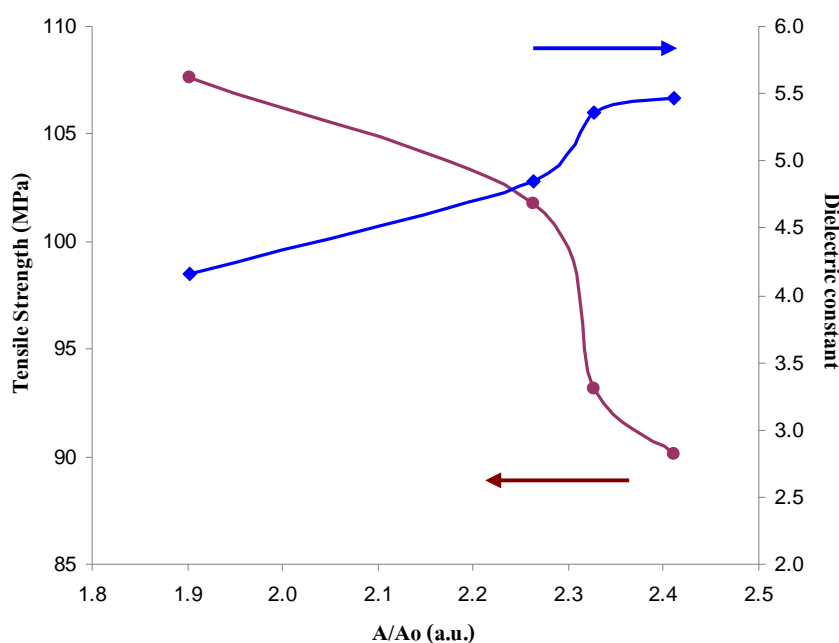
Figure 5.11 Tensile Strength and Dielectric constant of the 0.5wt% CB/PI nano-composites contain various CB/SDS ratios as function with Absorbance.

In the first experiment section, the CB/PI nanocomposite films, the effects of SDS surfactant on the dispersion state, electrical and mechanical properties of the CB/polyimide nanocomposite films were explored. This section can be concluded that the UV-vis spectra and TEM images were evidenced that the addition of surfactant increased level of dispersion of carbon black in the nanocomposite films due to the prevention of carbon black agglomeration and the improvement of transparent properties. When the concentration of surfactant was far above CMC, the dispersion

state and agglomerated size of carbon black in composite films were reverse. Dielectric properties of the CB/polyimide nanocomposite films without surfactant increase with increasing the CB loading and decreased as the addition of surfactant. The tensile properties of the CB/polyimide nanocomposite films were improved by surfactant amount until up to 1:2 CB/SDS ratio and optimum at 0.5 wt% of CB in composites. The incorporation of SDS into the CB/PI nanocomposites makes them more brittle. These results from the first section were used as a basic study for fine tune condition applicable of secondary experimental section, the aligned CNT/PI nanocomposite films.

5.2 The aligned CNT/polyimide nanocomposite films

5.2.1 SWNT and modified SWNT (SWNT-COOH)

The entire carbon nanotubes used in this experiment were purchased from Nanostructured & Amorphous Materials Inc., USA. According to the manufacturer's specifications, they were produced by catalytic CVD method, which have purity 95% CNT, 90% SWNT, 1-2 nm of average diameter and 5-30 µm in length.
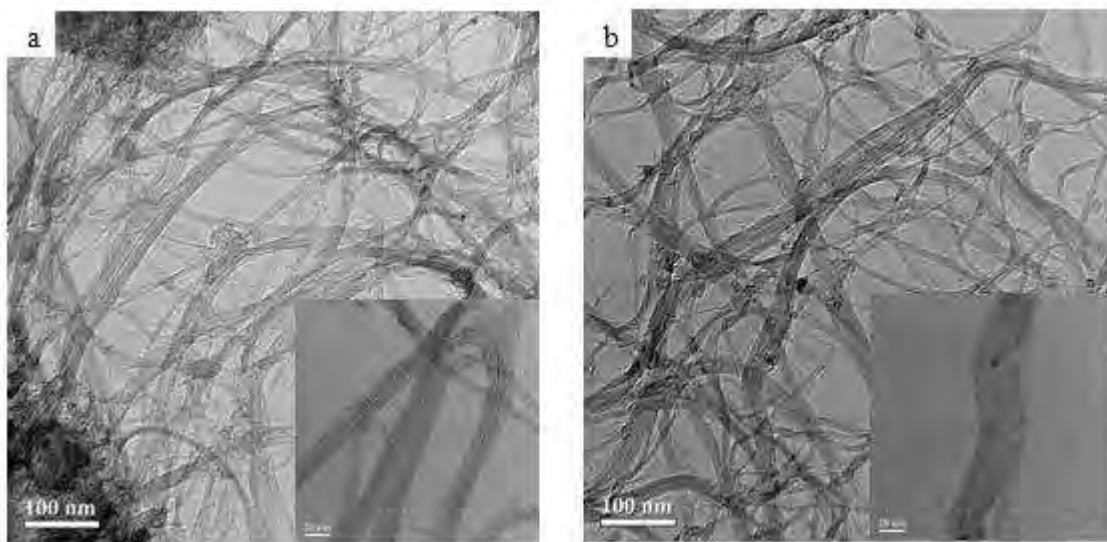

Figure 5.12 Typical TEM micrographs of SWNT (a) and SWNT-COOH (b).

Figure 5.12 showed the TEM images for these two kinds of nanotubes, evidence that the most of all as-synthesized CNT were curled and entangled into bundles structures with average size larger than 20 nm due to their high aspect ratio and strong Van der Waals interaction. Carbonaceous impurities typically include amorphous carbon, fullerenes, and graphite particles could also be observed. However, the easy to agglomerate, bundle together and entangle of CNT leading to many defect sites in the composites and limiting the efficiency of CNT on polymer matrices.
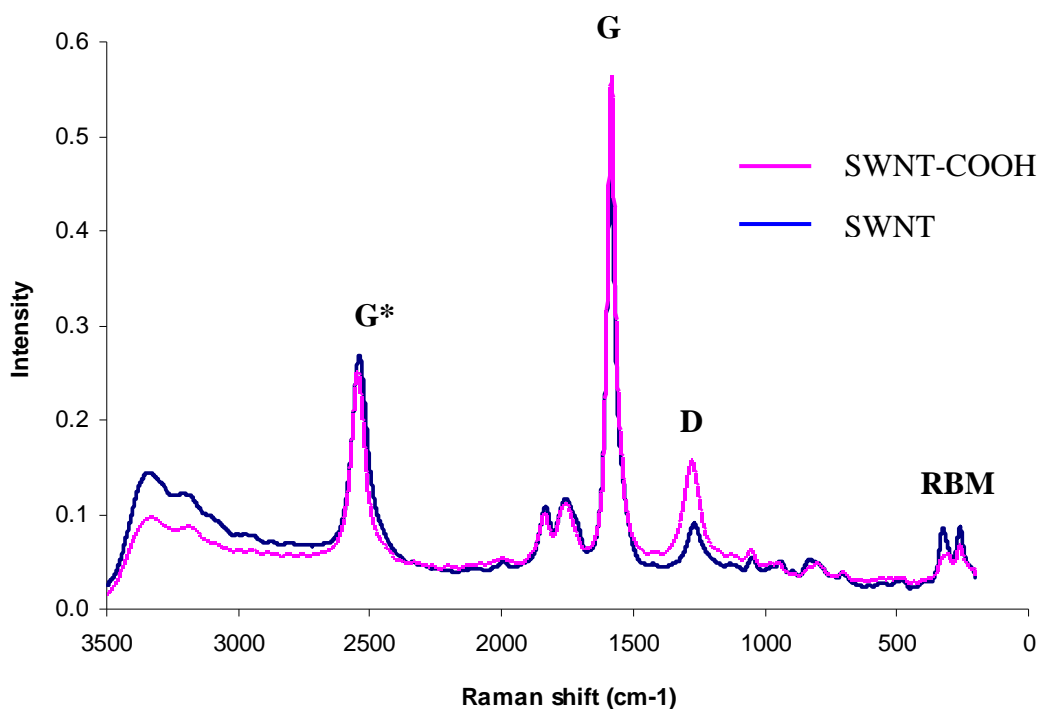
Figure 5.13 Raman spectrums of SWNT and SWNT-COOH.

The unique one-dimensional molecular nature of SWNT makes the resonance Raman technique an extremely useful and accurate method for the identification of materials through the characteristic vibration of certain structures. The Figure 5.13 is the full range Raman spectrum of a SWNT and SWNT-COOH. The most prominent Raman active peak in carbon nanotubs are the low frequency, radial breathing modes (RBM) and higher frequency, the disorder induce D-band, the tangential G-band (derived from the graphite like-in plane mode) and G* band (second-order Raman scattering from D-band vibrations). While D, G, and G* modes are also found in graphite, the RBM mode is a unique carbon nanotube mode.

The spectrum in the range of 150 to 350 cm^{-1} is the RBM, and is inversely proportional to the diameter of tube, making it an important feature for determining the diameter distribution of sample. Its absence in other graphite forms makes it a useful diagnostic for confirming the presence of nanotubes in sample. The feature in the range of 1250 to 1450 cm^{-1} is called D band, which is due to the defect on the nanotubes. The quality of a sample is often evaluated by comparing the D to G band intensity. For high-quality samples, without defects and amorphous carbon, the D/G ratio is often below a couple of percent. Also it can be used to qualitatively characterize the chemical functionalization of the tube. Side wall functionalization damages the tube, increasing the D band intensity. The G mode is a tangential shear mode of the carbon atoms. The most important aspect of this mode (1580-1590 cm^{-1}) is the characteristic Raman lineshape, which differs in accordance with whether the nanotube is semi-conducting or metallic. In case of semi-conducting tube, two Lorentzian features dominate the lineshape but in case of metallic tube, one Lorentzian is replaced by Breit–Wigner–Fano line. Also it can be used to mornitor the energy state change due to environment. The feature in the range of 2500-2900 cm^{-1} is the second order overtone of D band. It is an intrinsic property of the nanotube and graphite, and present even in defect-free nanotube when the D band is completely absent. It is widely used to monitor the load transfer between SWNT and matrix. In Raman spectrum, the D band intensity was increased in SWNT-COOH compared to raw SWNT. The I_D/I_G peak intensity ratios of SWNT-COOH exceed these of SWNT. This result provided direct evidence of the modification of SWNT.

5.2.2 Surfactants for dispersing carbon nanotubes

In the first of experiment section, the CB/PI nanocomposite films system, we concluded that the optimum ratio of CB to SDS in suspension which achieved well dispersion CB, good transparent property and the highest tensile strength in the nano-composite films was 1:2 (by weight). Therefore, this condition of the CB/PI nanocomposites system was used a reference to study the CNT/PI nanocomposites system. We made the CNT/SDS suspension by comparing the surface area between CNT and CB ($S_{CNT} = 569.57$ m^2/g and $S_{CB} = 76.76$ m^2/g), but the SDS amount was remained constant. Consequently, 1:14.8 CNT/SDS ratio of 0.0203 %w/v suspension was established. Junrong Y. *at el.* [45] has been reported that the optimum ratio of CNT to SDS was 1:1.5. Therefore, 1:1.5 of CNT/SDS ratio was also performed.
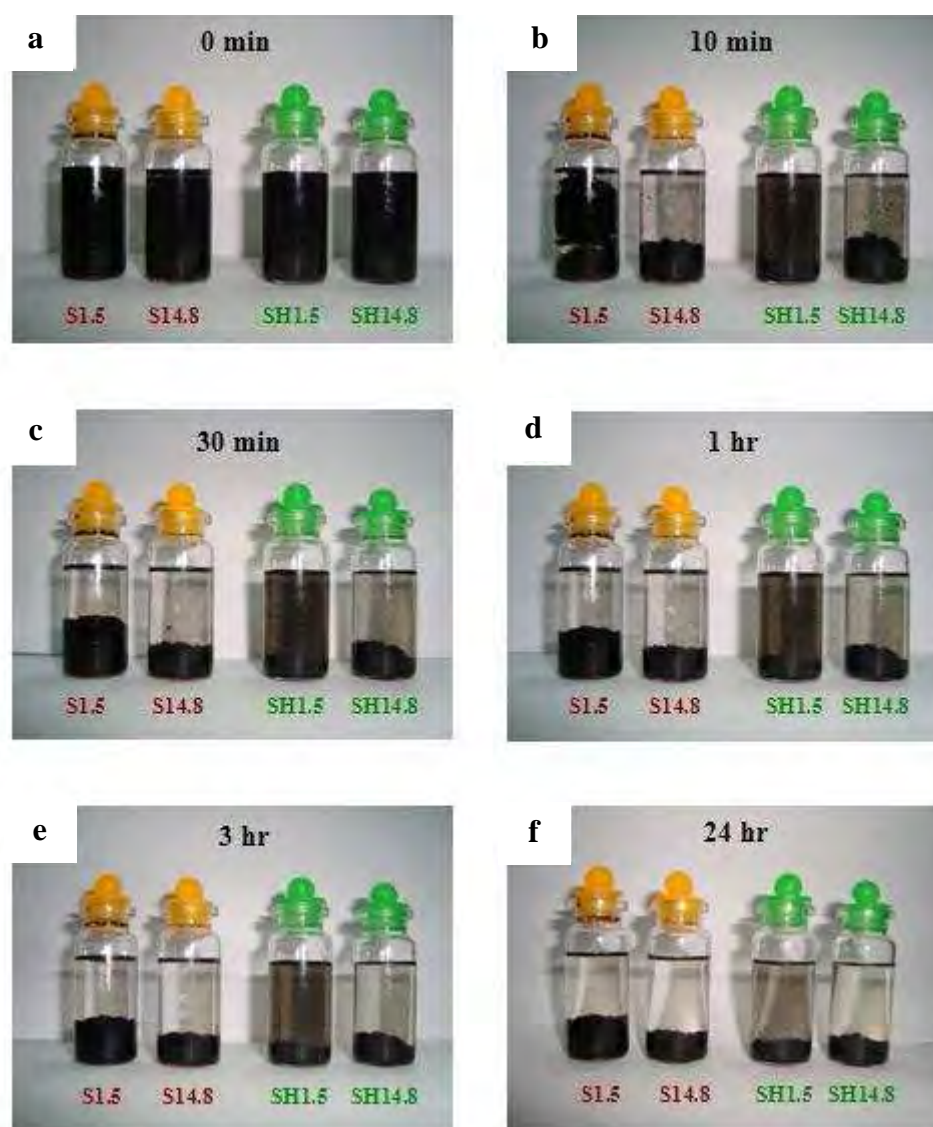
Figure 5.14 SWNT (S1.5 and S14.8 was 1:1.5 and 1:14.8 of SWNT/SDS ratio, respectively) and SWNT-COOH (SH1.5 and SH14.8 was 1:1.5 and 1:14.8 of SWNT-COOH/SDS ratio, respectively) suspension as function with stable time, after ultrasonication immediately (a), 15 min (b), 30 min (c), 1 hr (d), 3 hr (e) and 24 hr (f).

Figure 5.14 show these two kinds of CNT suspension as function with stable time. After the sonication process, visual observation indicates that both of the CNT suspension stabilized with SDS were kept with no precipitation of nonotubes and the color remained constant, in Figure 5.14 (a).

A mechanism of nanotube isolation from a bundle with the combined assistance of ultrasonication and surfactant absorption was proposed [45]. The role of ultrasonic treatment is likely to provide high local shear, particularly to the nanotube bundle end. During the sonication process, the bundle ends of SWNT were frayed by high local shear and became the site for additional SDS adsorption, and then the SDS molecules gradually exfoliate the SWNT bundles in an unzippering mechanism. The absorption of SDS on CNT surface can prevent the re-aggregated of individual nanotube to bundle, due to electrostatic repulsion force. However, the sedimentation of two types of SWNT can be observed in Figure 5.14 (b-f). At higher SDS concentration, the clusters become larger and denser. Such a behavior can presumably be ascribed to the reduction of electrostatic repulsion forces between CNT due to the large ionic strength and the increasing concentration of surfactant aggregates, known as micelles. Micelles cannot fit in between two CNT bundles that are close to each other. As a result, the osmotic pressure of the micelles around bundles creates an effective attraction; this attraction is known as a depletion attraction. Thus, stable time and saturated sediment point of whole SWNT in suspension are not different, and lower when comparing with CB system.

5.2.3 Raman spectroscopy of the SWNT/PI nanocomposite films

After sonication process, the homogeneous SWNT suspension (1:1.5 of CNT to SDS ratio) was obtained. This suspension was mixed with polyimide monomer, and then the SWNT/PI solution was cast onto a dried glass plate, followed by evaporation and thermal imidization to produce the random SWNT/PI nanocomposite films.

Raman spectroscopy was employed to confirm the presence of carbon nanotubes in the composites. The Raman spectrum of the composite containing 0.5 wt% SWNT is illustrated in Figure 5.15. The spectrum shows characteristic peaks around at 179 and 1590 cm^{-1}, which correspond to the diameter dependent radial breathing mode (RBM) and the tangential G band of the SWNT, respectively. The RBM mode is the real signature of the presence of carbon nanotubes in a sample, since it is not present in graphite. The neat polyimide film gives rise to a featureless spectrum in the composite, due to SWNT are exceptionally good scatters and it may be that the SWNT overwhelm the spectrum. So, the feature of composites spectrum is rather similar the raw carbon nanotubes.
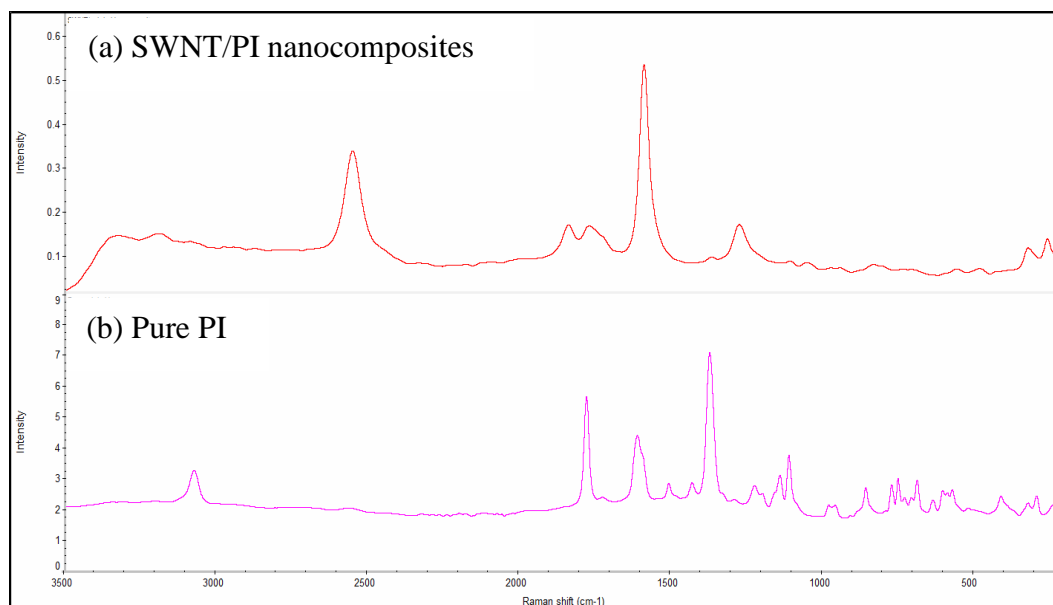
Figure 5.15 Raman spectra of (a) composite with 0.5wt% SWNT loading and (b) neat polyimide.

5.2.4 The optical microscopy of the aligned SWNT/PI nanocomposite films

After SWNT suspension was mixed with polyimide monomer, the SWNT/PI solution was cast onto a dried glass plate, a DC electric and magnetic field were separately and simultaneously applied for 7 min to induce the formation of an aligned structure, followed by evaporation and thermal imidization to produce the aligned SWNT/PI nanocomposite films. The optical images of some specimen are shown in Figure 5.16-5.18.
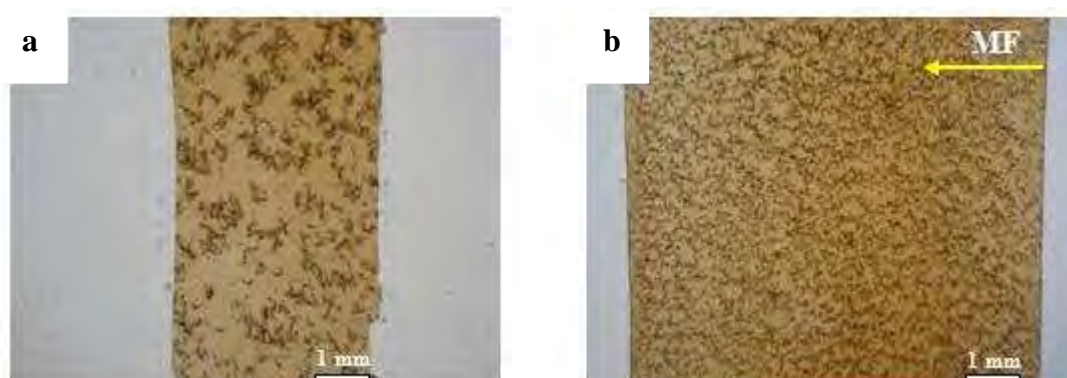

Figure 5.16 Optical micrographs of 0.5wt% SWNT/PI nanocomposite films; (a) random dispersion and (b) after applied 2 Tesla of magnetic field for 7 min.
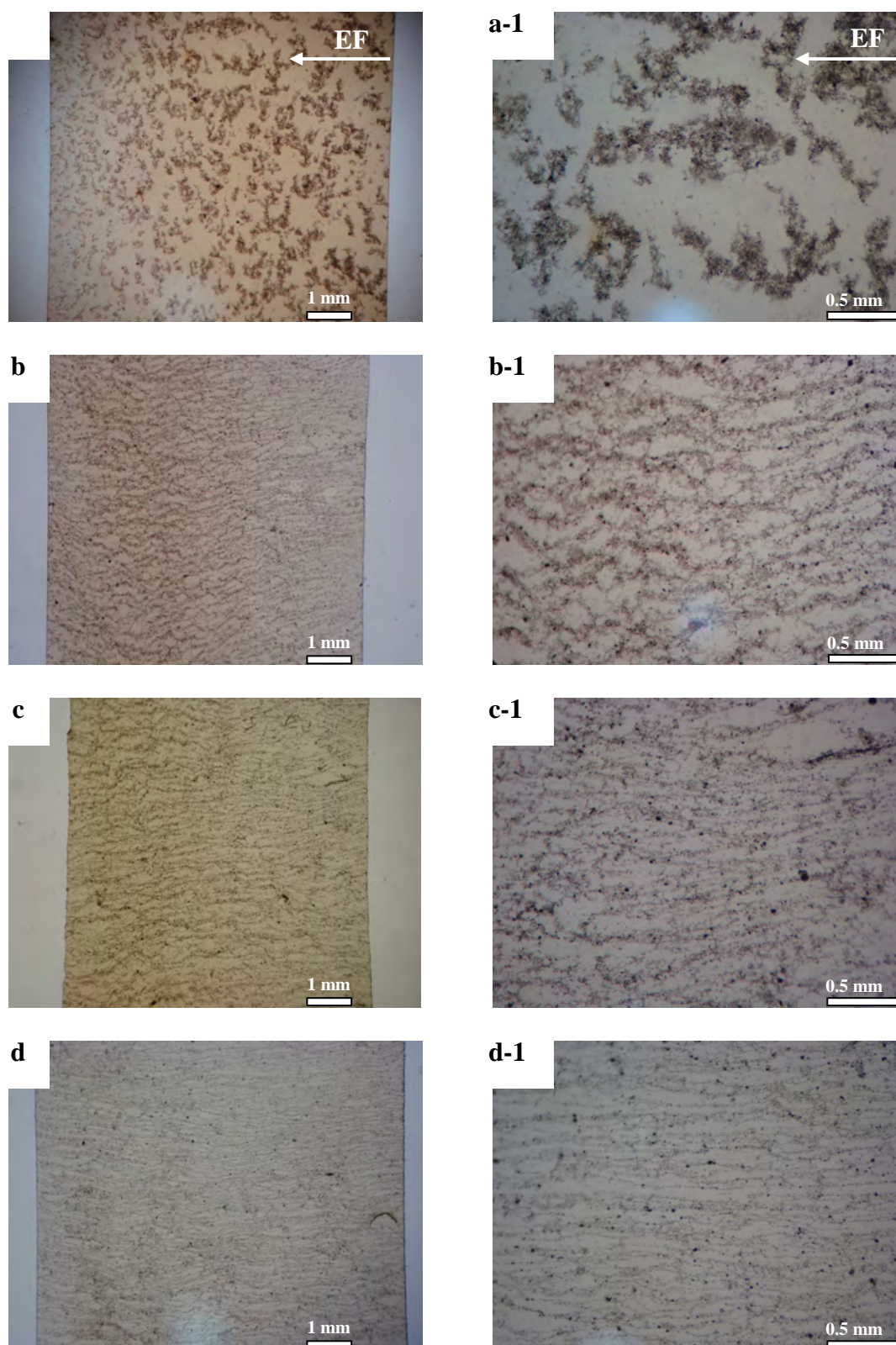
Figure 5.17 Optical micrographs of 0.5wt% SWNT/PI nanocomposite films with 7 min of applied DC electric field (a) 150 V/cm (b) 300 V/cm (c) 450 V/cm and (d) 600 V/cm. Magnification (right images) of the alignment structure of left images at (a-1) 150 V/cm (b-1) 300 V/cm (c-1) 450 V/cm and (d-1) 600 V/cm.
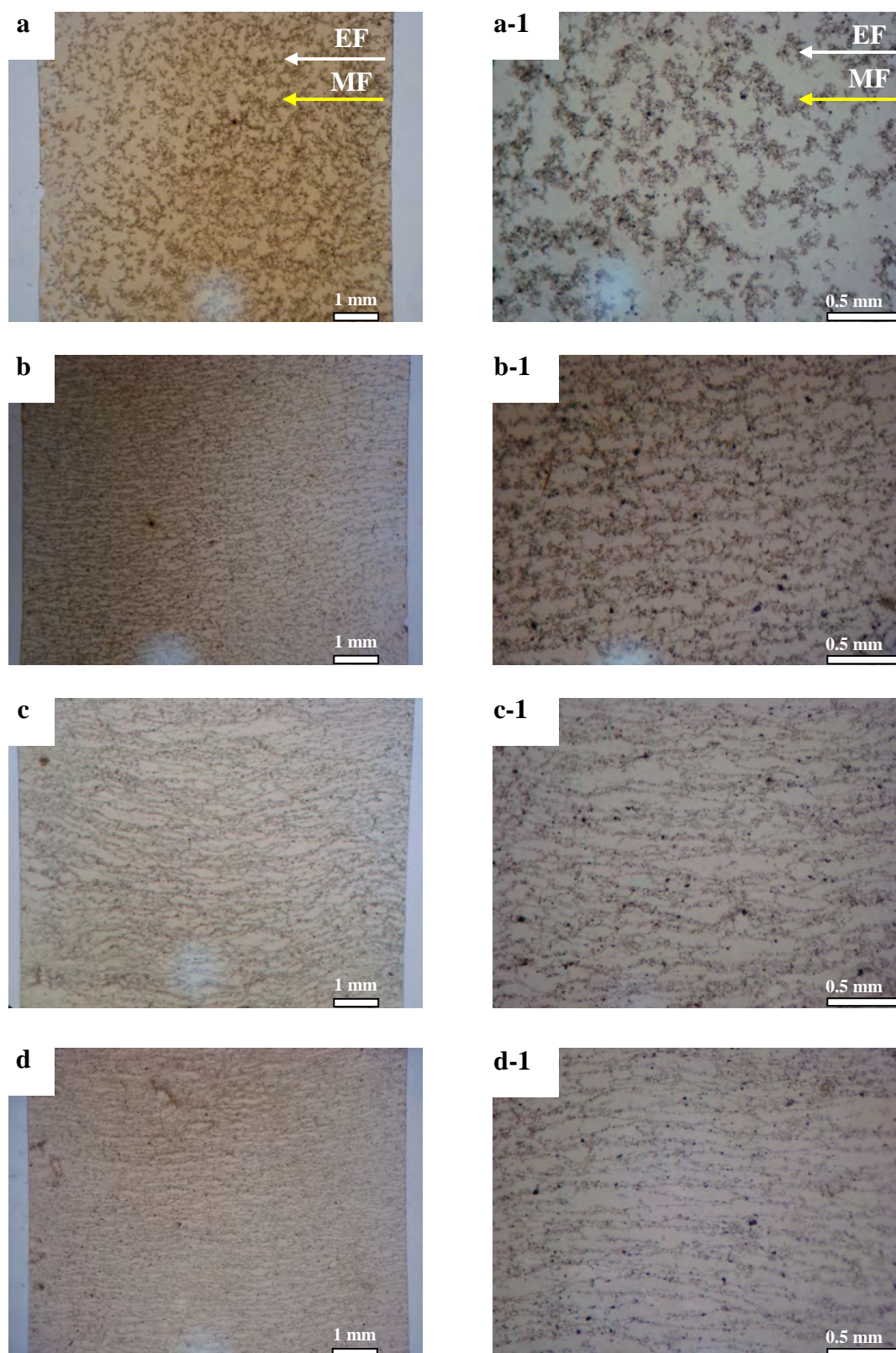
Figure 5.18 Optical micrographs of 0.5wt% SWNT/PI nanocomposite films with 7 min of simultaneously applied 2 Tesla magnetic fields and various DC electric field (a) 150 V/cm (b) 300 V/cm (c) 450 V/cm and (d) 600 V/cm (A system). Magnification of the left images show in the right image, (a-1) to (d-1) respectively.

To the study structural development of aligned carbon nanotubes in polyimide under the magnetic and electric field, the randomly and induce the orientation formation of nanotubes using external field were established. Figure 5.16 (a) shown the optical camera images of the 0.5wt% SWNT/PI nanocomposite film without inducing of electric and magnetic field. It was clearly seen that the distribution state of bundle SWNT in polyimide were not pattern, which indicate that random dispersion in composite film.

Carbon nanotubes have been shown to be highly susceptible to a magnetic field, which were materials in response to an applied magnetic field. Due to their magnetic susceptibility, it should be possible to place SWNT in a magnetic field and align them in common orientation parallel to the field direction. Figure 5.16(b) displayed the orientation of 0.5wt% SWNT in polyimide film under the effect of 2 Tesla magnetic fields for 7 min. Visible observation, SWNT slight generalized alignment while a large of quantity of the nanotubes are unextended. It would seem to indicate that the SWNT were in the process of aligning to directed towards the direction of the magnetic field, but were not able to completely alignment due to the 2 Tesla of magnetic field were not strong enough to achieve the perfectly structural alignment in the allotted processing time. The previously work [40], indicated that the much better nanotubes alignment was achieved when applied 15 Tesla of magnetic field.

A DC electric field applied to a dispersion containing 0.5wt% of SWNT in polyimide in parallel to the observation direction, as illustrated in Figure 4.9. Optical microscope observation allowed detailed characterization of the resulting aligned network structure of SWNT. Figure 5.17 shows a series of optical camera images of 0.5wt% SWNT/PI nanocomposite films as a function of DC field strength. At the lower field strength, Figure 5.17(a and a-1) (150 V/cm), SWNT in polyimide were slightly oriented, the most of nanotubes were retained to be agglomerated form. It was demonstrated that not sufficient field strength to induce the aligned structure. When field strength increases, the dispersed aligned SWNT were absorbed into an aligned and ramified network, show in Figure 5.17 (b-1)-(d-1). The better aligned structure of SWNT in composite films were achieved when field strength up to 600 V/cm, which demonstrated that the degree of alignment of nanotubes will be increase with

increasing the field strength. During the application of a DC electric field, a fraction of the carbon nanotubes was observed to move toward the anode, under electro-phoresis, verifying the presence of negative surface charges, but the deposition of all the SWNT in vicinity of the anode was not visible in the allotted processing time. We believed that 7 min of applied time was not enough to induce the deposition of the nanotubes at the anode, however, sufficient to the completely alignment formation of nanotubes across the Au electrode. The mechanism of the alignment and network formation of nanotubes under the effect of the electrode and magnetic field were illustrated in Figure 5.19 [38].
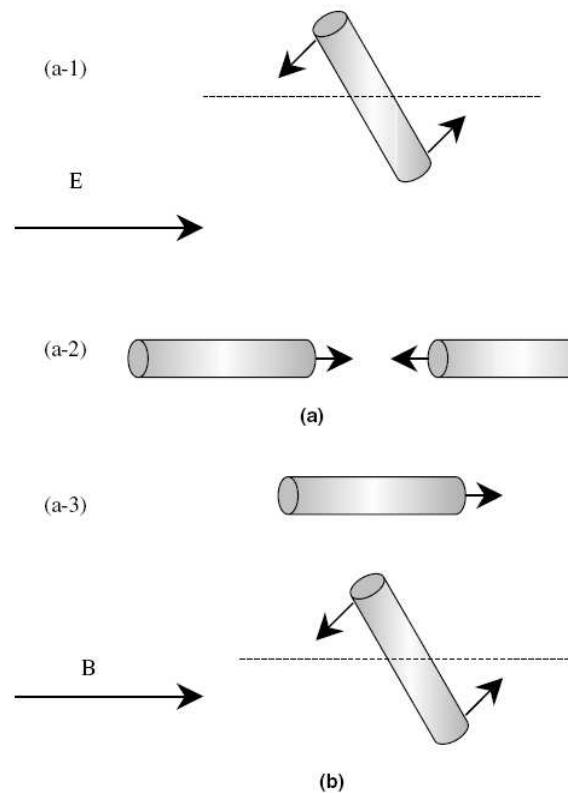

Figure 5.19 Schematic illustration of forces to which a CNT is subjected to under (a) a dc electric field ((a-1) rotation torque, (a-2) Coulomb force, and (a-3) electrophoresis, from top to bottom) and (b) a magnetic field (rotation torque).

Figure 5.19(a) shows a schematic illustrating the three forces, i.e., torque, Coulombic, and electrophoresis forces that act on each CNT due to a DC electric field. In the presence of the DC electric field, each CNT experience polarization. This polarization leads to a torque force (Fig. 5.19(a-1)) acting on each CNT. Columbic attraction (Fig. 5.19(a-2)) was generated among oppositely charged ends of different CNT. The

electrophoresis force (Fig.5.19 (a-3)) was induced by the presence of charged surfaces. Fig. 5.19(b) illustrates the torque force induce on a CNT by magnetic field. Under the effect of electric field, the SWNT were rotate, oriented, and moved toward the nearest electrode along the direction of the electric field. As soon as these nanotube are close enough to the electrode to allow charge transfer, the nanotubes discharge and adsorb onto the anode. Tip of nanotubes connected to the electrode then become sources of very high field strength and the location for adsorption of further filler particle. As a result, ramified nanotube network structures extend away from the anode, eventually reaching the cathode and providing conductive pathways throughout the sample.

A DC electric field and magnetic field were simultaneous applied to induce the aligned structure of SWNT in polyimide matrix along the supportive direction of the external field, as illustrated in Figure 4.10. It was believed that the incorporation of the electric and magnetic forces will be enhance the level of alignment that better than only using electric or magnetic field. The three forces of electric field (torque, Coulombic, and electrophoresis) and one force of magnetic field (torque) were displayed important role to improve the degree of alignment and ramified network formation for composite films. Figure 5.18 shows a series of the optical camera images of the aligned SWNT/PI nanocomposite films as a function various DC field strength with 2 Tesla of magnetic field constant. Figure 5.18 indicated that level of the alignment and ramified network structure was increased when increases DC field strength, and optimum reach to 600 V/cm with 2 Tesla

Comparison with the electric field system (Fig.5.17) at the same field strength, the lower field strength (below 450 V/cm), these systems with 2 Tesla of magnetic field are able to generate the well alignment more than the system without magnetic field, in which could visible observation. However, at higher field strength, the qualitative measurement of dispersed aligning by optical microscope can not use to verify because of both of system (with and without magnetic field) were slightly difference in the level of alignment and ramified network formation in composite films. Therefore, Raman spectroscopy was employed to qualitative assessment the degree of alignment of all the SWNT in polyimide matrix.

5.2.5 Raman spectroscopy of the aligned SWNT/PI nanocomposite films

Polarizer Raman spectroscopy is an important tool when attempting to characterize or assess the degree of alignment of carbon nanotubes in polymer matrix. SWNT nanocomposites show resonance-enhanced Raman scattering effect when a visible or near infrared laser is used as the excitation source, while the other pure polymers do not display such a resonance effect. The tangential peak (G-peak) of the SWNT in the Raman spectra is very sensitive to the polarizer, and is attributed to the elongation of the carbon-carbon bonds along the longitudinal axis of the nanotubes. Therefore, if the carbon nanotubes are aligned, there should be an increase in the G-peak intensity. When the polarizer is parallel to the aligned SWNT i.e. at an angle of 0°, the maximum intensity in the tangential peak is obtained. When the polarizer is perpendicular to the aligned SWNT i.e. at an angle of 90°, the minimum intensity in the tangential peak is obtained. When the polarizer angle is further increased to 180°, the maximum intensity of the tangential peak is obtained, as it is also again parallel to the aligned SWNT. The summery of the G-peak intensity of the whole specimens can be shown as below.
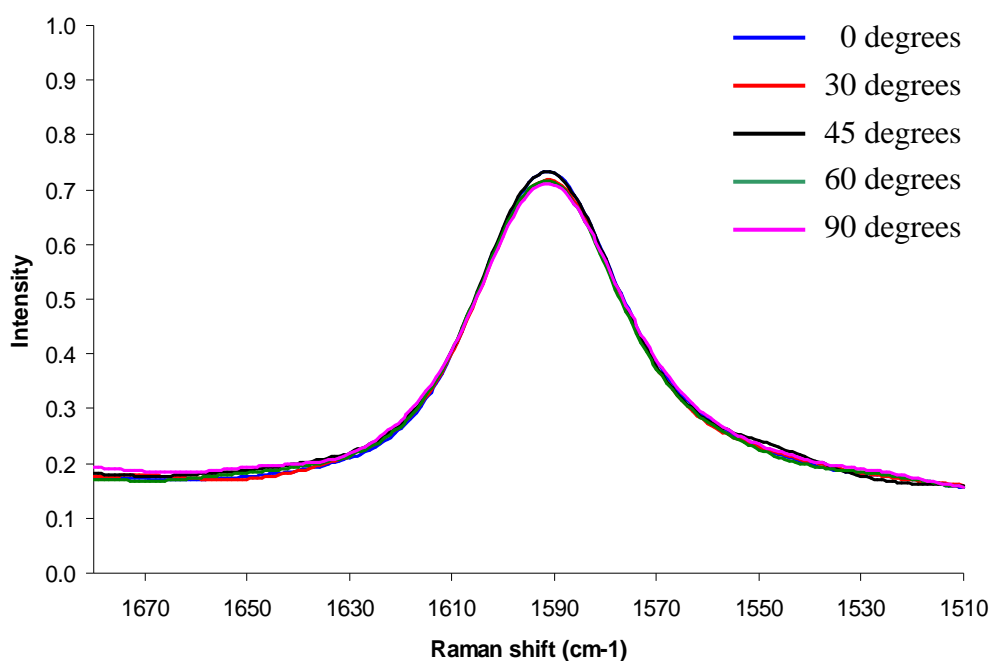

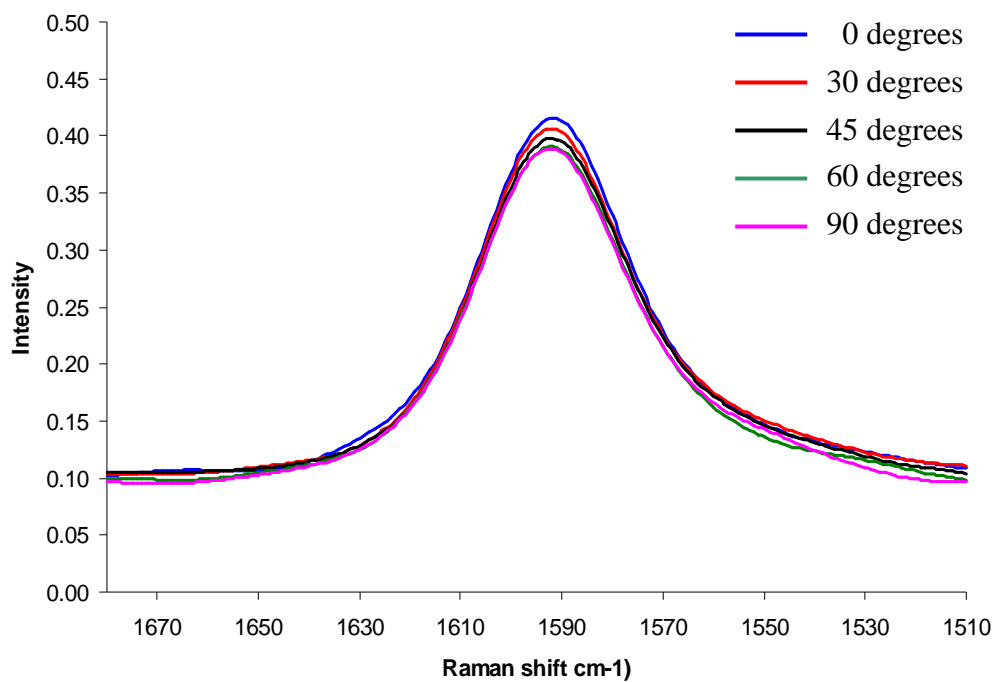**Figure 5.20** G-peak spectra of the random SWNT/PI nanocomposite films.

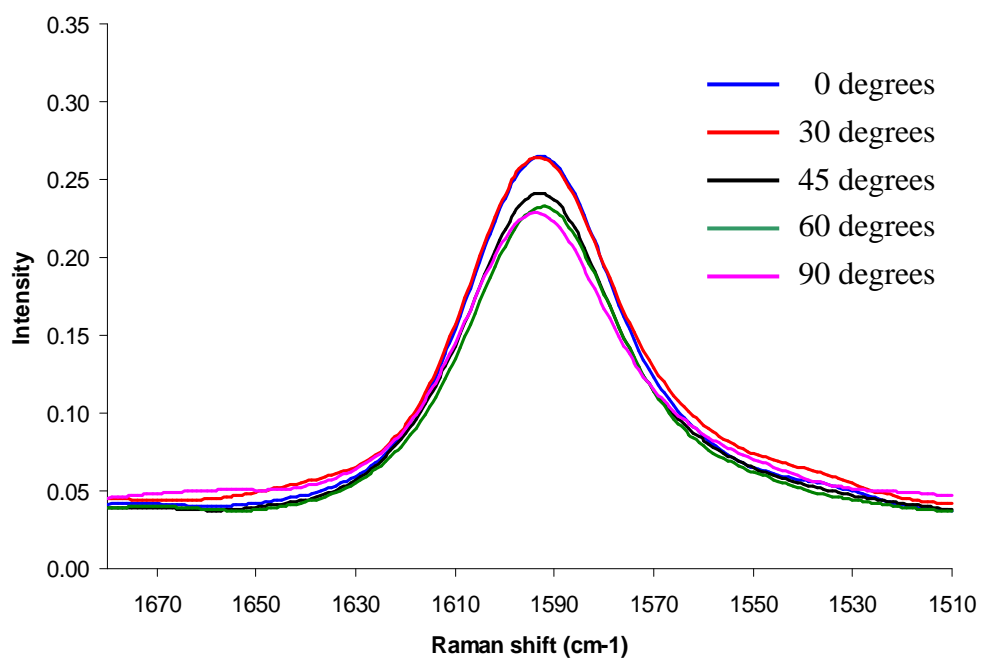**Figure 5.21** G-peak spectra of SWNT aligned by 2 Tesla of magnetic field.

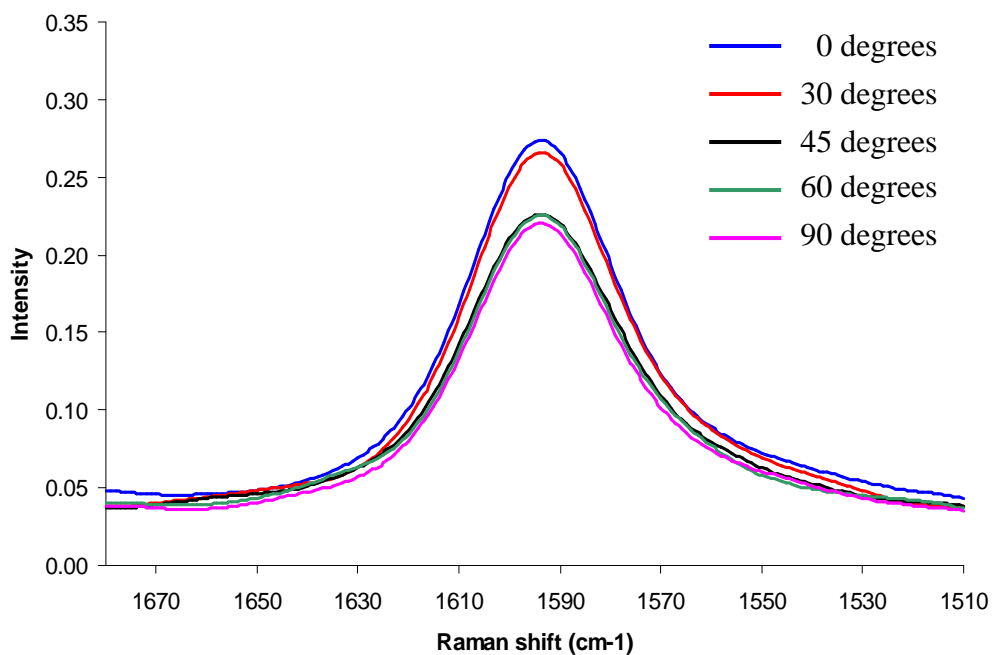**Figure 5.22** G-peak spectra of SWNT aligned by 150 V/cm of DC electric field.

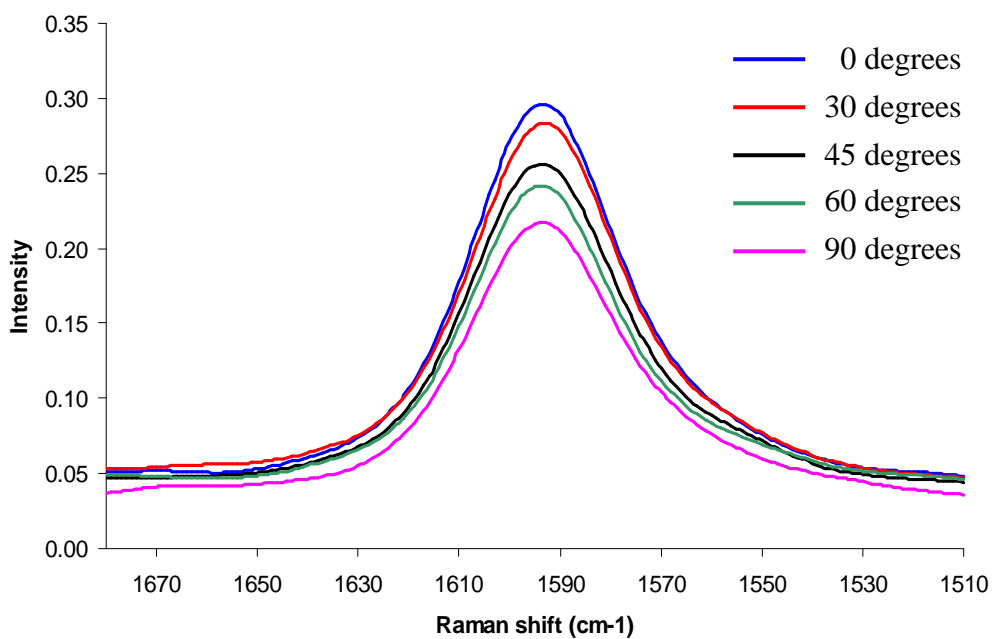**Figure 5.23** G-peak spectra of SWNT aligned by 300 V/cm of DC electric field.

Figure 5.24 G-peak spectra of SWNT aligned by 450 V/cm of DC electric field.
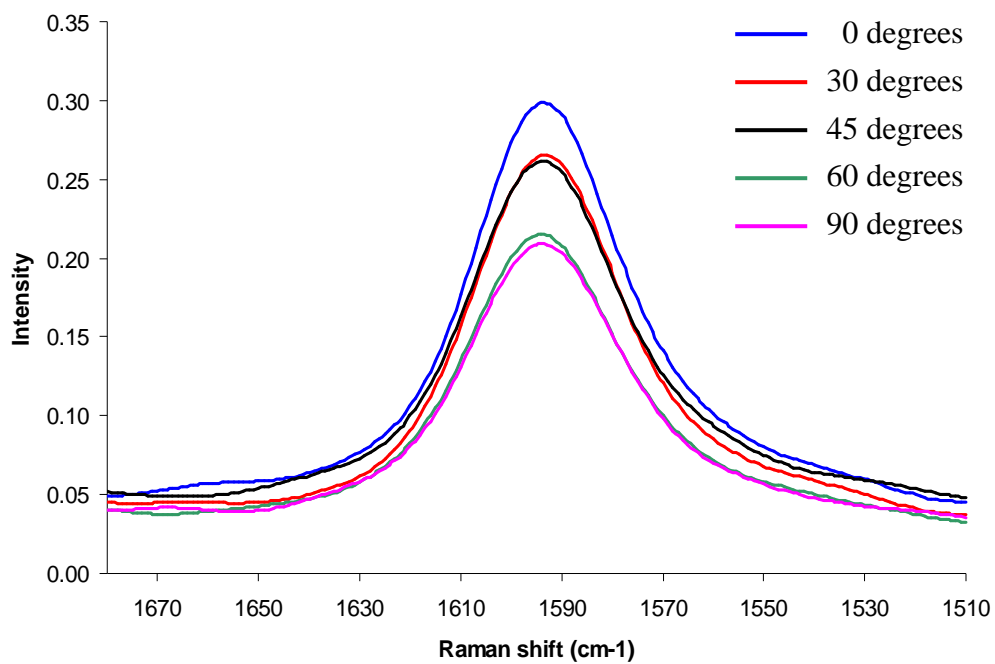
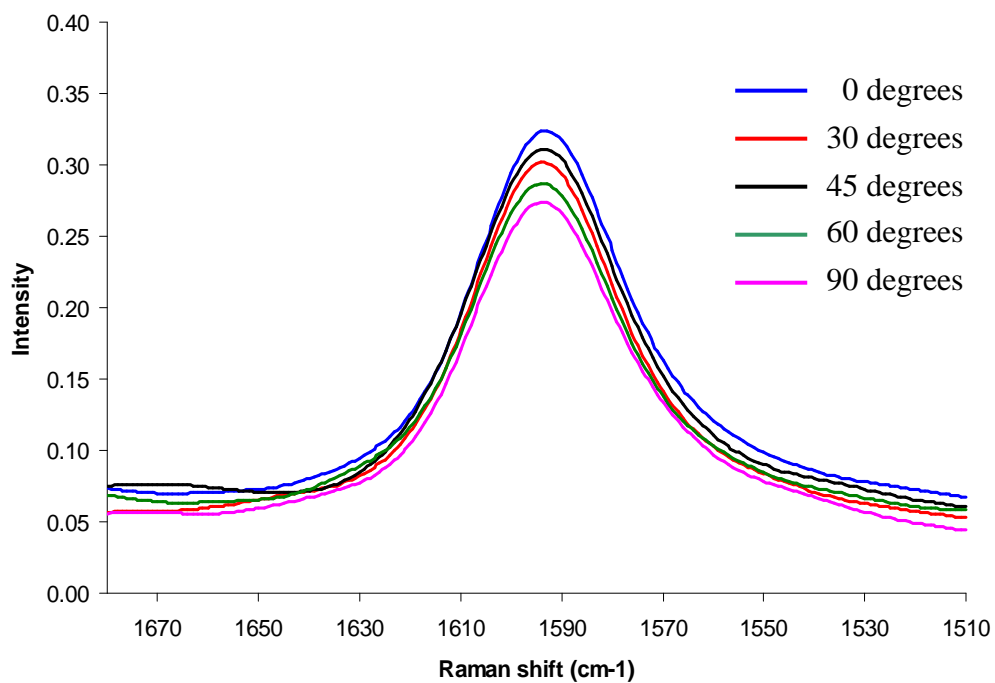**Figure 5.25** G-peak spectra of SWNT aligned by 600 V/cm of DC electric field.

Figure 5.26 G-peak spectra of SWNT aligned by 150 V/cm of DC electric field with 2 Tesla of magnetic field (A system).

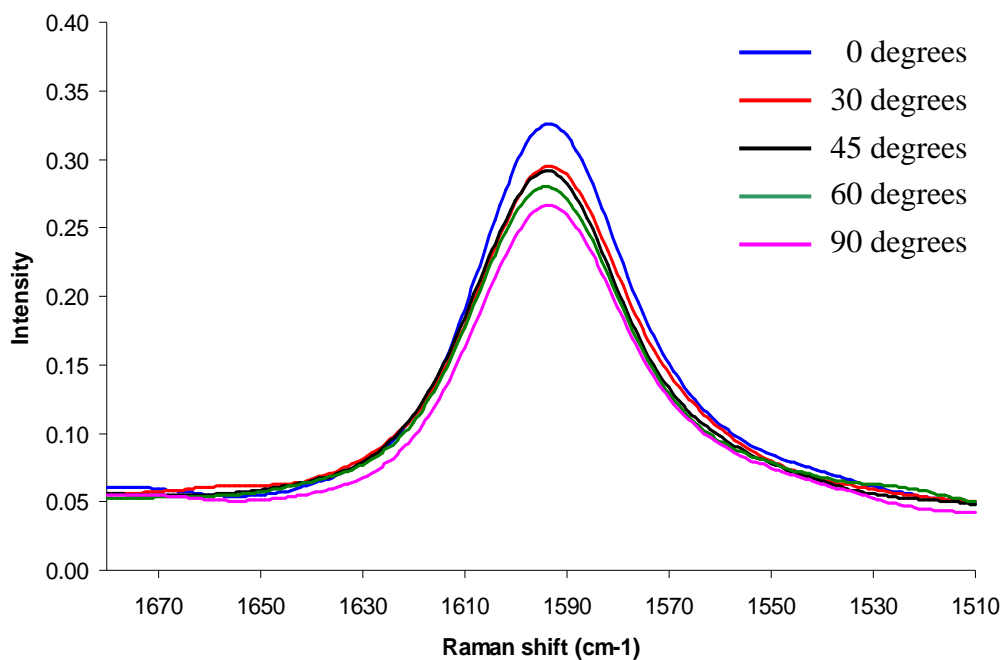**Figure 5.27** G-peak spectra of SWNT aligned by 300 V/cm of DC electric field with 2 Tesla of magnetic field (A system).
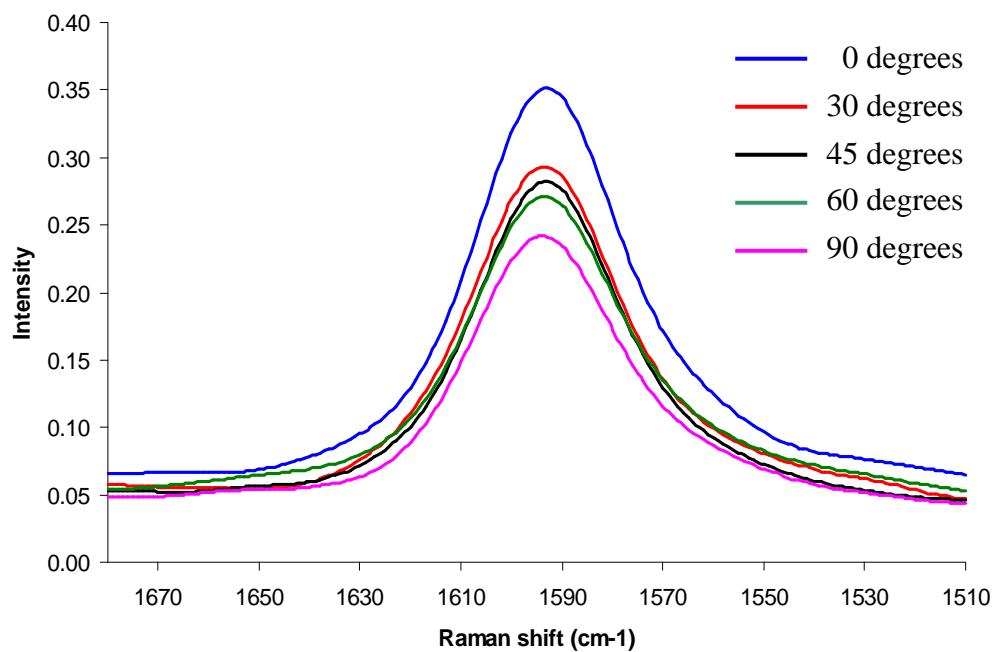
Figure 5.28 G-peak spectra of SWNT aligned by 450 V/cm of DC electric field with 2 Tesla of magnetic field (A system).
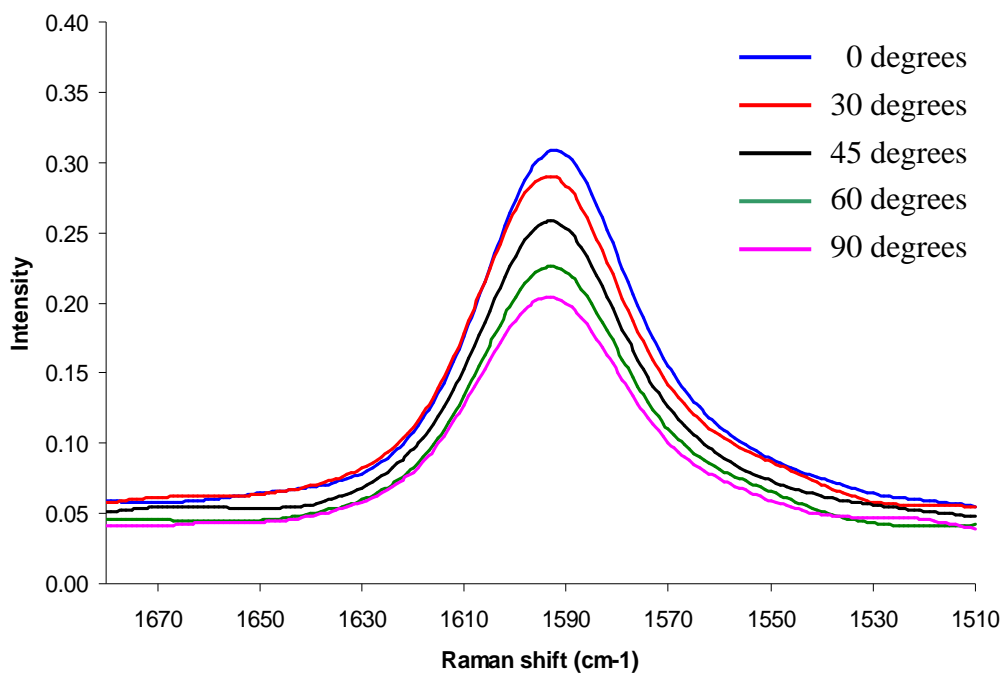
Figure 5.29 G-peak spectra of SWNT aligned by 600 V/cm of DC electric field with 2 Tesla of magnetic field (A system).
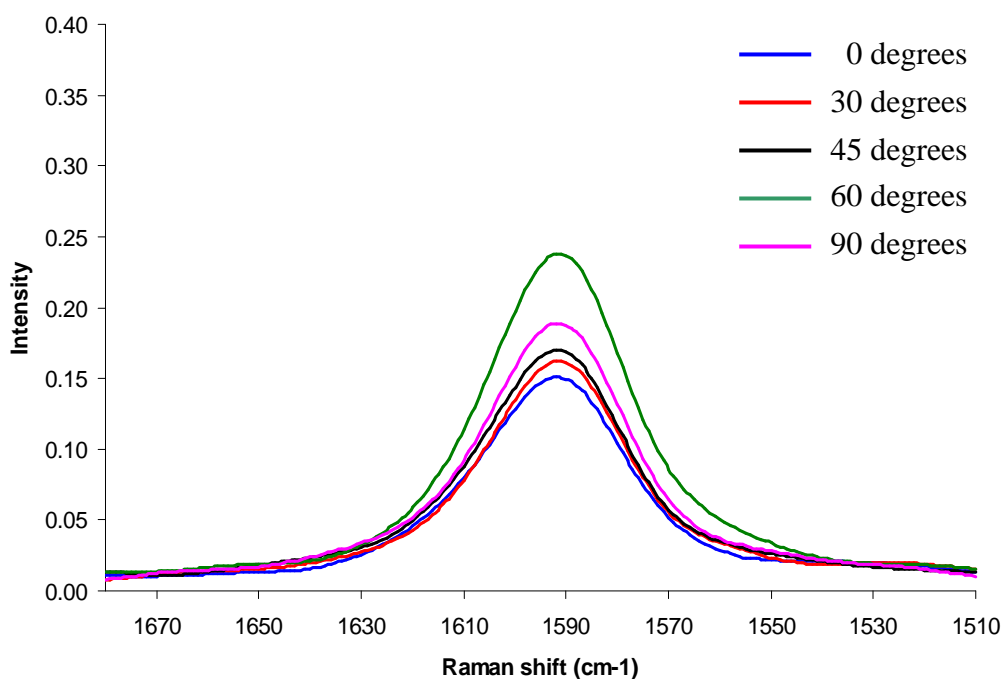
Figure 5.30 G-peak spectra of SWNT-COOH aligned by 600 V/cm of DC electric field with 2 Tesla of magnetic field (A system).

Figure 5.31 G-peak spectra of SWNT aligned by 150 V/cm of DC electric field with 2 Tesla of magnetic field (B system).

Figure 5.32 G-peak spectra of SWNT aligned by 300 V/cm of DC electric field with 2 Tesla of magnetic field (B system).

Figure 5.33 G-peak spectra of SWNT aligned by 450 V/cm of DC electric field with 2 Tesla of magnetic field (B system).

Figure 5.34 G-peak spectra of SWNT aligned by 600 V/cm of DC electric field with 2 Tesla of magnetic field (B system).
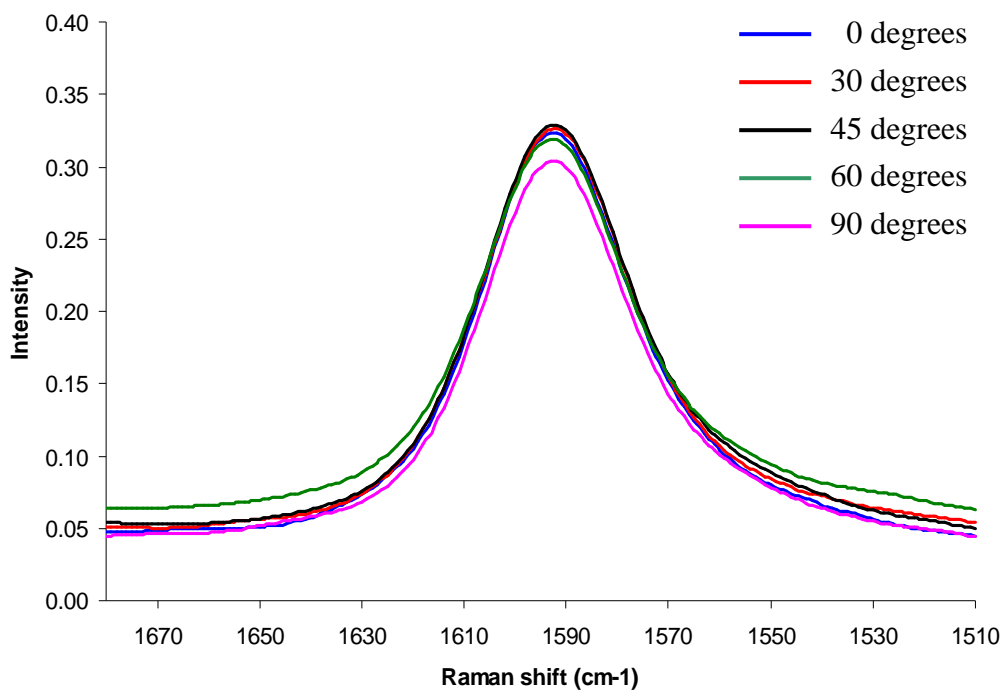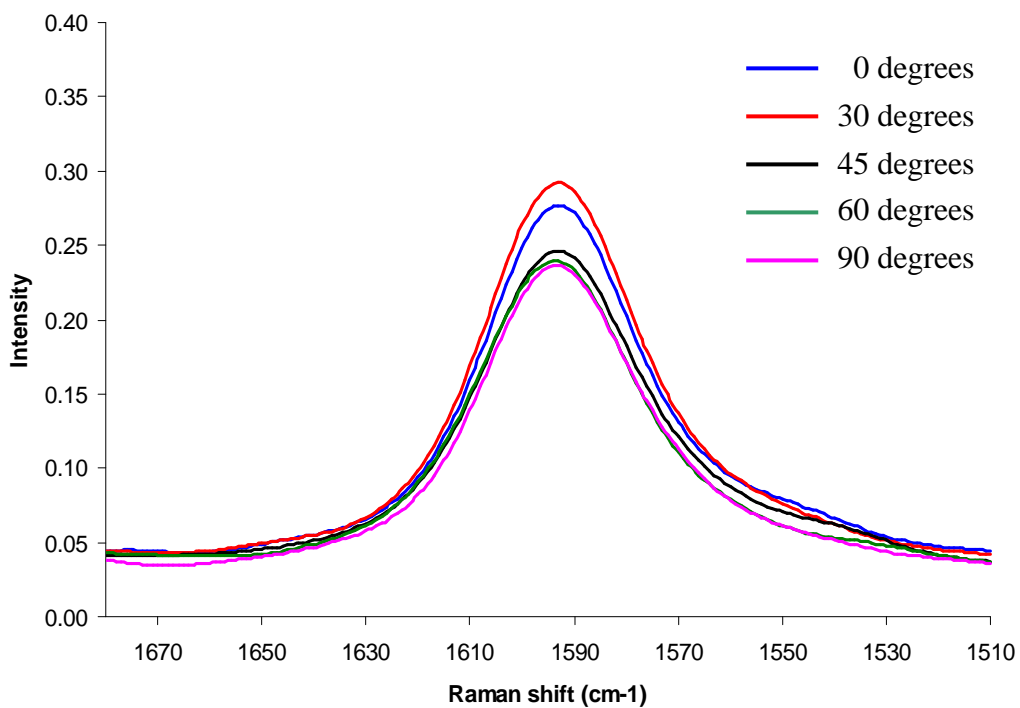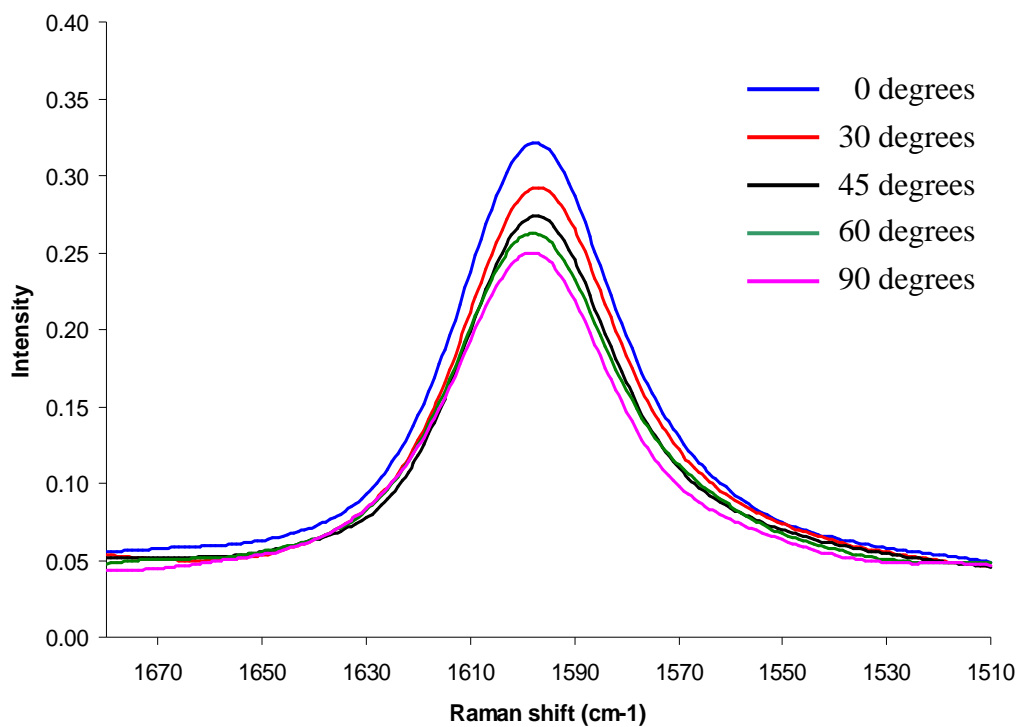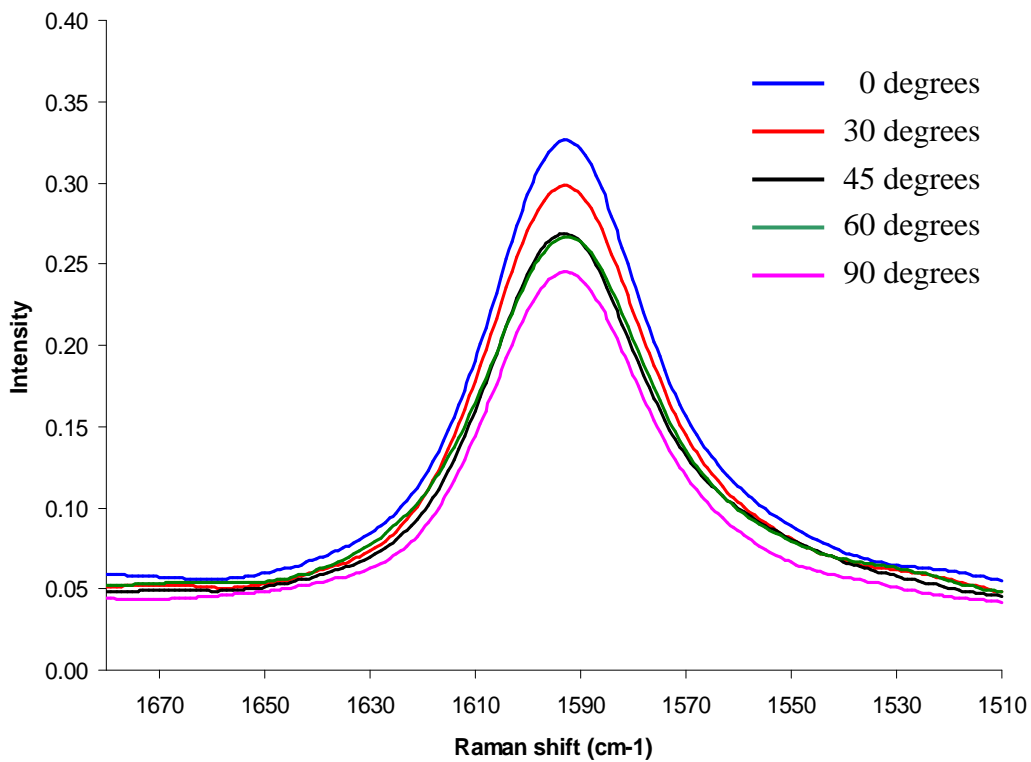
Table 5.3 Raman intensity of oriented SWNT at various external field strength.

Sample	Raman intensity of tangential peak (G-peak)					P0/P90
	0º (P0)	30º (P30)	45º (P45)	60º (P60)	90º (P90)	
random	0.732	0.718	0.732	0.717	0.711	1.030
2T	0.416	0.406	0.398	0.390	0.389	1.069
150 V	0.265	0.264	0.241	0.232	0.228	1.162
300 V	0.274	0.266	0.226	0.226	0.220	1.245
450 V	0.296	0.284	0.256	0.242	0.217	1.364
600 V	0.298	0.265	0.261	0.215	0.209	1.426
[A]150 V+2T	0.324	0.302	0.311	0.287	0.274	1.182
[A]300 V+2T	0.325	0.295	0.291	0.279	0.266	1.222
[A]450 V+2T	0.351	0.293	0.282	0.271	0.241	1.456
[A]600 V+2T	0.308	0.290	0.258	0.226	0.204	1.510
[B]150 V+2T	0.324	0.326	0.329	0.319	0.304	1.066
[B]300 V+2T	0.277	0.292	0.246	0.239	0.236	1.174
[B]450 V+2T	0.313	0.287	0.267	0.254	0.241	1.299
[B]600 V+2T	0.326	0.298	0.269	0.267	0.245	1.331
*600 V+2T	0.151	0.162	0.170	0.238	0.189	0.799

Superscript A and B is represented as A and B system, respectively.

* Condition of SWNT-COOH/PI nanocomposites in the A system

Raman intensity at various angle derived from the maximum point of G-peak

Figure 5.20 presents G-peak of random SWNT in polyimide. Each incident angle of polarizer with samples could indicate that there is no significant different of G-peak and independent with measurement angle. These results showed isotropic nature of unaligned CNT within composites. Figure 5.21 shows G-peak of 0.5 wt% SWNT sample proceeding under 2 Tesla magnetic field effect at various orientation angles. Peak spacing at each measurement angle was not faraway from the last orientation and ended at approximately 60º off-parallel. This suggested the incomplete alignment of SWNT in composites, which implied that the low magnetic field strength is not able to produce enough alignment samples.

Comparing with different DC field strength; 150, 300, 450 and 600 V/cm (Fig. 5.22-5.25). At DC field strength increase, increasing in G-peak spacing was observed. The G-peak spacing range was extended when field strength increased from 150 to 600 V/cm. These results demonstrated that the degree of alignment of SWNT were preferably occurred when the higher field strength were applied. The result obtained was correspond with the clearly observation of aligned network in optical images (Fig. 5.17). The similar trend could also be found in simultaneously applied electric and constant magnetic field system to induce the alignment of nanotubes in matrix, shown in Figure 5.26-5.30 (A system) and in Figure 5.31-5.34 (B system). However, the G-peak spacing of B systems at every condition is less than A systems or the only electric field systems. These unfortunately results exhibited that both of electric and magnetic forces were not assembled together in certain direction, which will be verified in the future. In the case of SWNT-COOH (Fig. 5.30), G-peak intensities were maximal around 60º and diminish from 90º to 0º which gave contrary results from SWNT at the same conditions. We believed that this phenomenon happened from interaction between $[SO_3]^-$ groups of surfactant and -COOH groups of SWNT-COOH, resulted in the refraction of alignment direction of SWNT-COOH.

The Raman intensity of the oriented SWNT at each measurement angle with different conditions was shown in Figure 5.35-5.38. Most of the samples had a similar trend, Raman intensity reaches maximum when the polarizer is parallel to the nanotubes axis (0º) and decreases as the angle of the polarizer increases from 0º to 90º. The maximum slope of the line was observed at the strongest field strength, and was gradually decreased with the reduction of field strength for all condition. The reduction of Raman intensity from 0º to 90º indicated that SWNT was induced to align in polyimide.

Raman spectra are successfully utilized to confirm alignment of SWNT in polyimide matrix. This method allows a qualitative assessment of the alignment of SWNT. Polarized Raman spectra proved that the SWNT are aligned in external field at 150, 300, 450, and 600 V/cm and 2 Tesla. It is believed that a combination of DC electric field and magnetic field can create a better alignment of the SWNT in the polyimide to certain direction than individual field. Therefore, to compare the degree

of alignment of nanotubes within the composites under each one and both of field effects should be investigated.

Raman spectra on different field strength can be used for comparison between the degrees of alignment of SWNT. Raman spectrum is obtained on the SWNT/polyimide nanocomposites with different field strength, to observe the difference in the alignment of the SWNT in polyimide matrix with various field strengths. The tangential peak of Raman intensity when the polarizer angle is at $0°$ and $90°$ is represented by P0 and P90, respectively. The relative intensity ratio (P0/ P90) is used for comparing the degree of alignment of SWNT in the composites with various conditions to observe the effect of field strength on the degree of alignment of nanotubes.
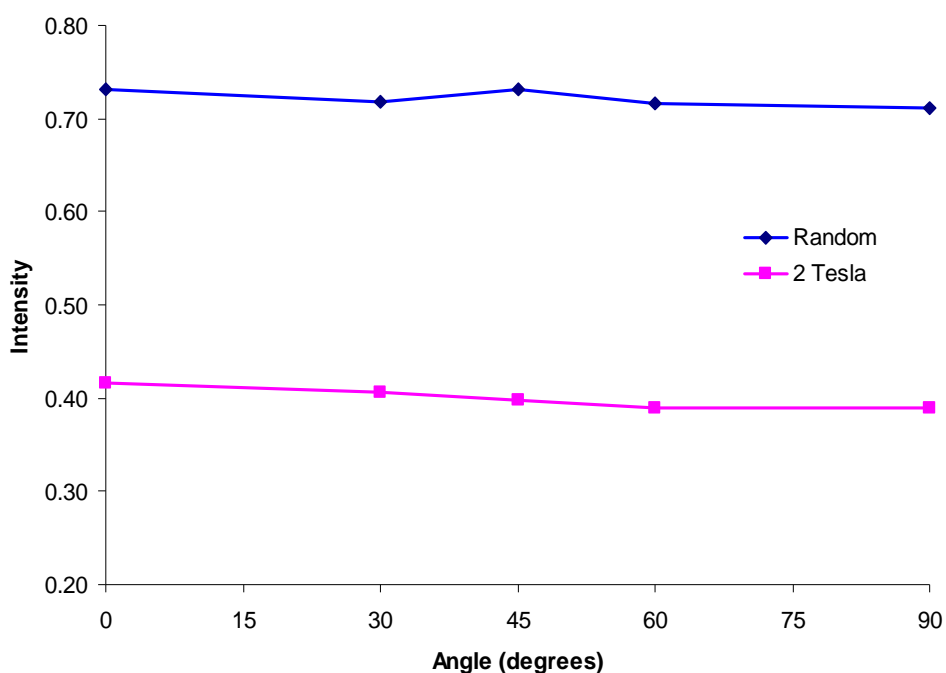

Figure 5.35 Maximal G-peak intensities at different measurement angles of randomly and aligned SWNT by 2 Tesla of magnetic field.
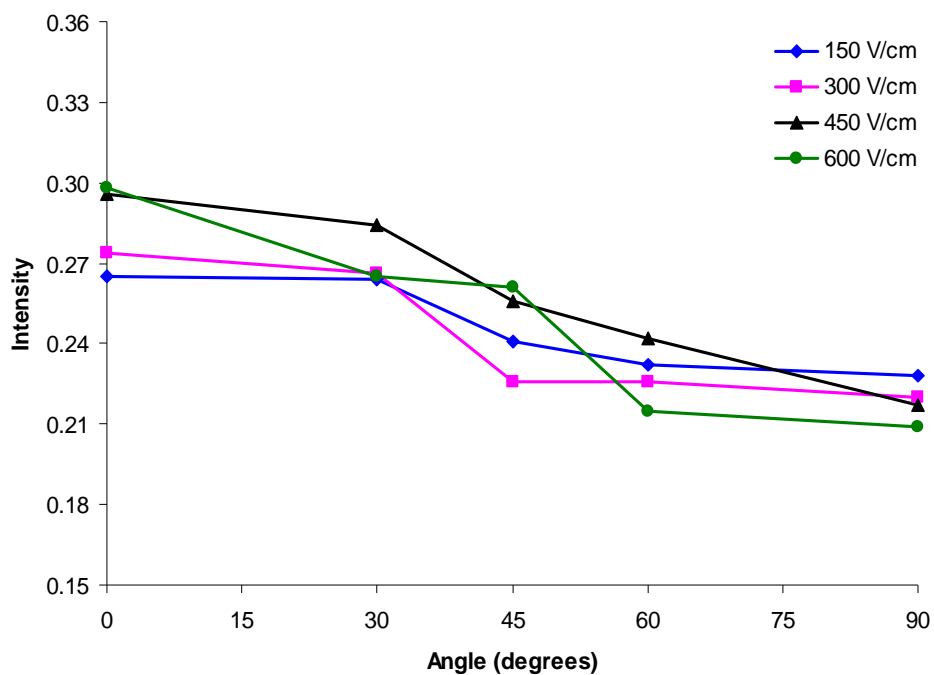
Figure 5.36 Maximal G-peak intensity at different measurement angles of SWNT was aligned by varies DC electric field (electric field system).

Figure 5.37 Maximal G-peak intensity at different measurement angles of SWNT were aligned by varies DC electric field with 2 Tesla of magnetic field (A system).
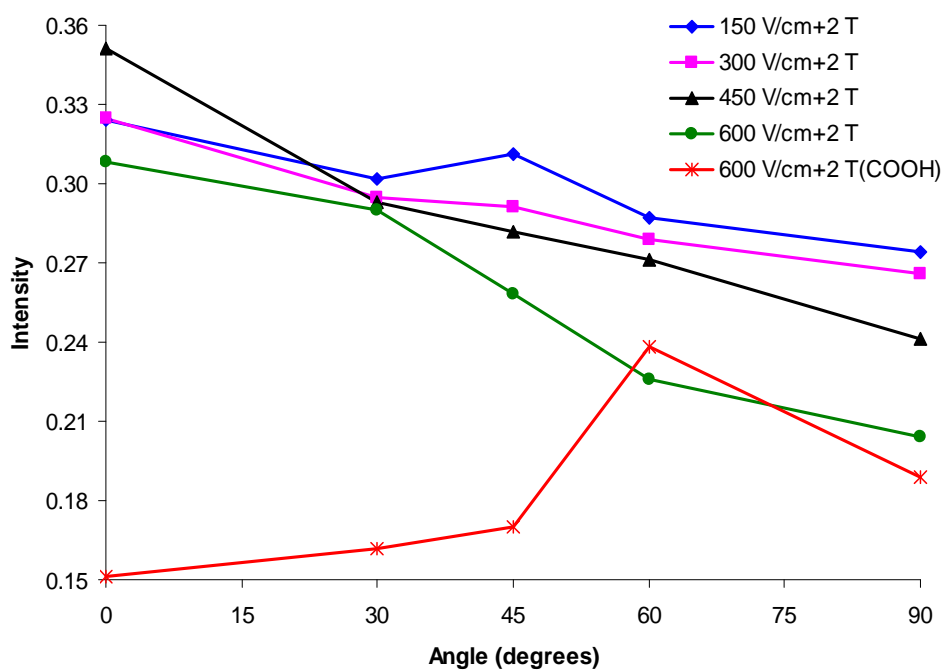
Figure 5.38 Maximal G-peak intensity at different measurement angles of SWNT were aligned by varies DC electric field with 2 Tesla of magnetic field (B system).
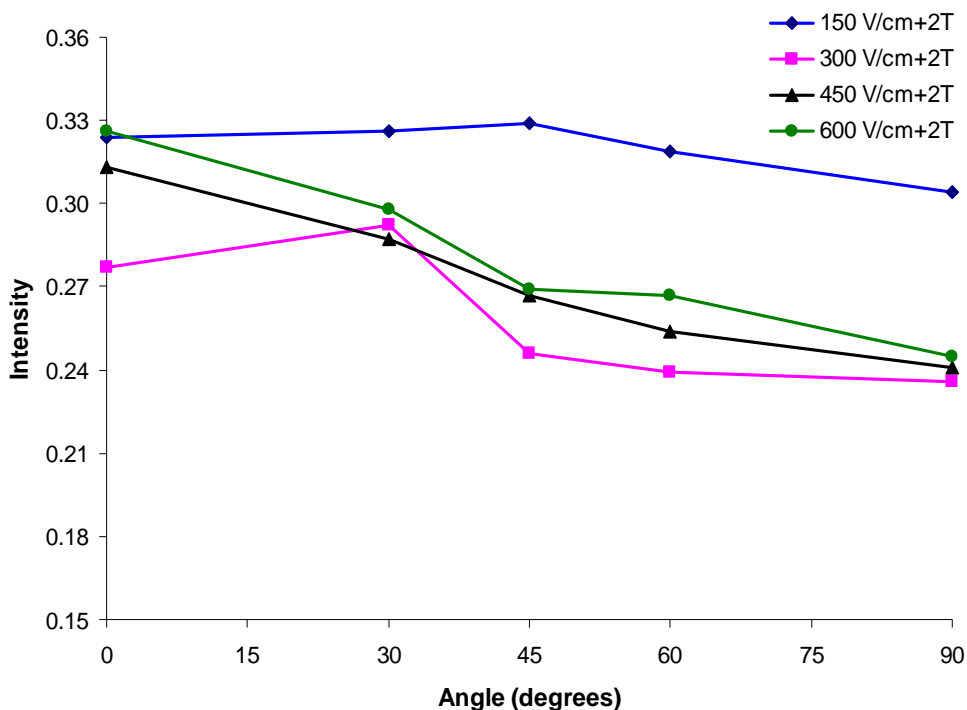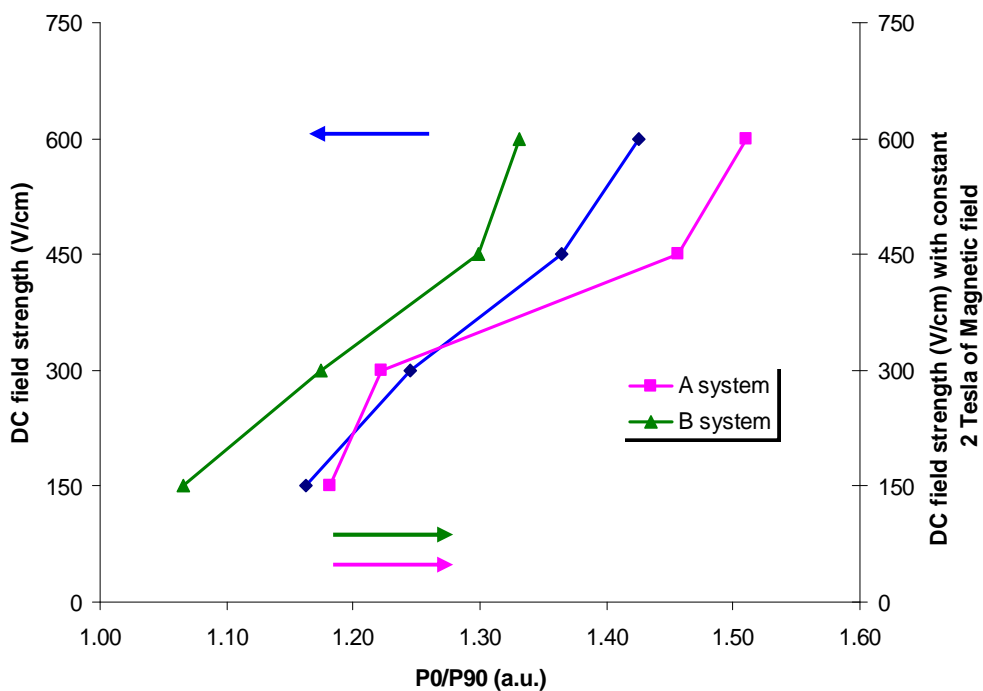

Figure 5.39 Relative Raman intensities (P0/P90) of aligned SWNT as function of the different aligned conditions.

Table 5.3 exhibits the Raman intensity of G-peak at various measurement angles and P0/P90 relative ratio of the entire samples. According to the theory, if the nanotubes were unaligned in composites, P0/P90 value should be equal to 1. On the other hand, if it had better degree alignment, P0/P90 value should be far away from 1. From Table 5.3, unaligned SWNT had 1.030 of P0/P90 value which differed from theoretical value about 3%. This small error could be acceptable. At the low external field strength (2 Tesla or 150 V/cm), relative ratio were 1.069 and 1.162 respectively. A little different relative ratio from the unaligned indicated that there was a tiny degree of alignment in composites. At the higher applied DC field strength; 300, 450 and 600 V/cm, the P0/P90 value will increase from 1.245 to 1.426 which can be concluded that the trends of the degree of alignment of SWNT under DC electric field effect follow: 600 > 450 > 300 > 150 V/cm. The similar trend could also be found in simultaneously applied electric and constant 2T magnetic field system (A and B system). The trends follow: 600 V/cm+2T > 450 V/cm+2T > 300 V/cm+2T > 150 V/cm+2T.

To compare the degree of alignment of both system, DC electric field and DC electric with magnetic field, the relationship between both system together with P0/P90 values were established in Figure 5.39. It was clearly seen that at the same DC field strength, P0/P90 values of the system without incorporation of constant 2T magnetic field were in the middle among the both of systems with magnetic field. This phenomenon displayed the effect of the different direction of magnetic forces on the degree of alignment of nanotubes in matrix. In the case of magnetic field (B) parallel to electric field (E) direction as supportive direction (A system), nanotubes in matrix were induced to align parallelly to the applied field. That means such nanotubes can be oriented in the plane of polymer surface. We believe that, in the direction of B//E, the three forces of electric field (torque, Columbic, and electrophoresis) and one force of magnetic field (torque) played an important role to improve the degree of alignment and the ramified network formation in composite films. Therefore, the P0/P90 value of A system are higher than the system with only electric field. The relative ratio was increased from 1.364 to 1.465 (approximately 6.7%) and from 1.426 to 1.510 (approximately 5.9%) when incorporate of 2T magnetic field at 450 and 600 V/cm, respectively. These results confirmed that 2

Tesla magnetic field in certain direction can improve the degree of alignment of nanotubes in composites.

When the magnetic field was perpendicular to the electric field (B⊥E), the contrary results were obtained. The P0/P90 value of B system was decreased about 8.3%, 5.7%, 4.8% and 6.7% when 2T magnetic field was incorporated respectively with 150, 300, 450, and 600 V/cm of DC field strength in perpendicularly direction. These results indicate that the degree of alignment of nanotubes in composites was decreased. For understanding the mechanism of the decrease of degree of alignment, the schematic image of the arrangement of nanotubes in film prepare with and without magnetic field can be described in Figure 5.40.
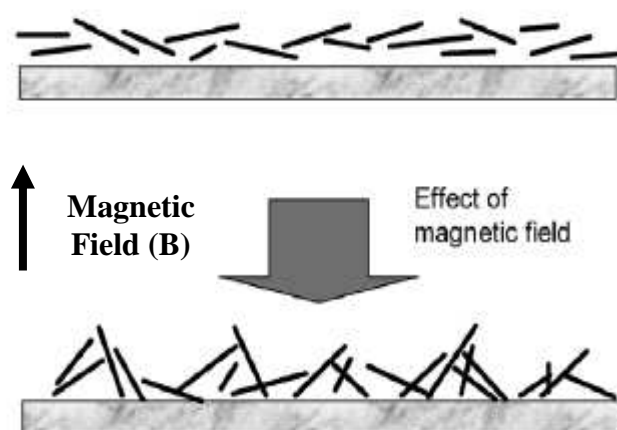

Figure 5.40 Schematic image of CNT-film structure prepared with and without magnetic field.

Under the effect of magnetic field, the torque force on CNT induced by magnetic field that can force the nanotubes to stand normally to the substrate surface. The nanotubes were also forced to rearrange in parallel to electric field direction. Therefore, the alignment direction of nanotubes under the force of electric and perpendicular magnetic field in B system was not in the same direction, which finally decreased the degree of alignment of nanotubes in composite films.

In this section, we assessed and verified the degree of alignment of carbon nanotubes in polyimide at various conditions of electric and magnetic field. Incorporation of electric and magnetic field in the same direction can create the maximal of degree of alignment due to torque, Columbic, and electrophoresis forces

of such external field. The more complete result will be achieved when there is an investigation on the properties of the aligned films for useful information of the applications in the future.

CHAPTER VI

CONCLUSIONS & RECOMMENDATIONS

6.1 Conclusions

In this research, the carbon black/polyimide nanocomposites were firstly investigated to create the basic information for studying the aligned carbon nanotube in polyimide matrix. DC electric and magnetic field was employed to induce the aligned and the network formation structure of CNT in polyimide matrix. Polarizer Raman spectroscopy was utilized to assess the degree of alignment of carbon nanotubes in composite films. The conclusions of this research can be summarized as follows;

6.1.1 The carbon black/polyimide nanocomposite films

In this section, the effects of SDS surfactant on the dispersion state, electrical and mechanical properties of the CB/polyimide nanocomposite films were explored. The UV-vis spectra and TEM images have confirmed that the addition of surfactant increased level of dispersion of carbon black in the nanocomposite films due to the SDS prevents the carbon black agglomeration and also improves the transparent properties. When the concentration of surfactant was far above CMC, the direction of dispersion state and agglomerated size of carbon black in composite films were opposite. Dielectric properties of the CB/polyimide nanocomposite films without surfactant increase with increasing the CB loading and decreased with the addition of surfactant. The tensile properties of the CB/polyimide nanocomposite films were improved by surfactant amount up to 1:2 CB/SDS ratio and were optimized at 0.5 wt% of CB in composites. The incorporation of SDS into the CB/PI nanocomposites makes the nanocomposites more brittle.

6.1.2 The aligned carbon nanotubes/polyimide nanocomposite films

Alignment of carbon natubes in polyimide was performed under the optimal condition for the CB/polyimide nanocomposites. 2 Tesla of magnetic field and various electric field included 150, 300, 450 and 600 V/cm were employed to induce the alignment of nanotubes in matrix. Raman spectroscopy was employed to confirm the presence of carbon nanotubes in the composites. The spectrum shows

characteristic peaks which corresponded to the diameter dependent radial breathing mode (RBM) and the tangential G band of the SWNT. The RBM mode is the real signature of the presence of carbon nanotubes in a sample, since it is not presented in graphite. Optical microscopy observation indicated that an alignment could clearly be found when increasing the field strength to the highest and decreased when the field strength are decreased. The incorporation of magnetic field in certain direction will be enhanced the level of alignment that are better than using electric or magnetic field alone. The three forces from electric and magnetic field displayed an important role for improving the degree of alignment in composites.

6.2 Recommendations

6.2.1 There should be more investigation in the other properties of the random and aligned SWNT /polyimide nanocomposite films.

6.2.2 There should be more investigation on parameter such as applied time, nanotubes concentration, viscosity of matrix and various magnetic field strengths.

6.3.3 AC electric field should be investigated to compare result with DC electric field.

REFERENCES

[1] Glushanin S, Topolov VY, Krivoruchko AV. Features of piezoelectric properties of the PbTiO3-type ceramic/polymer composites. **Materials Chemistry and Physics** 97(2006):357-364.

[2] Hine P, Broome V, Ward I. The incorporation of carbon nanofibres to enhance the properties of self reinforced, single polymer composites. **Polymer** 46 (2005):10936-10944.

[3] Cioffi N, Torsi L, Ditaranto N, Tantillo G, Ghibelli L, Sabbatini L, Bleve-Zacheo T, D'Alessio M, Zambonin PG, Traversa E. Copper nanoparticle/polymer composites with antifungal and bacteriostatic properties. **Chemistry of Materials** 17(2005):5255-5262.

[4] Pelaiz-Barranco A, Marin-Franch P. Piezo-, pyro-, ferro-, and dielectric properties of ceramic/polymer composites obtained from two modifications of lead titanate. **Journal of Applied Physics** 97(2005):034104-034105.

[5] Huang ZM, Zhang YZ, Kotaki M, Ramakrishna S. A review on polymer nanofibers by electrospinning and their applications in nanocomposites. **Composites Science and Technology** 63(2003):2223-2253.

[6] Jordan J, Jacob K,I Tannenbaum R, Sharaf MA, Jasiuk I. Experimental trends in polymernanocomposites - a review. **Materials Science and Engineering A-Structural Materials Properties Microstructure and Processing** 393 (2005):1-11.

[7] Gerard JF. **Fillers and filled polymers**. Wiley-VCH,Weinheim (2001).

[8] Wilson D, Stenzenberger HD, Hergenrother PM. **Polyimides**. London, New York, USA (1990).

[9] Siochi EJ, Dennis C, Park C, Lillehei PT, Rouse JH, Toppinga C, Bhattacharyyac AR, Kumar S. Melt processing of SWCNT-polyimide nanocomposite fibers. **Composites Part B** 35(2004):439–446.

[10] Smith JG, Delozier DM, Connell JW, Watson KA. Carbon nanotube-conductive additive-space durable polymer nanocomposite films for electrostatic charge dissipation. **Polymer** 45(2004):6133–6142.

[11] Wise KE, Park C, Siochi EJ, Harrison JS. Stable dispersion of single wall carbon nanotubes in polyimide: the role of noncovalent interactions. **Chemical Physics Letters** 391(2004):207–211.

[12] Jiang X, Bin Y, Matsuo M. Electrical and mechanical properties of polyimide–carbon nanotubes composites fabricated by in situ polymerization. **Polymer** 46(2005):7418–7424.

[13] Delozier DM, Watson KA, Smith JG, Connell JW. Preparation and characterization of space durable polymer nanocomposite films. **Composites Science and Technology** 65(2005):749–755.

[14] Delozier DM, Watson KA, Smith JG, Clancy TC, Connell JW. Investigation of aromatic/aliphatic polyimides as dispersants for single wall carbon nanotubes. **Macromolecules** 39(2006):1731–1739.

[15] Yu A, Hu H, Bekyarova E, Itkis ME, Gao J, Zhao B, Haddon RC. Incorporation of highly dispersed single-walled carbon nanotubes in a polyimide matrix. **Composites Science and Technology** 66(2006):1187–1194.

[16] Gosh MK, Mittal KL. **Polyimides: fundamentals and applications**. New York, Marcel-Dekker (1996).

[17] Tessler N, Medveder V, Kazes M, Kan S, Banin U. **Science** (2002):295-1506.

[18] Thostenson ET and Chou TW. Aligned multi-walled carbon nanotube reinforced composites: processing and mechanical characterization. **Journal of physics D:Applied physics** 36(2002):77-80.

[19] Saito R, Dresselhaus G, and Dresselhaus MS. Physical properties of carbon nanotubes**. Imperial College Press**, London (1998).

[20] Wong EW, Sheehan PE, Lieber CM. Nanobeam mechanics: Elasticity, strength, and toughness of nanorods and nanotubes. **Science** 277(1997):1971-1975.

[21] Lau KT, Hui D. The revolutionary creation of new advanced materials - carbon nanotube composites. **Composites Part B-Engineering** 33(2002):263-277.

[22] Li F, Cheng HM, Bai S, Su G, Dresselhaus MS. Tensile strength of single-walled carbon nanotubes directly measured from their macroscopic ropes. **Applied Physics Letters** 77(2000):3161-3163.

[23] Iijima S, Brabec C, Maiti A, Bernholc J. Structural flexibility of carbon nanotubes. **Journal of Chemical Physics** 104(1996):2089-2092.

[24] Ajayan PM, Schadler LS, Braun PV. **Nanocomposite Science and Technology**. Wiley-VCH, Verlag GmbH & Co.KGaA, Weinheim, Germany (2003).

[25] Nalwa HS. **Handbook of Nanostructured Materials and Nanotechnology**. Academic Press, New York, USA (2000).

[26] Hirsch A. **Angew. Chem. Int. Ed**. 41(2002):1853.

[27] Bubke K, Gnewuch H, Hempstead M, Hammer J, Green MLH. Optical anisotropy of dispersed carbon nanotubes induced by an electric field. **Applied Physics Letters** 71(1997):1906–1908.

[28] Yamamoto K, Akita S, Nakayama Y. Orientation and purification of carbon nanotubes using ac electrophoresis. **Journal of physics D:Applied physics** 31 (1998):34–36.

[29] Brezesinski G, Mo¨gel H-J, Grenzfla K, Mu¨nchen**. Spektrum Akademischer Verlag** (1993).

[30] Cheol P, Zoubeida O, Kent AW, Roy EC. Dispersion of single wall carbon nanotubes by in situ polymerization under sonication. **Chemical Physics Letters** 364(2002):303-308.

[31] Hyang HS, Jae WC, Nanda GS. Effect of carbon nanotubes on mechanical and electrical properties of polyimide/carbon nanotubes nanocomposites. **European Polymer Journal** 43(2007):3750–3756.

[32] Siu-Ming Y, Chen-Chi MM, Yao-Yu L, Hsu-Chiang K. Preparation, morphology and properties of acid and amine modified multiwalled carbon nanotube/polyimide composite. **Composites Science and Technology** 67 (2007):2564–2573.

[33] Yu A, Hu H, Bekyarova E, Itkis ME, Gao J, Zhao B, Haddon RC. Incorporation of highly dispersed single-walled carbon nanotubes in a polyimide matrix. **Composites Science and Technology** 66(2006):1187–1194.

[34] Martin CA, Sandler JKW, Windle AH, Schwarz MK, Bauhofer W, Schulte K, Shaffer MSP. Electric field-induced aligned multi-wall carbon nanotube network in epoxy composites. **Polymer** 46(2005):877–886.

[35] Park C and Wise KE. Aligned Single-Wall Carbon Nanotube Polymer Composites Using an Electric Field. **Journal of Polymer Science B: Polymer Physics** 44(2006):1751–1762.

[36] Donglu S and Peng H. Magnetic alignment of carbon nanofibers in polymer composites and anisotropy of mechanical properties. **Journal of applied physics** 97 (2005):064312-064315.

[37] Torsten P, Jean-Yves C, Wolfgang B. Electric anisotropy of carbon nanofibre/ epoxy resin composites due to electric field induced alignment. **Composites Science and Technology** 63(2003):1835–1841.

[38] Tatsuhiro T, Taichi M, Ayumu H, Hiroshi A, Koichiro Y. Aligning Vapor-grown carbon fibers in polydimethylsiloxane using dc electric or magnetic field. **Carbon** 44 (2006):1180–1188.

[39] Bangwen Z, Changsheng X, Junhui H, Huihu W, YangHai G. Novel 1–3 metal nanoparticle/polymer composites induced by hybrid external fields. **Composites Science and Technology** 66(2006):1558–1563.

[40] Erin C, Richard V, Marwan AH, Hamid G, Rina T. Properties of carbon nanotube–polymer composites aligned in a magnetic field. **Carbon** 45 (2007):2037–2046.

[41] Haiquan W, Hongyan Z, Weifeng Z, Wei Z, Guohua C. Preparation of polymer/oriented graphite nanosheet composite by electric field-inducement. **Composites Science and Technology** 68(2008):238–243.

[42] Brian W. Steinert, Derrick R. Dean. Magnetic field alignment and electrical properties of solution cast pet-carbon nanotube composite films. **Accepted Manuscript (Polymer)**, University of Alabama at Birmingham, Department of Materials Science and Engineering USA.

[43] Jeng-Shyong L and Hsien-Tang C. Preparation and Properties of Conductive Polyimide Films. **Journal of Polymer Research** 9(2002):189–194.

[44] Linqin J, Lian G, Jing S. Production of aqueous colloidal dispersions of carbon nanotubes. **Journal of Colloid and Interface Science** 260(2003):89-94.

[45] Junrong Y, Nadia G, Cor EK, Joachim L. Controlling the dispersion of multi-wall carbon nanotubes in aqueous surfactant solution. **Carbon** 45(2007): 618-623.

APPENDICES

APPENDIX A

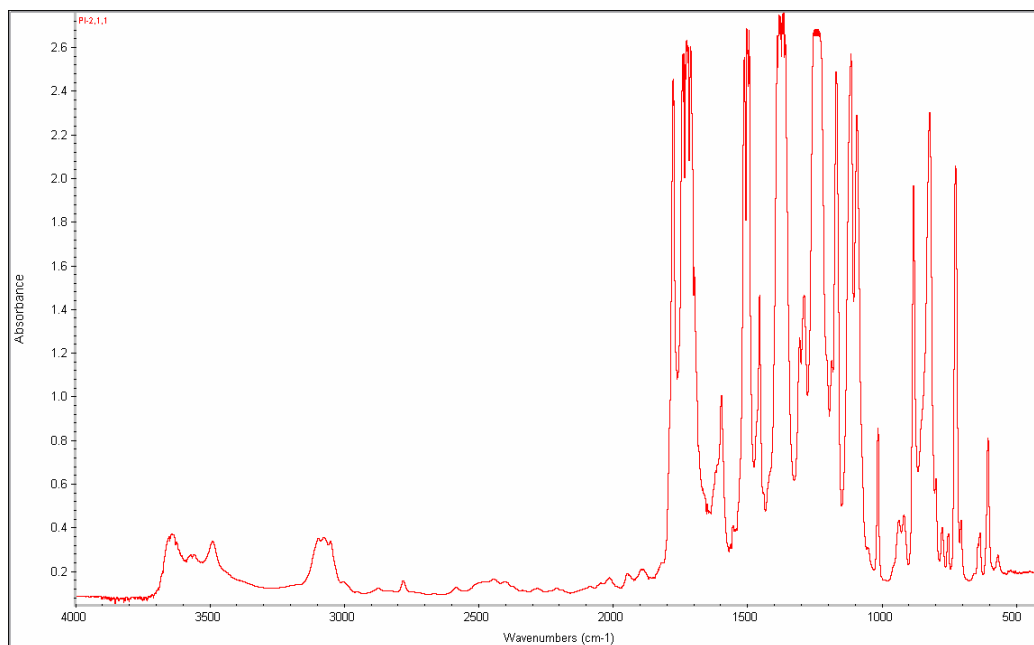# FOURIER TRANSFORM INFRARED SPECTROSCOPY (FTIR) CHARACTERIZATION

Figure A-1 FT-IR spectra analysis of pure polyimide film**.**

APPENDIX B

UV-VIS SPECTRASCOPY (UV-VIS)
CHARACTERIZATION

Table B.1 Absorbance (Ao) at 500 nm of pure polyimide films for calibration curve

Specimen code	Thickness (µm)	Absorbance (Ao)
P1	25	0.8048
P2	51	1.2582
P3	76	1.8590
P4	101	2.333
P5	125	2.8348

Table B.2 Absorbance (A) at 500 nm of nanocomposite films of 0.5wt% CB contents

Sample	CB/SDS ratio	Thickness (µm)	A	Ao	A/Ao
1	-	24	1.3540	0.5616	2.4110
2	1:0.4	21	1.1421	0.4914	2.3278
3	1:0.8	21	1.1376	0.4914	2.2625
4	1:2.0	18	0.8229	0.4212	1.9025
5	1:5.0	18	0.9962	0.4212	2.3653
6	1:10	20	1.1151	0.4680	2.4456

APPENDIX C

The dielectric constant and dissipation factor of the CB/PI nanocomposite films.

Calculation of dielectric constant (k) from capacitor formula:

$$k = Cd/AKo$$

C is the measured capacitance at any frequency.

d is thickness of sample.

A is area of sample

Ko is free permittivity = 8.854 pF

Table C.1 Summary of dielectric constant of nanocomposite films.

Specimen	CB/SDS ratio	Thickness (μm)	Cp (pF)	k
Pure PI	-	39	188.15	3.68
0.025wt% CB/PI	-	45	171.25	3.87
0.050wt% CB/PI	-	57	171.84	4.92
0.10wt% CB/PI	-	51	200.44	5.13
0.15wt% CB/PI	-	52	200.58	5.24
0.20wt% CB/PI	-	53	201.38	5.36
0.30wt% CB/PI	-	45	241.54	5.44
0.50wt% CB/PI	-	50	217.85	5.47
0.50wt% CB/PI	1:0.4	67	159.50	5.36
0.50wt% CB/PI	1:0.8	62	155.83	4.85
0.50wt% CB/PI	1:2.0	59	140.38	4.16
0.50wt% CB/PI	1:5.0	54	151.14	4.09
0.50wt% CB/PI	1:10.0	57	141.45	4.04

APPENDIX D

Calculation of magnetic field ($\overline{B}$) that is radiated from equipment as follow:

$$\overline{B} = N\mu I/L$$

$\overline{B}$ is magnetic field (Tesla)

N is number of coil round the iron core = 3656 (turns)

μ is The Absolute Permeabilities ($4\pi*10^{-7}$ (Wb/m^2)/(A/m))

I is a DC electric current (A)

L is spacing between air gaps (0.03 m)

Example

We would like to achieve 2 Tesla of the magnetic fields.

$$\overline{B} = N\mu I/L$$

$$I = \overline{B}L/N\mu$$

$$= (2 * 0.03)/(3656*4\pi*10^{-7})$$

$$= 13.06 \text{ A}$$

So, we have to apply 13.06 A of current to achieve the 2T magnetic field.

APPENDIX E

POLARIZER RAMAN SPECTROSCOPY CHARACTERIZATION
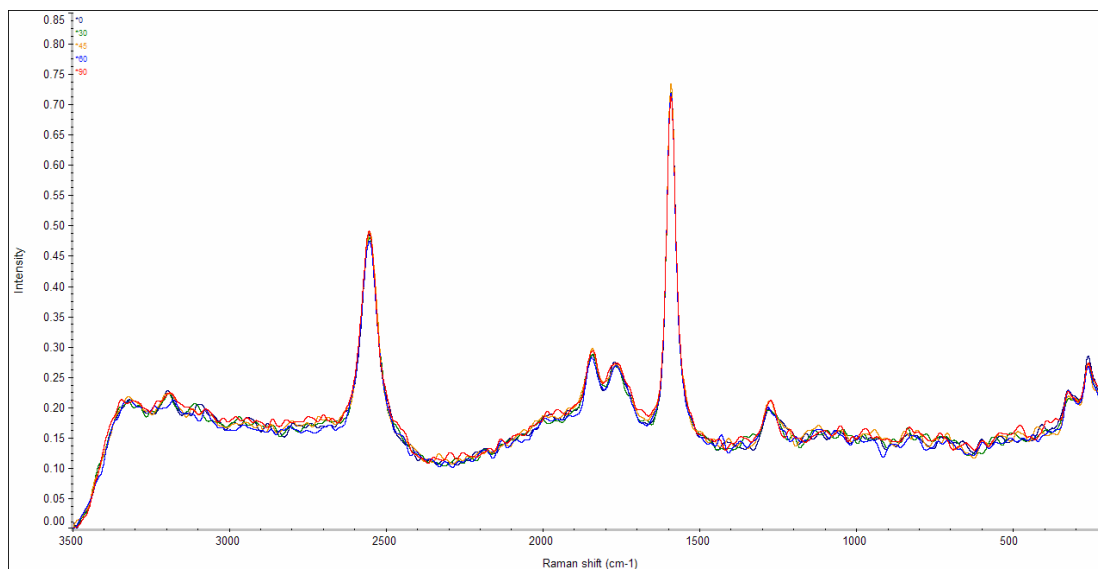
Figure E-1 Full Raman spectra of the random SWNT/PI nanocomposite films with various measurement angles**.**
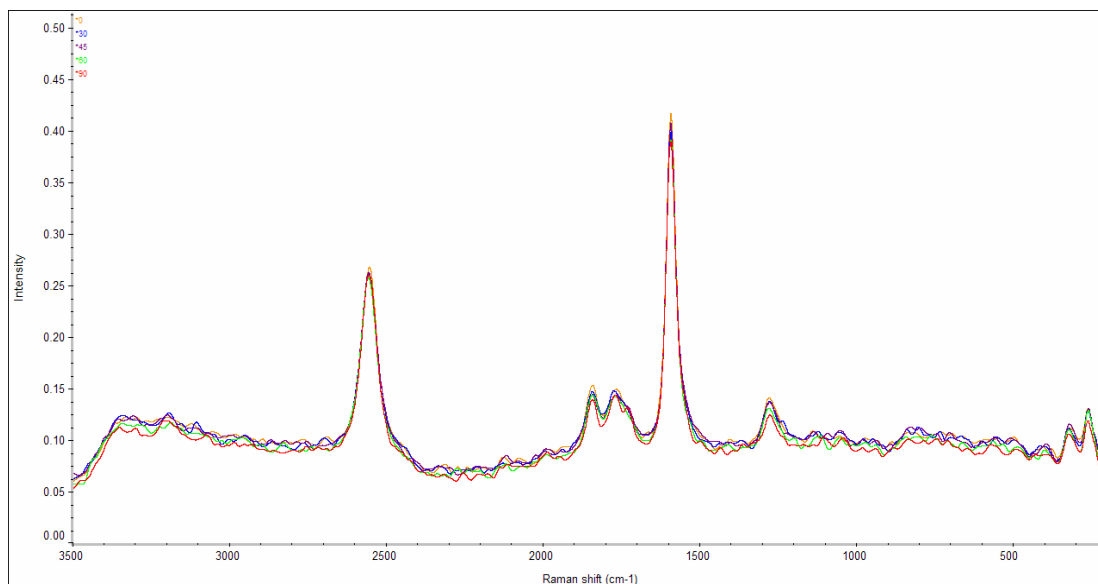
Figure E-2 Full Raman spectra of SWNT aligned by 2T magnetic field with various measurement angles**.**
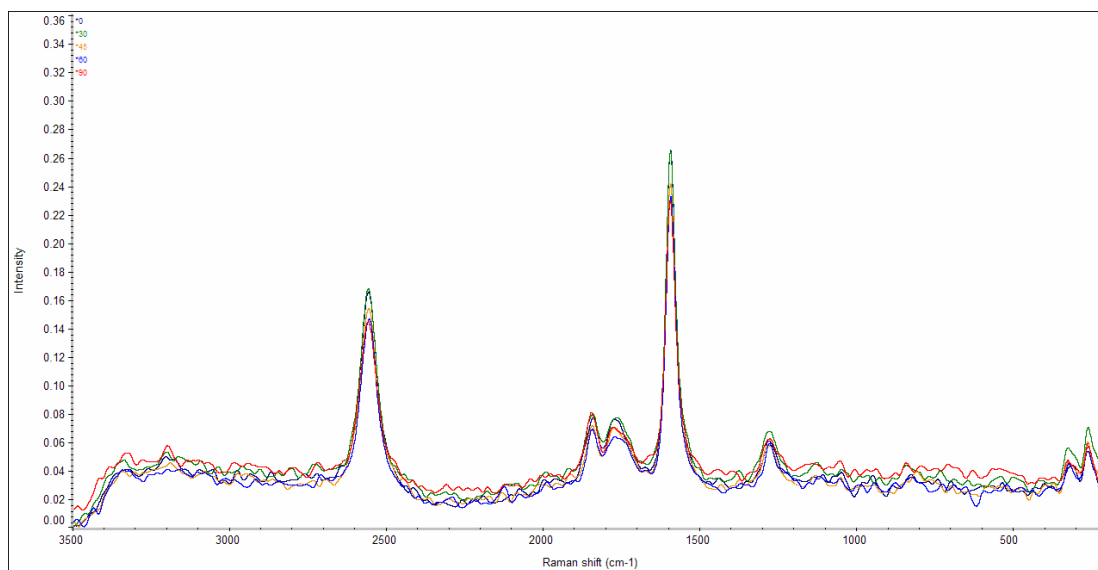
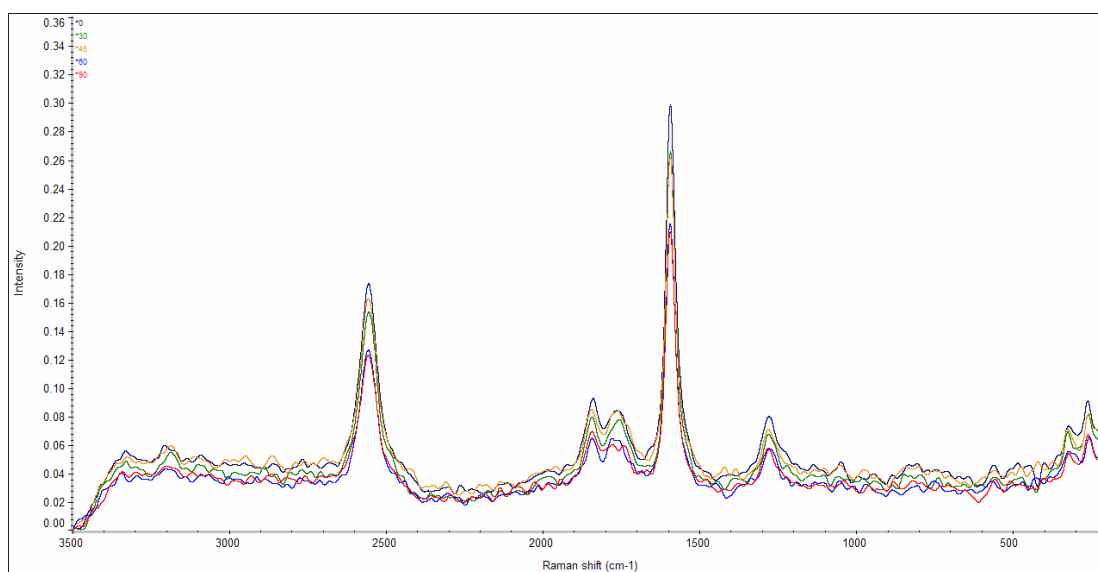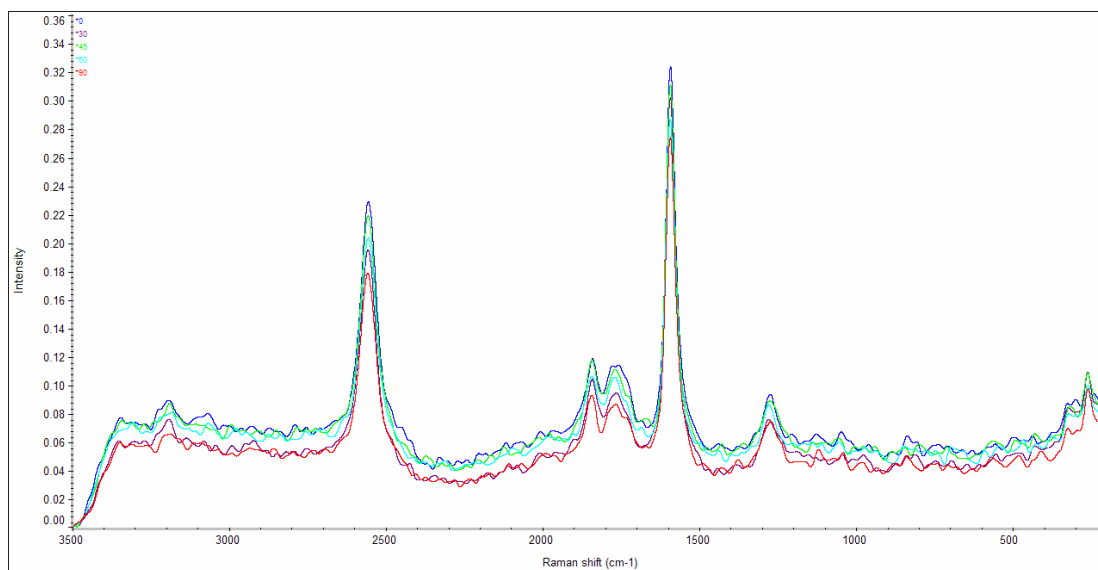**Figure E-3** Full Raman spectra of SWNT aligned by 150 V/cm of DC electric field with various measurement angles**.**
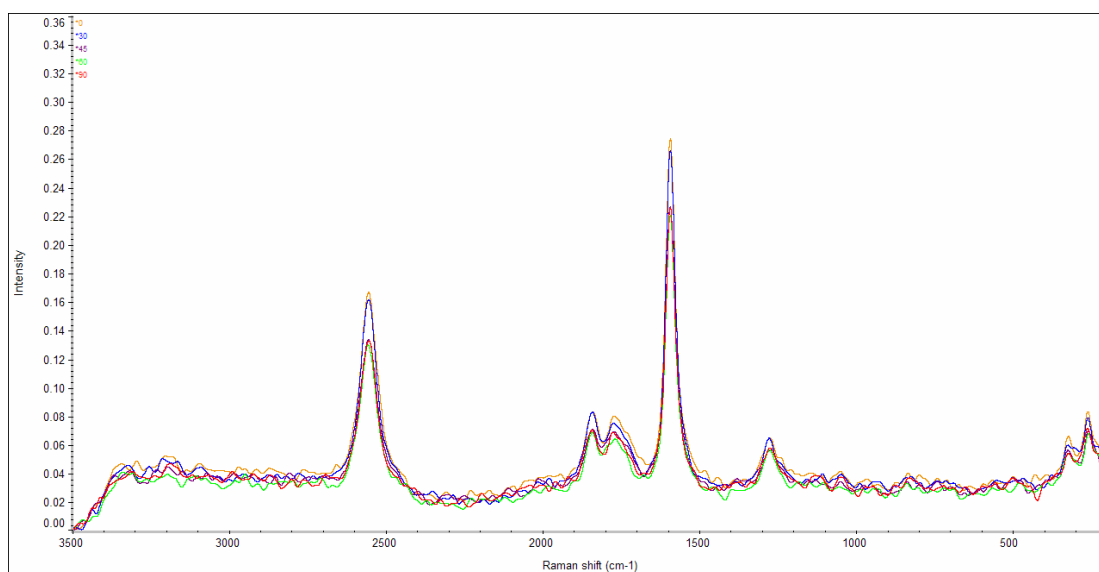
Figure E-4 Full Raman spectra of SWNT aligned by 300 V/cm of DC electric field with various measurement angles**.**
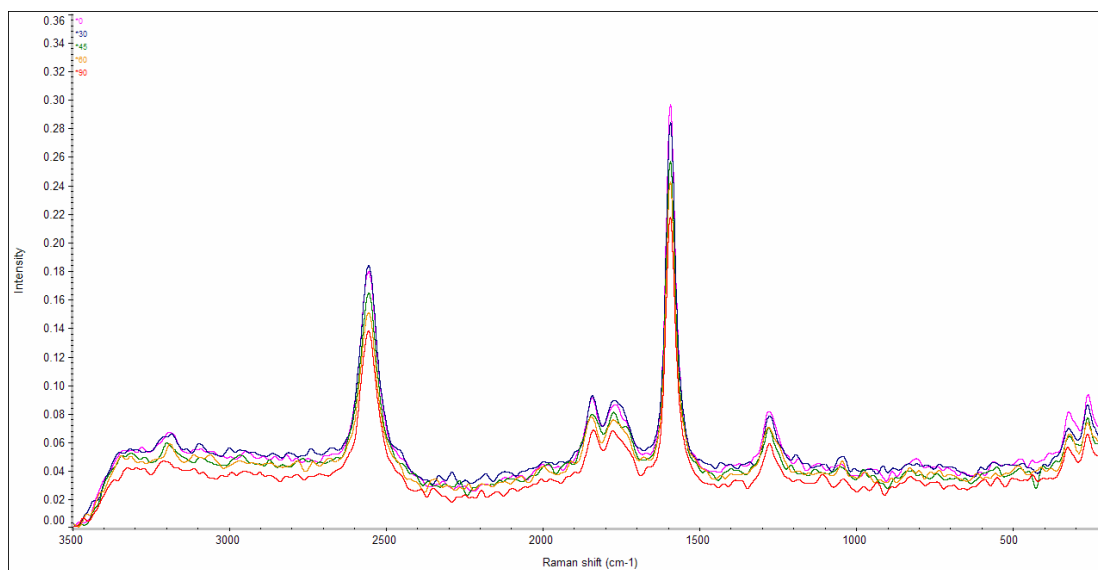
Figure E-5 Full Raman spectra of SWNT aligned by 450 V/cm of DC electric field with various measurement angles**.**

Figure E-6 Full Raman spectra of SWNT aligned by 600 V/cm of DC electric field with various measurement angles**.**
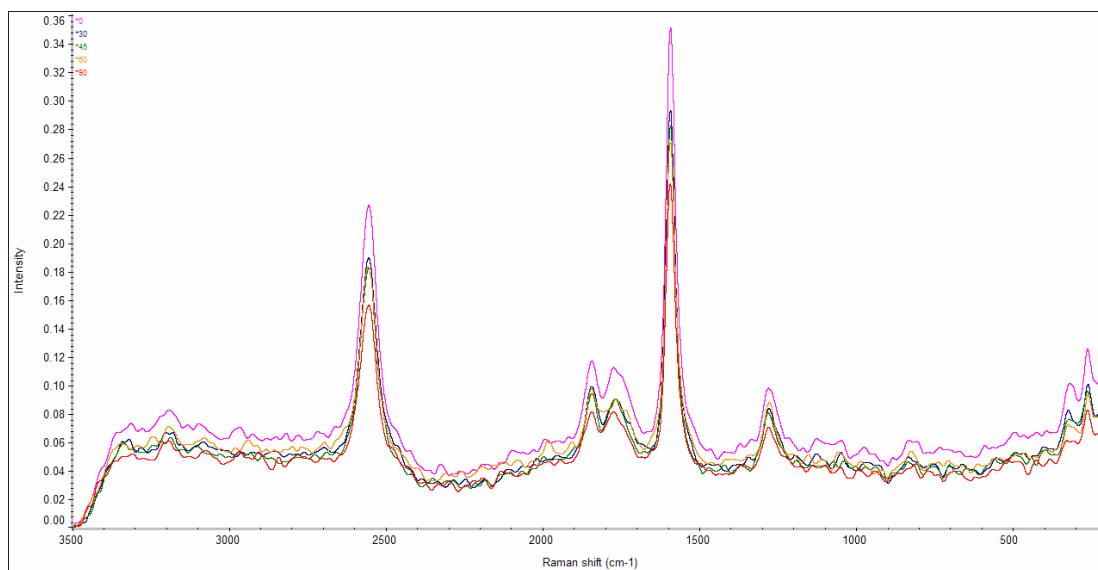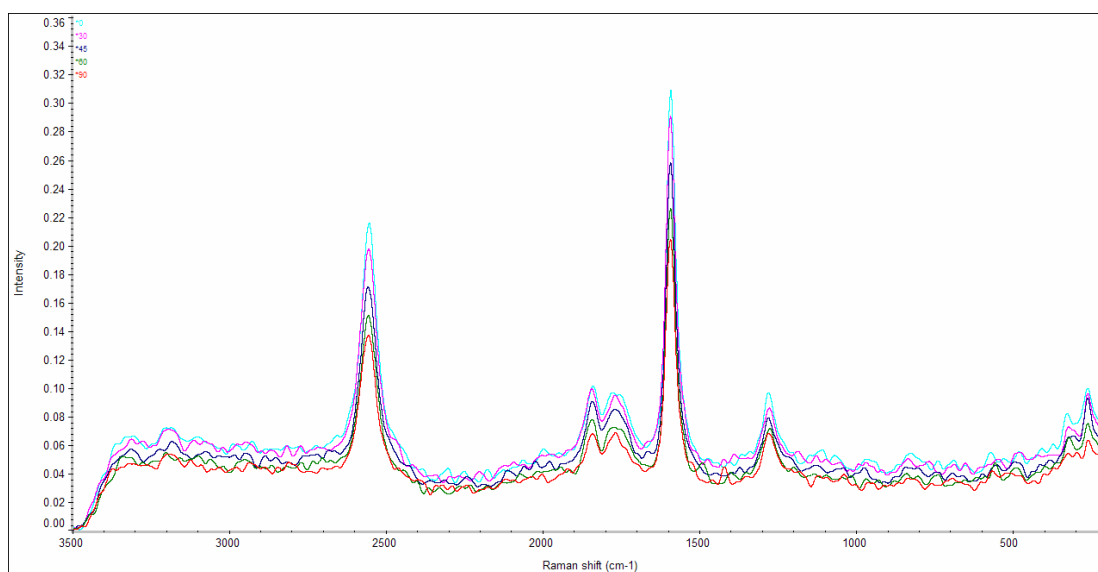
Figure E-7 Full Raman spectra of SWNT aligned by 150 V/cm of DC electric field with 2T magnetic field at various measurement angles (A system).
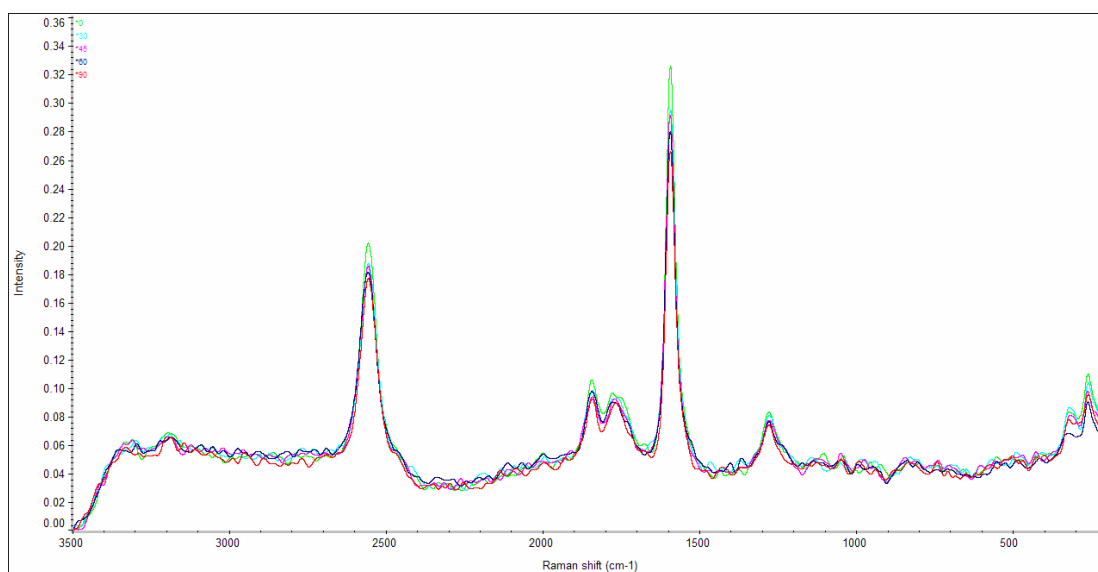
Figure E-8 Full Raman spectra of SWNT aligned by 300 V/cm of DC electric field with 2T magnetic field at various measurement angles (A system)**.**
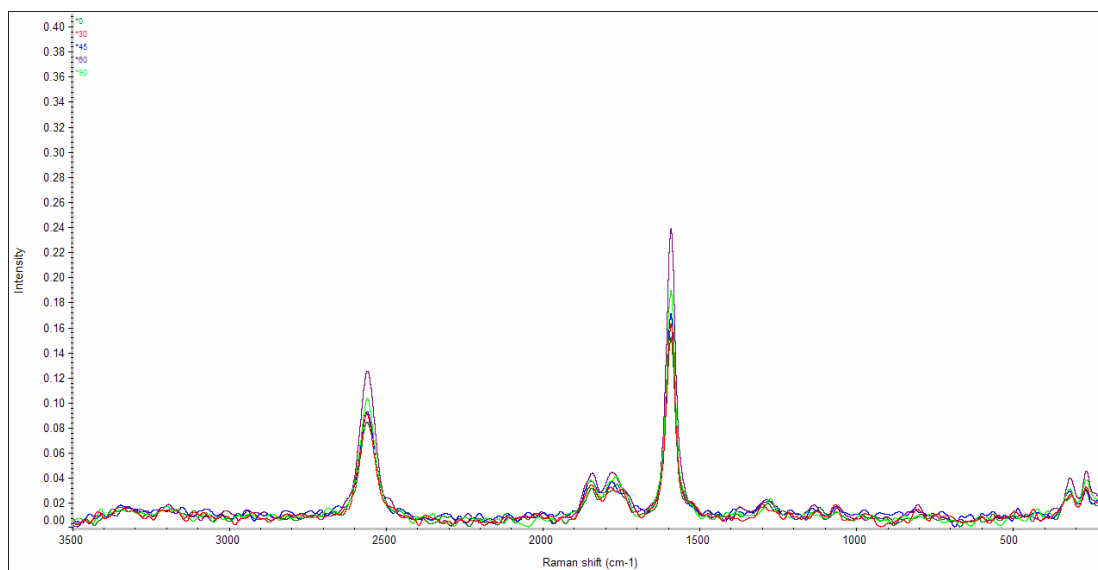
Figure E-9 Full Raman spectra of SWNT aligned by 450 V/cm of DC electric field with 2T magnetic field at various measurement angles (A system)**.**

Figure E-10 Full Raman spectra of SWNT aligned by 600 V/cm of DC electric field with 2T magnetic field at various measurement angles (A system)**.**

Figure E-11 Full Raman spectra of SWNT-COOH aligned by 600 V/cm of DC electric field with 2T magnetic field at various measurement angles (A system)**.**
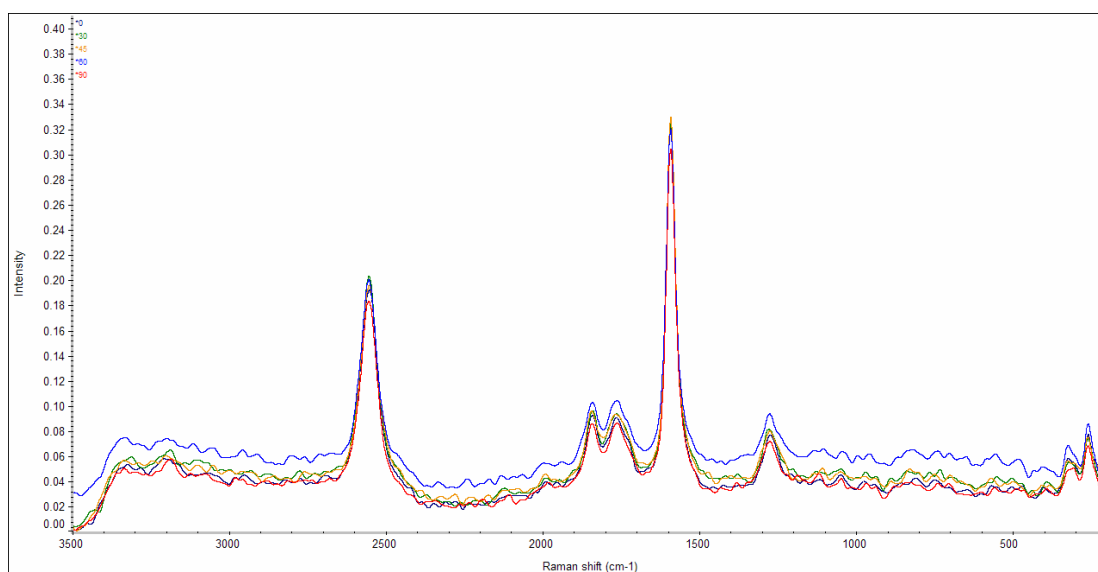

Figure E-12 Full Raman spectra of SWNT aligned by 150 V/cm of DC electric field with 2T magnetic field at various measurement angles (B system)**.**
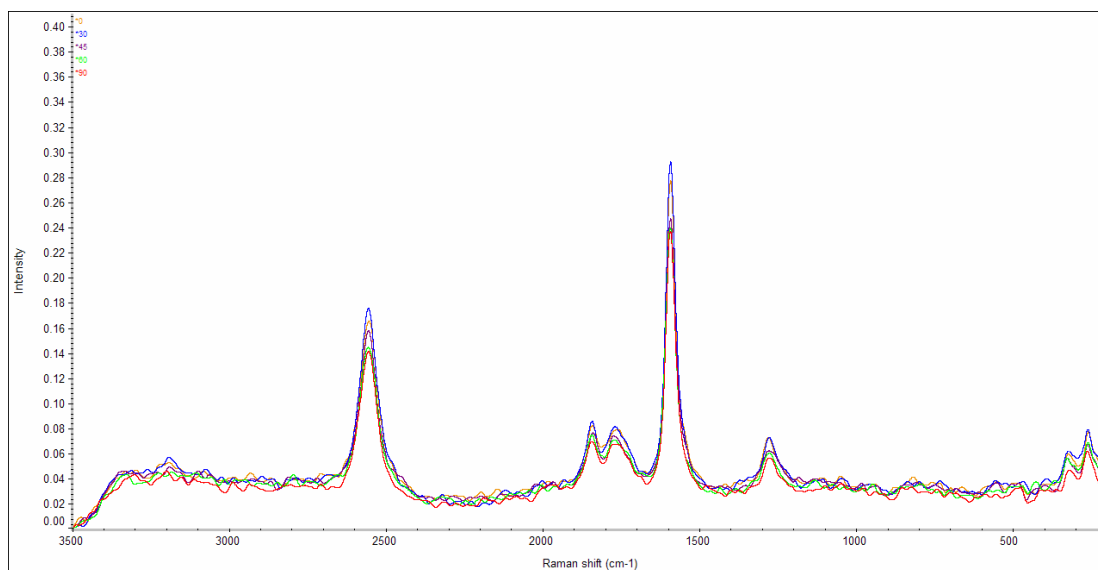
Figure E-13 Full Raman spectra of SWNT aligned by 300 V/cm of DC electric field with 2T magnetic field at various measurement angles (B system)**.**
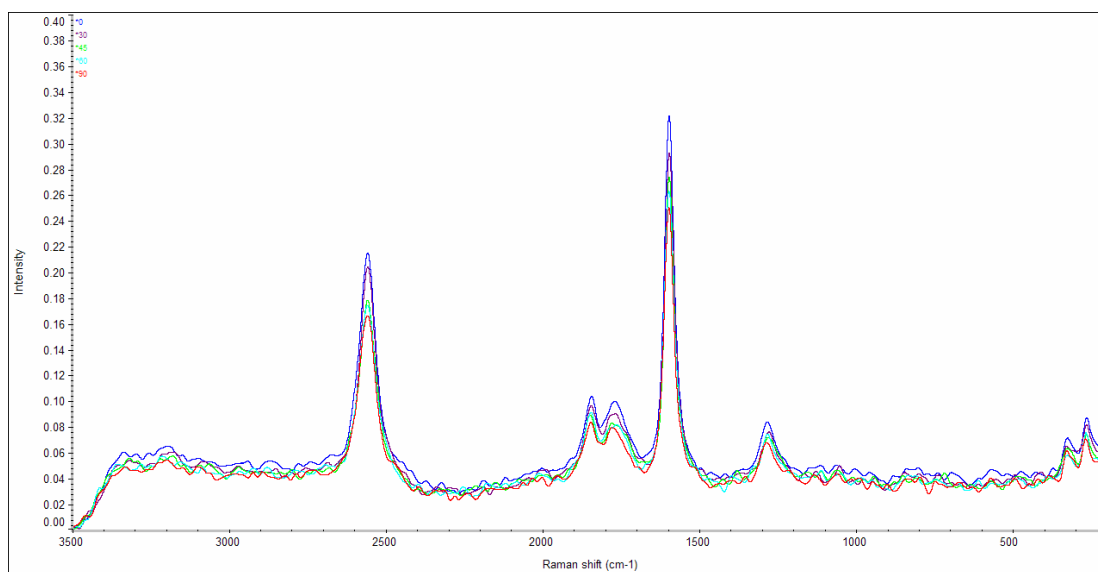

Figure E-14 Full Raman spectra of SWNT aligned by 450 V/cm of DC electric field with 2T magnetic field at various measurement angles (B system)**.**
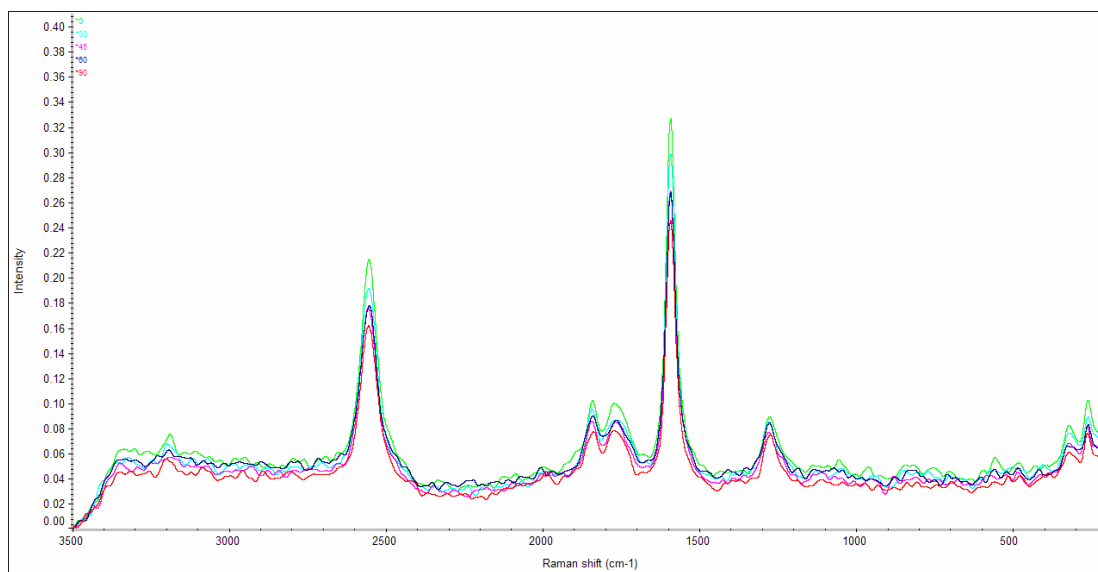
Figure E-15 Full Raman spectra of SWNT aligned by 600 V/cm of DC electric field with 2T magnetic field at various measurement angles (B system)**.**

VITA

Mr. Natthakarn Romyen was born on August 12, 1985 in Phrae, Thailand. He received the Bachelor's Degree in Chemical Engineering from Department of Chemical Engineering, Faculty of Engineering, Rajamangala University of Technology Thanyaburi in April 2007, He entered the Master of Engineering in Chemical Engineering at Chulalongkorn University in June, 2007.